School of

OCEANOGRAPHY

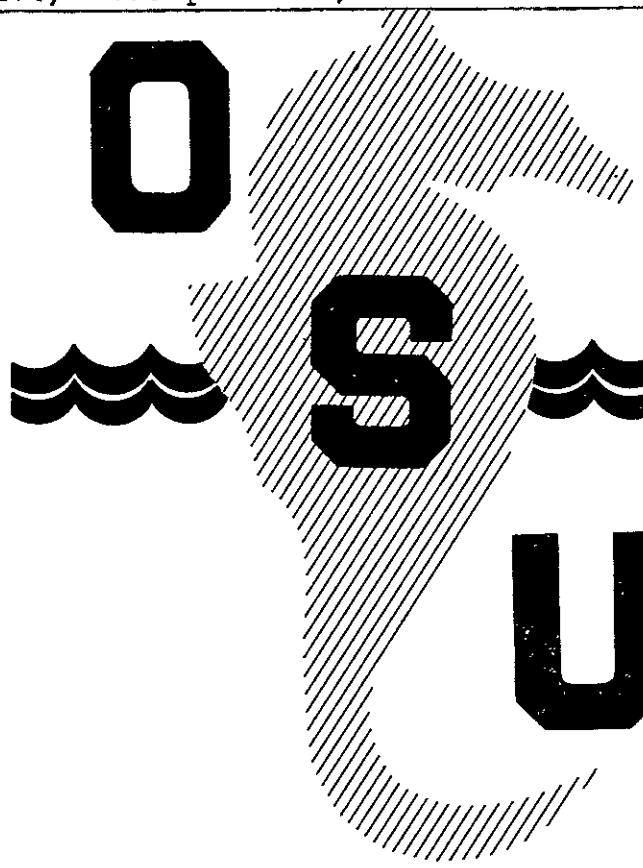

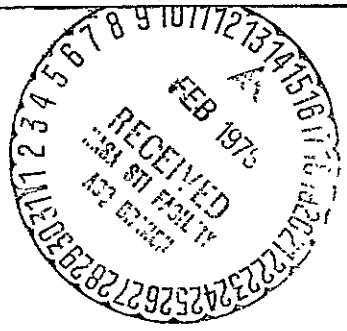

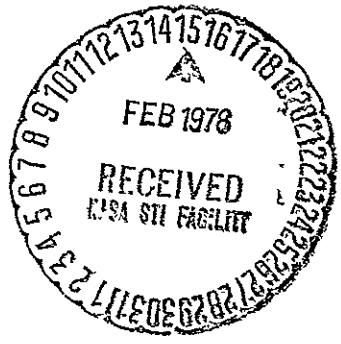

OREGON STATE UNIVERSITY

Particle Size Distributions and the Vertical Distribution of Suspended Matter in the Upwelling Region off Oregon

by

James C. Kitchen

Final Report
Contract NAS5-22319
to
National Aeronautics and Space Administration
Reference 77-10 August 1977

ACKNOWLEDGMENTS

I am very grateful to Hasong Pak for giving me the opportunity to work with the Optical Oceanography group at Oregon State University and to J. Ronald V. Zaneveld for continued encouragement and guidance.

Larry Small provided the nutrient and pigment data and was an exacting reviewer at all stages of the production of this dissertation and related manuscripts. David Menzies provided much technical and scientific discussion and helped collect and reduce the nutrient and pigment data. William Peterson provided the zooplankton data.

Section III has been previously published in Limnology and Oceanography with David Menzies, Hasong Pak and J. Ronald V. Zaneveld as co-authors.

ABSTRACT

Various methods of presenting and mathematically describing particle size distribution are explained and evaluated. The hyperbolic distribution is found to be the most practical but the more complex characteristic vector analysis is the most sensitive to changes in the shape of the particle size distributions.

Particle size distribution, nutrient concentrations, temperature and other biological and hydrographic data were taken during two cruises off the Oregon coast. The first, in late July, 1973, was during a period of consistent upwelling-favorable winds. The second cruise, in August, 1974, was during a period of intermittently favorable winds. Thus the data presented represent several different upwelling situations. Two distinct vertical structures of suspended particulates and two types of particle size distributions were found, separated by a particle front. On the offshore side of the front, the structure was characterized by dominantly small particles and a subsurface maximum of suspended matter. On the other side of the front, the structure shows a particle maximum at or very near the surface with dominantly large particles.

A method for determining onshore-offshore flow patterns from the distribution of particulates was presented. The method was applied to the data from the two cruises. A further experiment was suggested with an emphasis on determining three-dimensional current patterns at the same time as particle distributions. Such data would be used for a three-dimensional numerical model.

A numerical model of the vertical structure of two size classes of particles was developed. The results show a close similarity to the observed distributions but overestimate the particle concentration by forty percent. This was attributed to ignoring grazing by zooplankton. Sensitivity analyses showed the size preference was most responsive to the maximum specific growth rates and nutrient half saturation constants. The vertical structure was highly dependent on the eddy diffusivity followed closely by the growth terms.

TABLE OF CONTENTS

LIST OF FIGURES

LIST OF TABLES

PARTICLE SIZE DISTRIBUTIONS AND THE VERTICAL DISTRIBUTION OF SUSPENDED MATTER IN THE UPWELLING REGION OFF OREGON

I. INTRODUCTION

During the summer months, the prevailing North winds along the Oregon coast produce a transport in the surface water which is directed away from the coast because of the effect of the rotation of the earth. The coastal water is thus mixed with the warmer, less saline Columbia River plume water which separates the coastal from the oceanic waters (Pattullo and Denner, 1965). The advected surface water is replaced by cold, deep water upwelled near the coast. This nutrient-rich water can then support large phytoplankton blooms. The phytoplankton may act as tracers of the water masses (Jerlov, 1976; Pak, Beardsley and Smith, 1970) and thus can possibly be used to describe the dynamics of the circulation. Phytoplankton, however, have their own growth dynmamics, rendering any conservative assumption questionable. This increases the complexity of using optical parameters (functions of the suspended and dissolved matter in the water) to map circulation patterns off the Oregon coast.

The purpose of this dissertation is to describe the relationship of the particle size distribution and vertical distribution of suspended matter in the surface layer to the circulation patterns common in the upwelling region. Data from two cruises has been analyzed to determine what the important processes are. A model will be developed to show that these processes can produce the observed distributions. The inverse problem (determining the circulation given a distribution

of suspended matter and particle sizes) will be discussed. This dissertation is a step toward the ultimate goal of monitoring circulation by remote sensing of optical parameters.

The distribution of a substance P is governed by the equation:

$$\frac{\partial P}{\partial t} = \frac{\partial}{\partial x_i}\left(A \frac{\partial P}{\partial x}\right)_i - \frac{\partial}{\partial x_i}(U_i P) + R(x,t,P) \qquad (1)$$

where repeated indices imply summation over three directions, x_1, x_2 and x_3. A is called the eddy diffusivity and is a constant of proportionality relating the flux of a substance due to random motions to the gradient of that substance in space. The flux of the substance in the direction x_i due to the organized or average velocity U_i in that direction is $U_i P$. The change in concentration of the substance P in an element of space is the flux into the element minus the flux out divided by the volume of the element, which, in the limit as the volume of the element goes to zero, is the first two terms of equation 1. The last term represents all the nonconservative processes. These are mainly biological or chemical. Since this dissertation deals only with the relationship between circulation and suspended matter it is not necessary to know the contribution of each of the nonconservative terms separately. Most of these terms are proportional to the concentration of suspended matter P so it is not difficult to combine them all into one term.

A very high correlation between the concentration of suspended matter and chlorophyll and particulate carbon (Kitchen, Menzies, Pak and Zaneveld; 1975) indicates that the suspended particles in the Oregon upwelling region are predominantly phytoplankton and their

byproducts. Thus marine ecology will play an important role. However, no attempt will be made to provide new insights into biological processes. Only the simple concept of the total optically active matter increasing in concentration at a rate related to the nutrient and light levels is used. Thus phytoplankton and suspended matter or particulates will be used interchangeably in this dissertation. Allowance is made for the fact that different size phytoplankton may have different growth kinetics. In this way the models will be kept as simple as possible and the emphasis placed on the physical processes and results.

The most remarkable feature of the distribution of any parameter is a front. A front is here defined as a region with a relatively large horizontal gradient of the parameter. It is a practical analogue to the interface between two bodies of differing properties. Of particular interest are a temperature (or density) front and a particle front. For the purposes of this dissertation a temperature front is said to exist if the horizontal gradient of surface temperatures is greater than $0.5°C\ km^{-1}$. A particle front exists if the concentration in any size class changes more than an order of magnitude in two kilometers. This is equivalent to a change of about one in the log-log slope (to be defined and discussed in section II) of the particle size distribution. The temperature and particle fronts generally but not necessarily coincide. The mechanisms producing the characteristic particle size distribution and vertical distributions on each side of the front will be investigated.

Organization

The second section is background information on and evaluation of methods of parameterizing particle size distributions. This is presented merely to help the reader understand and evaluate data presented in later chapters. Sections III and IV present data collected during two cruises and contains conclusions based on the data about the importance of the various processes in controlling the distributions. These conclusions will be used in developing the model. The first cruise (section III) was during a period of steady upwelling-favorable winds. The second cruise (section IV) was during a time of periodically favorable winds. The numerical model is developed and the results evaluated in section V. The last section discusses the problem of determining the flow field from measurements of suspended matter and particle size distributions. Improvements to be considered in future research are also presented in this section.

Literature Review

Upwelling Circulation

Two different circulation patterns have been described as typical of coastal upwelling off Oregon. The first is very simple; onshore flow predominates over most of the water column and a fast offshore flow exists in a shallow surface layer (Huyer, 1976). The second pattern occurs when a sloping pycnocline (density front) intersects the surface near the coast. Then the offshore flow meets a much lighter water mass and is forced under it. Another upwelling cell may be found offshore of the density front (Mooers, Collins and Smith,

1976). The distinction between the two patterns may be only whether or not the density front is in the region of observation. Stevenson, Garvine and Wyatt (1974) interpret the frontal circulation pattern as a relaxation of upwelling with sinking of unstably stratified water maintaining upwelling at the coast by continuity restraints. There seems to be general agreement of the magnitude of upwelling motions. Huyer (1976) computes an upwelling velocity of $2.x10^{-2}$ cm sec^{-1} by displacements of the isopycnals (equal density surfaces). Johnson (1977) achieves the same results by a mass balance calculation using a high resolution profiling current meter. Both agree that upwelling motions persist to some degree when the winds slacken after an upwelling event. An in-depth description of Oregon coastal upwelling is given in Huyer (1973).

Models of Suspended Particulate Distributions

A simple steady state analytical solution of the relative vertical distribution of phytoplankton is given by Riley (1963). He uses a two layer system with constant net production in the upper layer (euphotic zone where light levels allow phytoplankton growth to exceed death) and constant negative production in the lower layer (aphotic zone). Settling rates and mixing were constant with depth. By varying the eddy diffisivity, Riley produced solutions qualitatively similar to the vertical distributions studied in this dissertation. However, his assumptions of depth uniform eddy diffusivity and negligible vertical water movements make application to the coastal upwelling regime of little value. Riley's model may be more applicable to the offshore vertical maximum between the permanent and seasonal pycnoclines as described by Anderson (1969). Anderson believes that stability (low

eddy diffusivity) plays an important role in the formation of this maximum but does not extend any of his conclusions to a coastal upwelling feature he briefly mentions.

Ichiye, Bassin and Harris (1972) use a simple model in which all terms of the dispersion equation except settling and vertical diffusion are combined into one term T(z) which they later assume to be constant with depth. They facilitate this simplification by using an average profile of several stations from one region. It is hoped that this would eliminate terms which are random in space or time. Using this procedure they obtain a vertical distribution of eddy diffusivities, all of order 1 cm^2 sec^{-1}. Eittreim, Biscaye and Gordon (1973) point out that constant A_z and varying T(z) is at least as likely. In this dissertation both functions will be assumed to vary with depth.

Wroblewski (1976) presents an extensive numerical model of nutrient flow through two living food chain levels and detritus (nonliving material of biological derivation). The biological model is superimposed on a two-dimensional flow field determined by a numerical model of the wind-driven upwelling circulation off the Oregon coast. The upwelling model is patterned after that of Thompson (1974). Wroblewski's model includes self-shading, the diurnal periodicity of the light field, and the effect of nitrate and ammonia on the uptake rate of one another. But the paper does not include a reduced value of eddy diffusivity in the thermocline. As a result his maximums are much deeper than those shown in this dissertation. However, it is likely that we are modeling two different phenomena as data can be found to support both models.

Phytoplankton Cell Size

Semina (1972) demonstrates a correlation between mean cell size and vertical water velocities, value of the density gradient and phosphate concentration. A slightly more analytical approach is used by Parsons and Takahashi (1973). They relate phytoplankton growth rate μ to species-specific (and therefore size-specific) light and nutrient half saturation constants K_I, K_N (the light intensity and nutrient concentration at which the growth rate is half the maximum), maximum specific growth rate μm (in units of inverse time), cell sinking rate s, upwelling velocity U and depth of the mixed layer D as follows:

$$\mu = \mu_m \left\{\left(\frac{<I>}{K_I+<I>}\right)\left(\frac{[N]}{K_N+[N]}\right) - \frac{s-U}{D}\right\}$$

where <I> is the average light intensity in the mixed layer and [N] is the concentration of the limiting nutrient.

Dominant cell size is determined by comparing the computed growth rates μ of two different species. To be dimensionally correct the advective term (already in units of inverse time) should be outside the brackets. Of the examples that Parsons and Takahashi present, only in the estuarine case, where D is very small, does the advective term play any role at all. They do not present any case of strong upwelling (i.e. U > s). In that case the validity of their advective term may fail as upwelling of clean water through the thermocline and the divergence of the surface water should be a negative influence on suspended particulate concentrations. Hecky and Kilham (1974) point out that half saturation constants may be more a function of cell history than a species specific property. Parsons and Takahashi's method may be

adequate to explain cell size differences between large general regions of the Pacific Ocean. Their method will not be used in its present form for explaining smaller scale variation in the coastal upwelling region. However, most of the factors used by them and by Semina (1972) will be included in the modeling.

Seasonal changes in the ratio of nanoplankton (not retained by nets) to netplankton were studied by Malone (1971). He found that netplankton only become abundant during strong upwelling (as evidenced by high nutrient concentrations) and that nanoplankton exhibit less variability because of the stronger coupling of production and grazing. He postulates the stronger coupling to be due to the shorter life span of the protozoans which may be the primary grazers of the nanoplankton. During June and July the netplankton were selectively grazed and reduced in number in spite of relatively high nutrient concentrations.

Response of Inhomogeneous Distributions to Physical Processes

Inhomogeneity of a substance in the ocean is often referred to as "patchiness". This is especially true of suspended matter in the surface layer. Monitoring the behavior of a patch may provide information about the physical processes active in the area. Many experiments have been performed with artificially generated patches. Several of these are reviewed in Okubo (1971). Okubo presents a relationship between the apparent eddy diffusivity and the length scale of the patchiness. He also discusses the effect of current shear on increasing the dispersion of the patch. Theoretical considerations of phytoplankton patchiness are presented by Wroblewski, O'Brien and

Platt (1975) and by Wroblewski and O'Brien (1976). The former paper derives a critical length scale for a patch to maintain itself against diffusion and grazing. The latter includes numerical models of the growth of decay of one dimensional patches. Kamykowski (1974) presents several mechanisms by which internal tides can produce patchiness. One of these is the convergence of surface waters over the trough of the internal tide.

Studies of natural patches are not as plentiful. Pearcy and Keene (1974) described the patchiness of ocean color spectra of Oregon. They discovered parallel bands of differing color composition corresponding to the upwelled water, the Columbia River plume, and the oceanic waters. Beers, Stevenson, Epply and Brooks (1971) found two circular patches of chlorophyll pigment off Peru. They monitored the evolution of these patches with quasi-synoptic shipboard measurements. One of these patches was bordered by a density front on two sides and was believed to be a cyclonic eddy of the Peru coastal current. Temperature and salinity indicated that the water at the center of the eddy was upwelled. The patch moved west at about 23 cm sec^{-1}. The water to the west of the patch was moving north. In general the motion of a patch does not reveal the velocity of the water but the boundaries of a patch may divide regions of differing circulation patterns.

II. PARTICLE SIZE DISTRIBUTIONS

The size of the particles suspended in the water is an important factor in determining their optical properties and settling rates. If the particles are phytoplankton, their size or more specifically their surface area to volume ratio may affect the ease with which nutrients are transferred through their cell walls. Particle size may also be used as an identifying characteristic of the water mass in which the particles are suspended.

In actual water samples, the particles will have a wide range of sizes. Thus a function describing how the particles are distributed over the various sizes must be used. Such a function is called a particle size distribution (psd).

There are three ways of presenting size distributions: 1) histograms; 2) cumulative distributions; and 3) incremental distributions. Histrograms superficially appear to be the most direct method, but are in fact somewhat ambiguous as the choice of windows is critical to the shape of the distributions and to the amount of information portrayed. Sheldon and Parsons (1967) recommend windows which cover particle volumes between consecutive powers or half powers of 2 μm^3. Such a scaling can also be represented as a logarithmic scale of particle diameters. In very productive waters narrower windows may be needed to record peaks corresponding to abundant species with a small range of cell volumes. The cumulative distribution is computed by finding the amount (e.g. number (N) or volume (V)) of particulate volume larger (or smaller) than given sizes (D). The incremental size distribution is the derivative (dN/dD) with respect to size of the cumulative size

distribution. The cumulative size distribution is, by definition, monotonic which helps when trying to find a simple mathematical expression to describe the curves. By the same token, it also conceals some of the irregularities. The incremental distribution (dN/dD) is usually monotonic also, and is often fit well by the same type of mathematical expressions that describe the cumulative curve.

Methods of Parameterization

Suspended material in the oceans and many other natural collections of particles often have a cumulative psd which is fitted very well by the hyperbolic curve $N = kD^{-c}$ (Bader, 1970) where N is the number of particles per unit volume larger than diameter D, and k and c are constants to be determined for each sample. This is equivalent to an incremental size distribution $dN = -mD^{-b}$ where $m = ck$ and $b = c + 1$. c and b are both called slopes of the distributions as they are the slopes of the corresponding distributions as plotted on full logarithmic graph paper. There may be some confusion when giving slopes unless it is clearly stated whether the cumulative or incremental size distributions are used. The slopes are also a measure of the number of small particles relative to the number of larger particles, the larger the slope, the greater the relative number of small particles.

Carder, Beardsley and Pak (1971) suggest the Weibul distribution, $F = 1-\exp(-(D/D_0)^f)$, where F is the percentage of particles smaller than diameter x and D_0 and f are constants] as a good fit to samples taken from the eastern equatorial Pacific. But the samples they show are partitioned into three segments with widely differing values of c

for each segment. This hardly constitutes a good fit especially considering the narrow range of diameters (2.2-7.1 μm) which the three segments cover. The exponential distribution, $N = a \exp(-dx)$, can be obtained from the Weibul distribution in the special case that $f = 1$. The exponential distribution is easier to work with and is more widely used (e.g., Zaneveld and Pak, 1973). Coastal particle size distributions (by number of particles on a log-log scale) have a definite curvature and sometimes even a maximum at about 5 μm spherical equivalent diameter. Parsons (1969) described similar distributions by an index of diversity $D = \Sigma P_i \log P_i$ where P_i is the fraction of the total volume in the ith window, the range of particle volumes in each window being twice that of the previous window as was suggested above. This gives a single value corresponding to community diversity as measured by species counts, but the size distribution cannot be reconstructed from it.

Another method of reducing particle size distributions to two parameters is by characteristic vector analysis, CVA (Kitchen, Menzies, Pak and Zaneveld, 1975). Given r different kinds of information about each of N samples, CVA finds the system of orthogonal axes in r-space for which the variability is concentrated in as few dimensions as possible. The first characteristic vector, V1, is the axis along which the most variation occurs and the second characteristic vector, V2, is in the direction of the most remaining variability and so forth. For each characteristic vector there is a corresponding root, λ which is a solution of the equation $\det(S - \lambda I) = 0$ where S is the variance-covariance matrix and I is the r by r identity matrix. The proportion

of the original variance in the direction of any characteristic vector is given by the ratio of the corresponding root to the sum of the diagonal terms (trace) of the variance-covariance matrix. A computational method for obtaining the first few vectors and roots is given by Simonds (1963). The Fortran rendition of Simonds' Algorithm used for this dissertation is given in Appendix A. CVA has been used by Mueller (1973, 1976) in studying ocean color spectra and by Kopelevich and Burenkov (1972) for light scattering functions.

Comparison of Methods to Fit Particle Size Distributions

To compare some of the various methods of fitting size distributions from coastal waters, a set of 204 samples from the first six transects of cruise Y7408B (see Chapter 3) has been chosen. The fit to each data window (size classes) will be tested by comparing the residual sum of squares, $RS_i = \sum_{i}^{n}(X_i - Y_i)^2$ where X_i is the actual data in the ith window and Y_i is the predicted value, to the total sum of squares corrected for the mean, $TS_i = \sum_{i}^{n}(X_i - \overline{X}_i)^2$ where $\overline{X}_i$ is the average of the n samples for the ith window. The test statistic shall be called $R_i^2 = 1. - RS_i/TS_i$ with the result that a negative R_i^2 value can occur when the given fit is worse than using just the average concentration for the window. The best possible R_i^2 is 1.0.

The mean vector for the 204 samples is: 925.01, 602.43, 333.11, 138.10, 60.585, 32.374, 17.419, 10.457, 6.0023, 3.4122, 2.3042, 1.2218 particles per ml. The total sums of squares corrected for the mean (TS_i) are: 8.0731×10^7, 3.5279×10^7, 1.5214×10^7, 4.0756×10^6, 1.3127×10^6, 490270, 143320, 73627, 24244, 7559.5, 3830.4, and 1129.3.

Table I. A quantitative comparison of various methods of fitting particle size distributions.

$$R^2_i = 1 - \frac{\Sigma(X_i - Y_i)^2}{\Sigma(X_i - \bar{Y}_i)^2}$$

Windows / Method	1	2	3	4	5	6	7	8	9	10	11	12	Av
Exponential	0.88	0.94	0.93	0.85	0.94	0.94							0.91
Exponential	-0.80	-0.33	0.36	0.83	0.59	0.18	-0.76	0.00	0.35	0.80	0.91	0.59	0.23
Hyperbolic	0.71	0.93	0.81	0.88	0.97	0.93							0.87
Hyperbolic	0.56	0.82	0.78	0.83	0.84	0.87	0.87	0.89	0.94	0.97	0.93	0.89	0.85
CVA (number)	0.999	0.978	0.979	0.87	0.68	0.64	0.58	0.56	0.59	0.58	0.53	0.45	0.70
CVA (log number)	0.61	0.76	0.85	0.83	0.80	0.83	0.85	0.85	0.92	0.97	0.97	0.93	0.85
Cumulative hyper	0.38	0.94	0.88	0.88	0.90	0.95							0.82
Cumulative hyper	-0.30	0.73	0.84	0.85	0.87	0.88	0.87	0.84	0.87	0.90	0.78	0.80	0.74
Cumulative exp.	0.49	0.79	0.96	0.71	0.57	0.89							0.74
Cumulative exp	-1.61	-1.21	-0.33	0.57	0.88	0.57	-0.63	-0.27	-0.11	0.52	0.96	0.64	0.00

The fit of the exponential, the hyperbolic and the CVA distributions are compared in Table I. The first six lines of Table I all pertain to the psd's expressed as histograms. The exponential fits the first six windows better than the hyperbolic but when one tries to fit all twelve windows the exponential becomes very bad. The hyperbolic fits twelve windows almost as well as it fits 6 windows. CVA of the number distributions fits very well on the first three windows but then becomes mediocre on the rest of the distribution. This results because most of the total variability is in the small sizes which have very large numbers of particles. Thus the most efficient way to reduce the total variance is to fit the small sizes very well. The ratio of the characteristic roots to the trace of the variance covariance matrix indicates that the first two vectors eliminate 98% of the total variance. The average R^2 statistic used in Table I is different because it gives equal weight to each window. Only two vectors are used so that all the comparisons are between fits using two parameters. If log particle concentrations are used instead, then the total variance is more evenly spread over the windows. When we transform the numbers back to particle concentration our statistics show a better fit than using just the concentration to begin with. The CVA method indicates 95% of the variance of the log values is accounted for by two vectors. The CVA fit is as good as the hyperbolic fit. Some samples are shown in Figure 1 with their hyperbolic and log CVA fits. The last four lines of Table I refer to the cumulative size distributions. The cumulative size distributions may look like a better fit on graph paper but after converting the numbers back to a histogram they are seen not to do a good job.

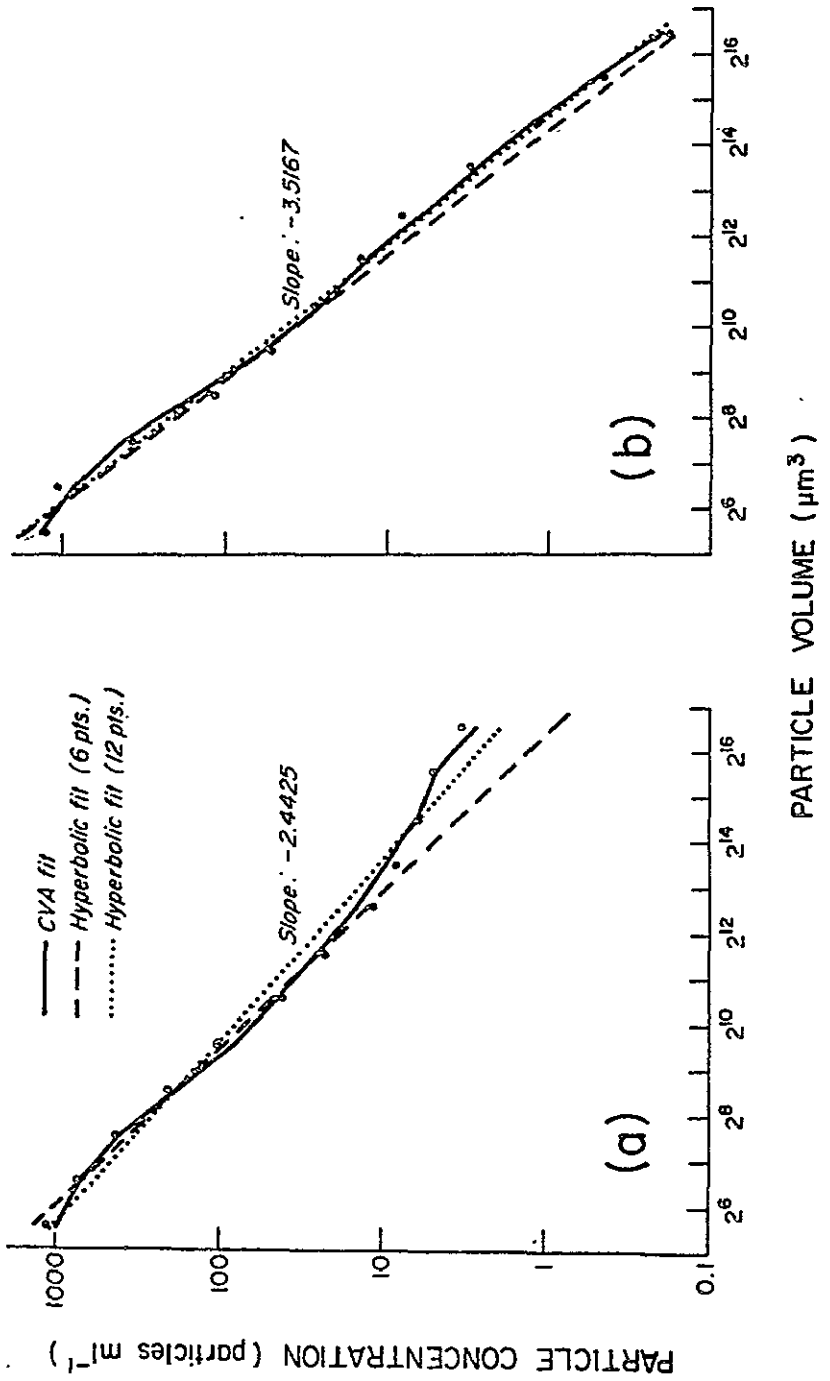

Figure 1. A comparison of various methods of fitting particle size histograms. The large dots show the actual data points.

There is a close relationship between the hyperbolic fit to the cumulative size distribution and to the histogram. Assuming the hyperbolic distribution, $dN = N_0 D^{-b} dD$, describes the particles, we can compare the two fits. The cumulative distribution is given by $\int_x^\infty N_0 D^{-b} dD = N_0 x^{1-b}/(b-1)$. A doubling in volume results in the diameter changing by a factor of 2 so the number of particles in a window of a histogram can be expressed as:

$$\int_x^{2^{1/3}x} N_0 D^{-b}\, dD = \frac{N_0(1 - 2^{(1-b)/3})}{b - 1} x^{1-b}$$

Both have the same log-log slope, (b-1). The slopes were computed both ways and a correlation of 0.96 and a mean difference of 0.029 were found. For almost all the samples, the two slopes were within 0.5 of each other. The range of c-1 was approximately 1.8 to 4.7. Such a close relationship between the cumulative and histogram distributions cannot be found for the exponential function.

Much of the variation that we have tried to model in Table I is due to changes in the total numbers of particles. The same tests can be performed on normalized distributions where each window is divided by the total number of particles in the sample. Thus the variance is due only to changes in the shape of the psd, not to changes in the total amount of suspended matter. The results of this refinement are shown in Table II. The mean vector of the data is: 0.44685, 0.28177, 0.15244, 0.063123, 0.026850, 0.013395, 0.0069944, 0.0038370, 0.0021892, 0.0012555, 0.00083686, 0.00046300 and the corrected sum of squares are: 0.98782, 0.20774, 0.17269, 0.094027, 0.041057, 0.016543, 0.0045693, 0.0026460, 0.00097616, 0.000038095, 0.00023685, 0.000084677. We see that only

CVA provides an accurate fit to the normalized psd's. CVA, however, produces weighting factors (Kitchen et al., 1975) whose physical meaning is not always apparent. Generally the first weighting factor corresponds well with total particulate matter (not in the case of the normalized distributions though) and the second adjusts the ratio of small to large particles. Until some sort of universal data set is found CVA must be performed anew for each data set with different ectors and different weighting factors resulting. The last line of Table II is an attempt to see what would happen if one set of characteristic vectors is used on a larger data set. The results were not drastic but it can be seen that the use of these particular vectors could not be expanded much farther.

Characteristic vector analysis and hyperbolic distributions give equally good fits to size distributions which are in terms of concentrations (e.g. particles per ml). For relative distributions (absolute concentration ignored) only CVA is better than using the average relative psd as representative of all samples. However, the hyperbolic function gives a reasonable fit over a wide range of particle sizes. Since it is much more widely used and easier to present and understand than characteristic vector analysis, the hyperbolic distribution is the logical choice when presenting data to other people. For narrow ranges of particle sizes the exponential distribution may give a better fit. Characteristic vector analysis has the potential of being the best choice where subtle differences in the shape of the particle size distributions are important as may be the case in studies of nutrient-phytoplankton relationships. In the case of particle size distributions using volume

Table II. A quantitative comparison of various methods of fitting relative (number of particles in each size class is divided by the total number of particles) size distributions.

$$R_i^2 = 1 - \frac{\Sigma(X_i - Y_i)^2}{\Sigma(X_i - \bar{Y}_i)^2}$$

Windows	1	2	3	4	5	6	7	8	9	10	11	12	Av
Method													
Exponential	- 0.16	--0.45	0.46	0.48	0.80	0.86							0.33
Exponential	-23.76	-35.20	- 6.55	0.50	-0.52	-2.17	-4.77	-2.21	-0.66	0.67	0.87	0.44	-6.11
Hypertolic	- 2.68	-- 0.58	- 0.81	0.63	0.89	0.89							-0.28
Hyperbolic	- 4.82	- 3.53	- 1.12	0.47	0.60	0.64	0.71	0.76	0.90	0.97	0.90	0.86	-0.22
Cumulative exp.	- 5.11	- 2.50	- 2.74	-0.34	-0.33	0.73							-1.72
Cumulative exp.	-34.40	-57.14	-14.66	-1.06	.63	- .65	-4.05	-2.84	-1.70	0.18	0.95	0.52	-9.52
Cumulative hyper	- 5.64	- 0.33	- 0.19	0.61	0.76	0.87							-0.65
Cumulative hyper	-15.04	- 5.06	- 0.48	0.56	0.64	0.68	0.76	0.74	0.84	0.87	0.71	0.70	-1.17
CVA log	0.55	0.04	0.22	0.42	0.72	0.83	0.82	0.84	0.92	0.95	0.98	0.96	0.69
CVA log*	0.41	-0.57	0.00	0.41	0.71	0.82	0.81	0.81	0.94	0.97	0.986	0.96	0.60

*CVA was performed on the first 51 samples only but the resulting vectors were applied to all 204 samples.

concentration, CVA may be the only choice as volume distributions tend to be very irregular.

III. OBSERVATIONS DURING A PERIOD OF STEADY NORTH WINDS

Data were obtained during a ten day multidisciplinary coastal upwelling experiment (CUE) cruise in late July, 1973, during a period of consistent upwelling favorable winds that had commensed about ten days previously. Discrete water samples were obtained by a pumping system attached to a salinity-temperature-depth (STD) recorder with deck readout. Sampling depths were selected to characterize the source of the upwelling water, the surface euphotic zone (where phytoplankton growth takes place), the pycnocline, and the thermal inversion when present.

Particle size distributions (PSD) were measured from eight to one hundred and five μm spherical equivalent diameter in twelve bands with an electronic particle sizer interfaced to a Nuclear Data 2400 Multi-channel Analyzer. Phytoplankton standing stock was measured as chlorophyll _a_ concentration, determined by a continuous flow Turner 111 fluorometer, and as particulate carbon, determined by combustion of glass fiber filters in a Carlo Erba model 1100 CHNO elemental analyzer.

The particle count data was reduced to incremental volume distributions dV/dD by dividing the volume concentration in parts per million by the bandwidth in micrometers. This scaling maximizes the systematic variations (peaks at nine and thirty μm) and minimizes the variations in the size bands that contain the most statistical uncertainty (the largest sizes). These distributions were then subjected, with the aid of a computer, to characteristic vector analysis (CVA).

Results, Characteristic Vector Analysis

For the 263 samples collected during this cruise, the CVA method indicates that the first characteristic vector (CV) removes 74% of the variance, the second CV removes 18% and the third CV only 3%. Thus, for a given sample:

$$C_1 \cong \langle C_1 \rangle + W1V_{1,1} + W2V_{2,1}$$
$$C_2 \cong \langle C_2 \rangle + W1V_{1,2} + W2V_{2,2}$$
$$C_i \cong \langle C_i \rangle + W1V_{1,i} + W2V2,i$$

C_i is the incremental volume concentration for the sample in the ith psd band, $\langle C_i \rangle$ is the average concentration in the ith band for all samples, W1 and W2 are the weighting factors determined for the sample, and $V_{1,i}$ and $V_{2,i}$ are the ith components of the first and second CV's determined for the entire sample set. The average vector and the two CV curves are shown in Figure 2.

The first CV weighting factors (W1) have been plotted against the second CV weighting factors (W2) in Figure 3 for all samples analyzed. Samples from the homogeneous, clean, deep water are shown as a dense patch of points with W1 values near -0.05. Samples from the surface waters form the two arms, one with positive W2 values and one with negative W2. Notice that the positive arm represents almost exclusively samples with sigma-t greater than 25.5. To see what these arms mean, the sum of the average data and different proportions of the two CV curves have been plotted in Figure 4. The total volume varies most with W1. Negative W2 values indicate that a large fraction of the particulate volume is contributed by particles with diameters less than 20 μ,. and positive W2 values represent samples that have a well defined

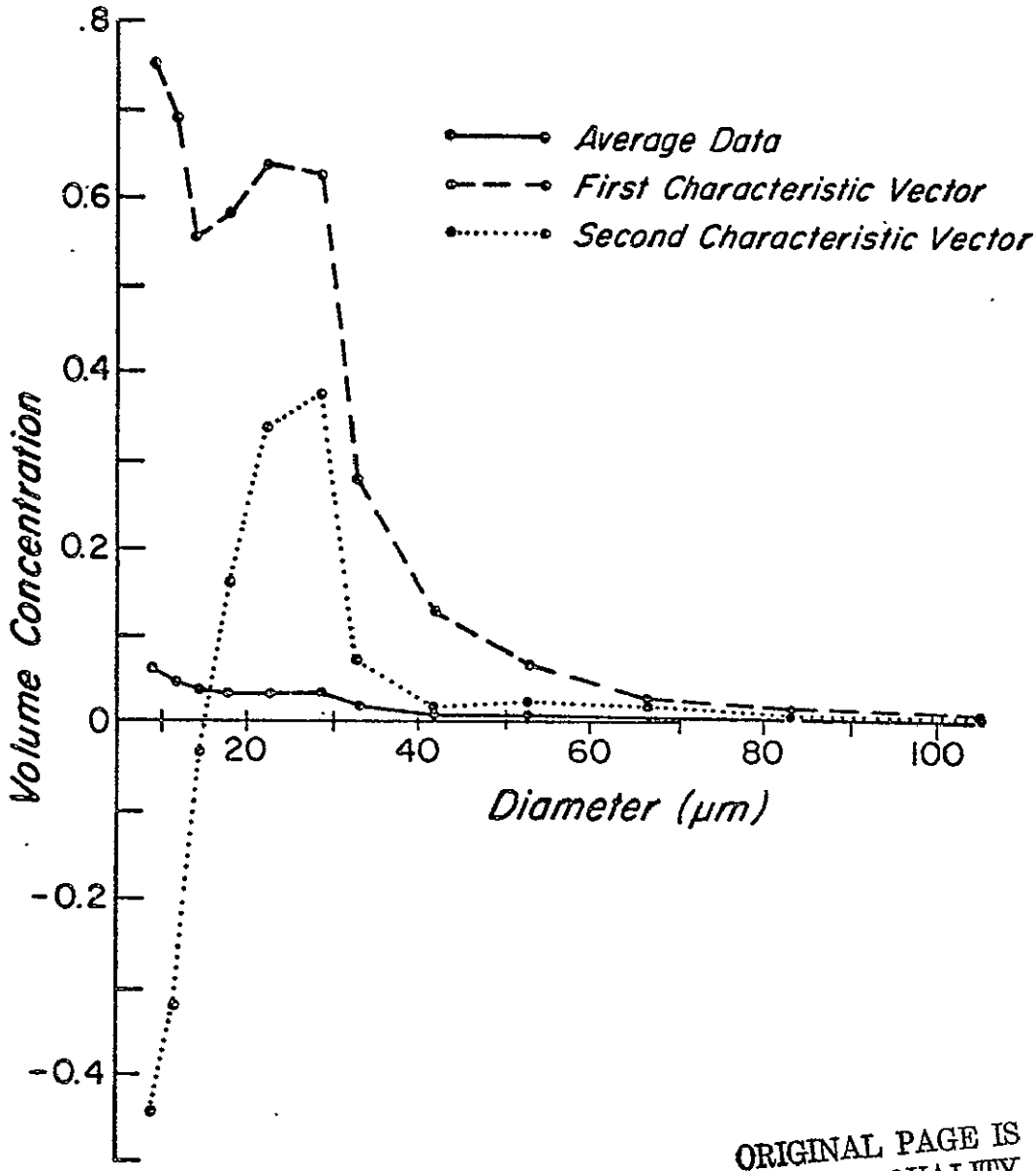

Figure 2. The incremental volume concentration (ppm/μm bandwidth) for the average of the 263 samples, the first characteristic vector and the second characteristic vector

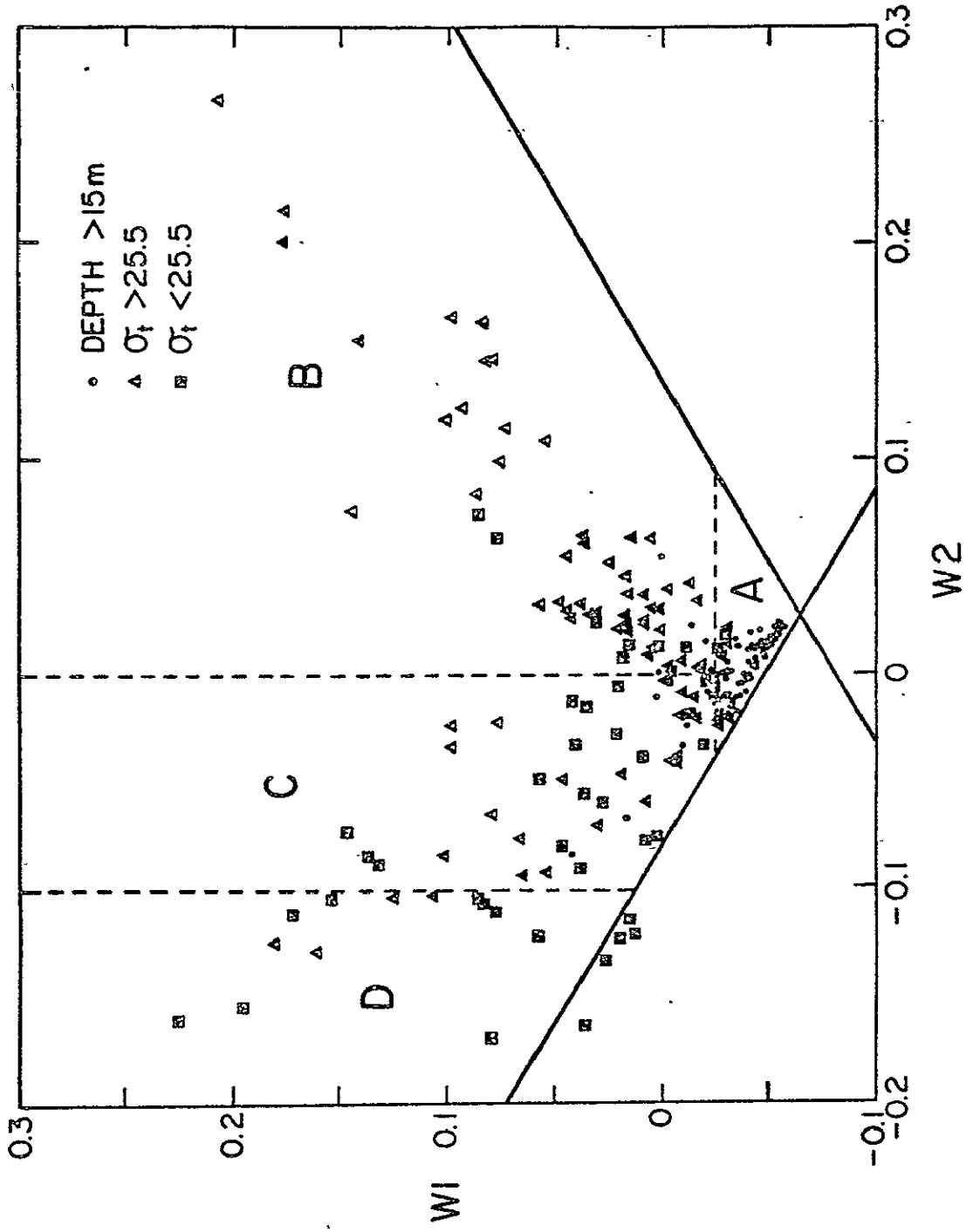

Figure 3. The distribution of the first characteristic vector weighting factors (W1) versus the second characteristic vector weighting factors (W2). Points in region A represent primarily samples taken below the euphotic zone. The other groups are predominantly samples from the top 15 m.. Samples from the surface layer are symbol coded according to their sigma-t values.

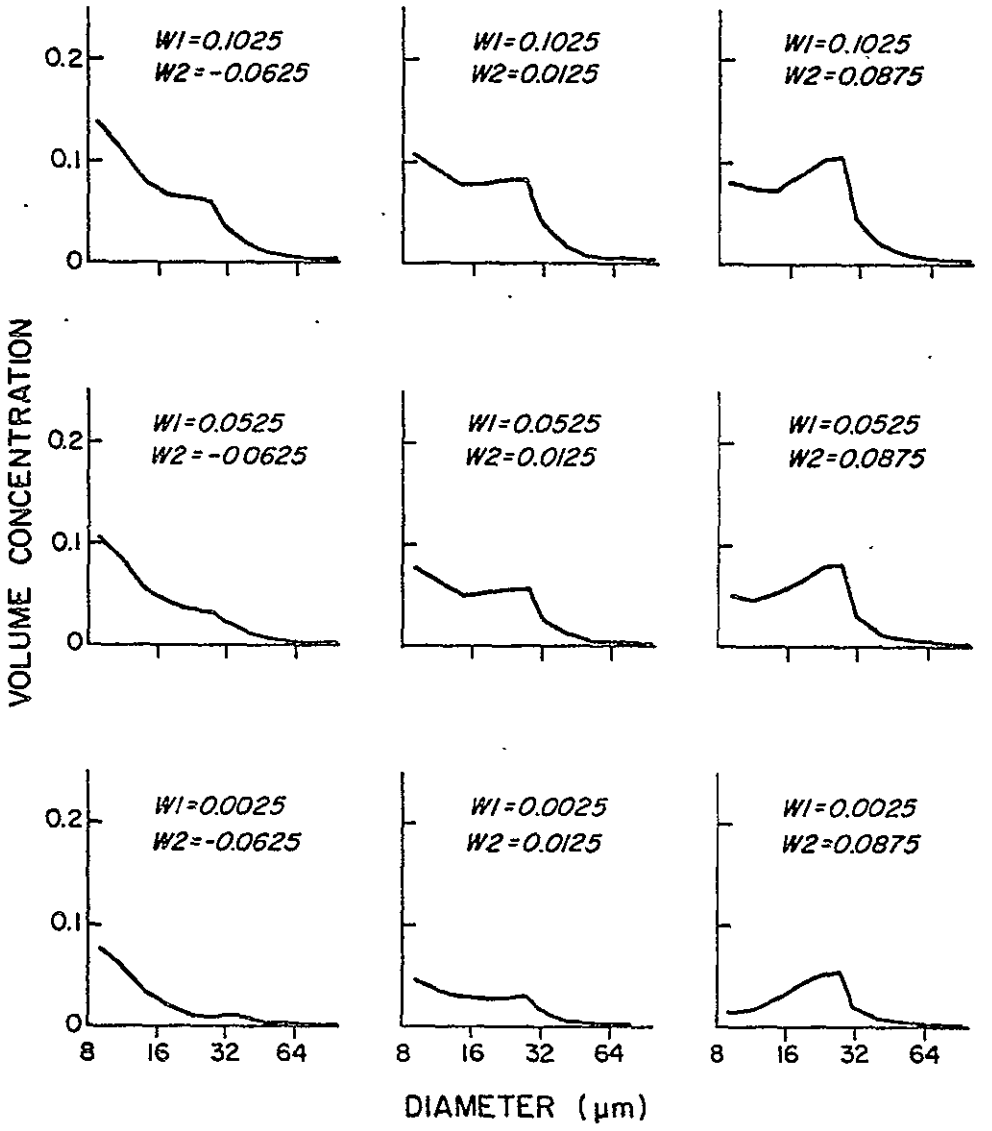

Figure 4. The sum (ppm/μm bandwidth) of the average volume concentration curve and various proportions of the two characteristic vectors as defined by their weighting factors, W1, W2.

peak in volume concentration between 20 and 50 μm diameter. Thus, for this data set, the weighting factors are directly comparable to the slope and intercept of the hyperbolic distribution. Both the slope and W2 are measures of the relative amounts of small and large particles. The intercept and W1 are measures of the total amount of suspended matter. The intercept may be the more ambiguous of the two since it depends greatly on the slope of the distribution. The sign of the second weighting factor (W2) also discriminates between two distinct types of distributions.

The slanted lines of Figure 3 indicate the region of possibility. That is, below these lines the sum of the average vector and the weighted characteristic vectors produces negative volume concentrations in certain psd bands; i.e. below the line with negative slope

$$\langle C_6 \rangle + W1V_{1,6} + W2V_{2,6} < 0$$

and below the line with positive slope

$$\langle C_1 \rangle + W1V_{1,1} + W2V_{2,1} < 0 \ .$$

These particular bands are the first to go negative to each case. Since negative volume has no meaning here, these lines delineate the region of possibility. The reason that some points do, in fact, lie outside this region is that not all of the variation is accounted for by the first two characteristic vectors. The psd curves of the actual data represented by points outside the region of possibility have high volume concentration at the smallest diameter measured and fall rapidly with increasing size. The psd values represented by points almost on but above the line are very smooth in shape, and those farther removed are more irregular. In Figure 5 the volume concentration curves for some representative samples are given along with their CV representation. The samples were chosen to illustrate the variation between the clean

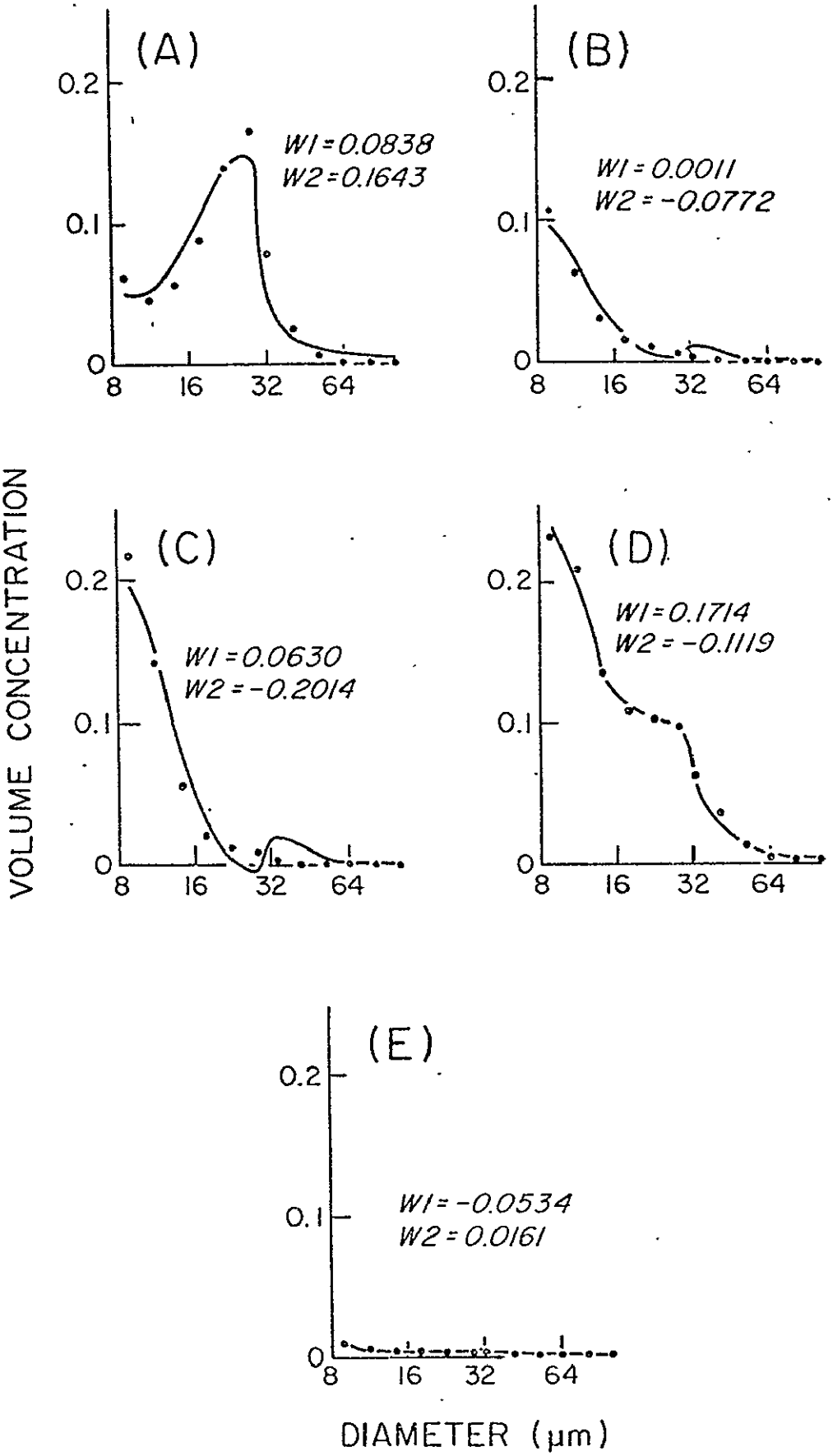

Figure 5. Volume concentration (ppm/m bandwidth) as given by the measured data (dots) and by the characteristic vector representations (lines) for samples taken d km from shore at a depth z, (d,z) as follows: A, (1.85,1); B, (37.1); C, (15.5); D, (9.25); and E, (7.5,20).

in the whole transect but a relative minimum occurs at station six. Potential productivity (Figure 6h) also shows a relative minimum at station six.

Figure 7 shows W1, W2, and temperature for a transect taken a day later at 45° 12.2' N lat. A significant temperature inversion is noticeable at three consecutive stations and the large temperature gradient seen in the previous transect is not present. Low surface temperature are prevalent throughout the transect. Correspondingly all samples from the surface layer have large positive values of both W1 and W2 increasing with distance from shore.

In order to compare the W1-W2 water mass characterization with the standard temperature-salinity diagrams, Figure 8 was constructed. It is a T-S diagram with the points coded according to their position on the W1-W2 diagram. Each kind of symbol represents one of the regions marked off in Figure 3. On Figure 8 the symbols form overlapping but distinct groups of points. The diagram shows that warmer, less saline water contains a greater proportion of small particles (as shown by negative W2 values) than the cold salty water. The points representing the samples from group A have a broad range of temperature and salinity but for a given salinity are usually colder than the other three groups. This is as expected since group A represents the deep samples. Group B is concentrated below 10°C and greater than 33 $^{o}/_{oo}$ salinity. Groups C and D are spread through the warmer, less saline water. The averages of temperature and salinity (T,S) for the groups are: A--(7.61,33.47); B--(8.31,33.41); C--(9.35,33.01); D--(10.49,32.65). The data for the station producing the outlying group of points at the top of Figure 8 have not been used in these averages. This group of points represents

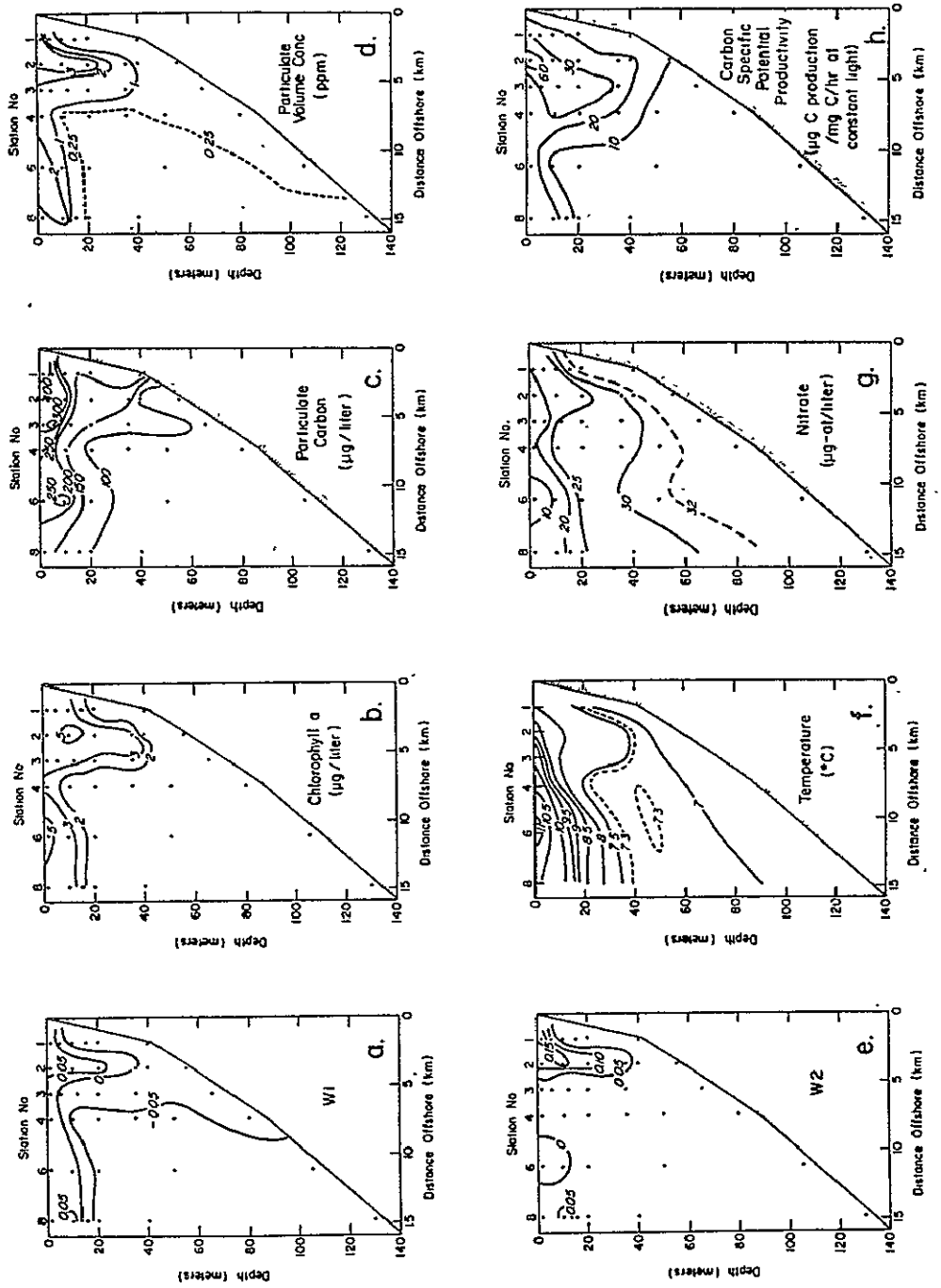

Figure 6. A transect sampled 30 July 1973 along a line of latitude 45°05' North off the Oregon coast.

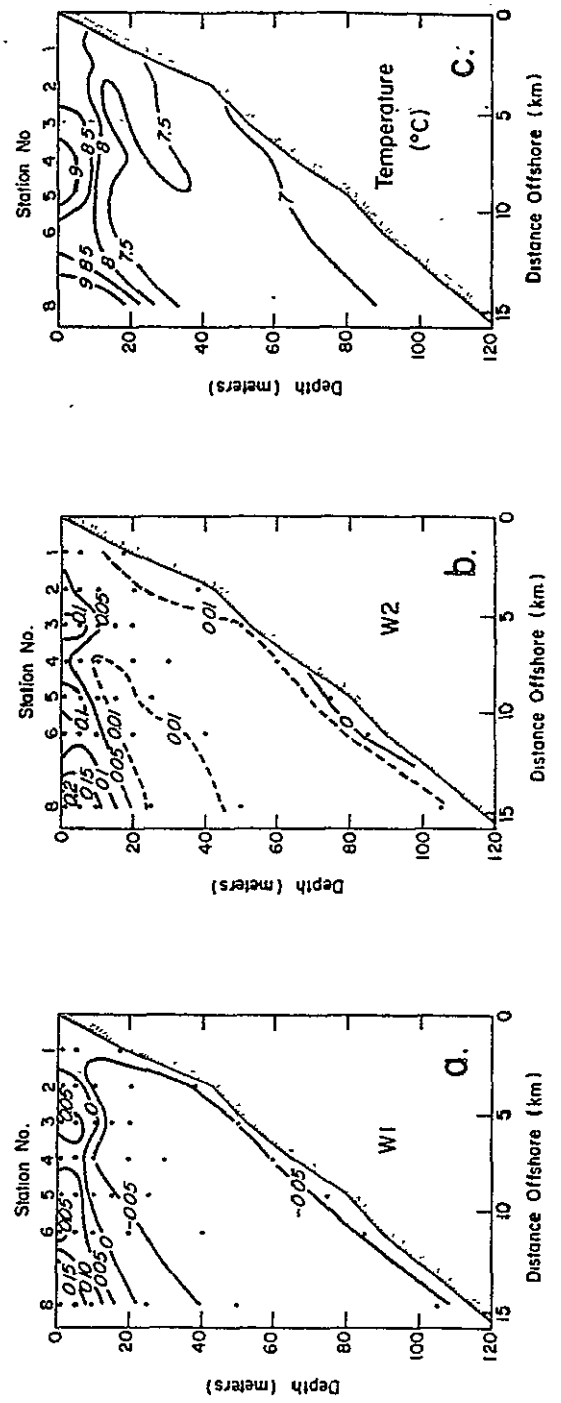

Figure 7. A transect sampled 31 July 1973 along a line of latitude 45°12.2' North off the Oregon coast.

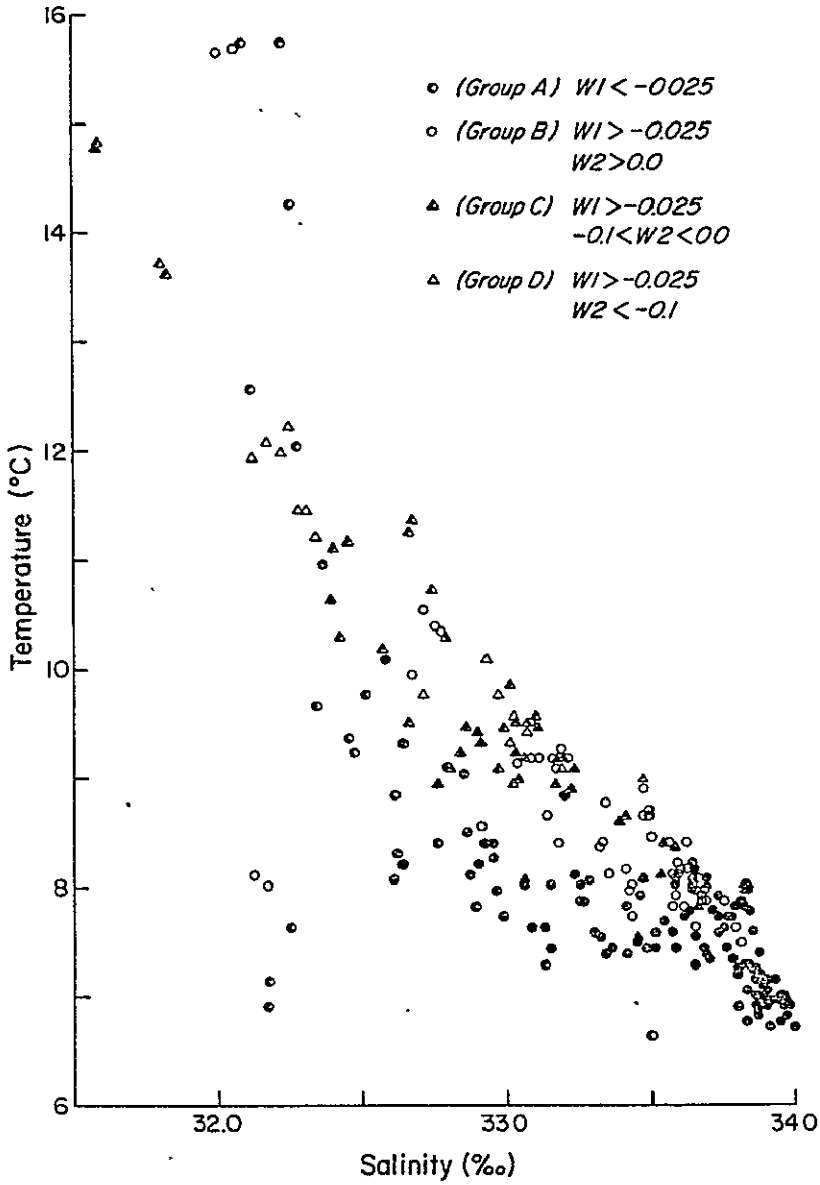

Figure 8. A temperature-salinity plot of the samples coded according to their characteristic vector weighting factors. Each type of symbol represents one of the regions outlined in Figure 3.

a station taken 75 km from shore, the farthest out we went, and is believed to be an isolated station in an open ocean water mass.

DISCUSSION AND CONCLUSIONS

Parsons (1969) presented psd curves (in Parsons' case, volume histograms) very similar to those presented here. In his study, change in particulate volume compared favorably with production as determined by the ^{14}C method. Also, the correlation of particulate volumes with carbon and chlorophyll *a* was highly significant. In our study, the weighting factors W1 and W2 also correlated well (Table III) with particulate carbon and chlorophyll *a*, leading to the conclusion that the large volumes of suspended particulates were due to phytoplankton. Accepting Parsons' designated value of 20 μm diameter as the boundary between nanoplankton and microplankton, negative W2 values indicate a predominance of nanoplankton and positive W2 values indicate that a greater proportion of the particulate volume represents the larger microplankton.

Table III shows that for our 263 samples, W1 correlates better with carbon and chlorophyll *a* than does total measured volume. Also, a linear combination of W1 and W2 correlates with chlorophyl *a* and carbon equally well as a linear combination of the volume in the first three psd bands V1-3 and the volume in the second three psd bands V4-6. Thus, for some applications at least, we lose nothing by using CV weighting factors instead of volume. In fact, we gain psd shape information that volumes alone do not give us. Figures 3 and 5 suggest that, a lot of qualitative information is given by the weighting factors that cannot be expressed in terms of ratios of volumes.

TABLE III. REGRESSION COMPARISON OF PARTICULATE VOLUME AND CV WEIGHTING FACTORS VS. CHLOROPHYLL a AND PARTICULATE CARBON.

Regression equation	R	df	levels of sign
CHL = 0.99(±0.12) + 1.35(±0.07) VOL*	0.78	260	< 0.001
CHL - 2.65(±0.07) + 31.5(±1.2)W1	0.86	260	< 0.001
CHL = 0.60(±0.1) + 5.12(±0.28)V_{1-3} + 0.49(±0.14)V_{4-6}†	0.87	260	< 0.001
CHL = 2.65(±0.07) + 31.5(±1.2)W1 - 7.3(±1.1)W2	0.88	260	< 0.001
CARB = 89.97(±9.4) + 68.9(±5.3)VOL	0.64	249	< 0.001
CARB = 175.0(±6.2) + 1658.9(±101.7)W1	0.72	249	< 0.001
CARB = 68.65(±9.0) + 243.95(25.3)V_{1-3} + 41.61(±12.3)V_{4-6}	0.726	249	< 0.001
CARB = 175.0(±6.1) + 1667.3(±100.4)W1 - 271.4(±98.6)W2	0.730	249	< 0.001

* Numbers in parentheses are the standard errors of the regression coefficients.

† V_{1-3} is the particulate volume in the first three particle size distribution bands, and V_{4-6} is the volume in bands 4 through 6 of the particle size distributions.

Figure 3 lacks points in the top center. This indicates that size distributions similar to the first CV (e.g. the case that W2 $\cong$ 0.0 and W1 > 0.1) are lacking. Figure 2 shows that the first CV has large volumes of both microplankton and nanoplankton. The lack of similar curves in the data suggests that competition between the microplankton and nanoplankton does not allow them to grow in this proportion to each other. The "V" shape of the W1-W2 diagram suggests that mixing of the two extreme water types does not occur, but that both types grow from the same type of particle collections.

Except for a few samples, the positive W2 leg (Figure 3) represents water with sigma-t values greater than 25.5. The negative W2 leg has two extensions. The extension along the lower boundary is comprised of samples having lower density (σ_t < 25.5). The rest of the leg seems to be equally represented by both water types. The samples with CV weighting factors not near the lower boundary have psd curves similar to D of Figure 5. Even though the smaller particles predominate, there is still a large population of microplankton. Many of these samples have sigma-t values near 25.5. This may suggest either an intermediate environment or that changes in circulation or mixing caused the growth pattern to shift at the same time as the temperature and salinity.

In Figure 6 a downward flow at station two and an upward flow at station four is indicated by all of the parameters. Between these two stations is a large temperature gradient. This is very consistent with the two-cell circulation pattern suggested by Mooers, Collins and Smith (1976). These transects are also similar to those presented in (Stevenson, Garvine and Wyatt, 1974). In this context a different psd is associated with the surface water of each cell. In neither cell are

nutrients very low. In Figure 7, the features indicate a more simple surface flow pattern and correspondingly only one type of psd.

IV. OBSERVATIONS DURING A PERIOD OF VARIABLE WINDS

The data analyzed in this section were obtained during August, 1974. Several modes of sampling were used along the Oregon coast: 1) a transect at 45°00'N latitude was repeated three times; 2) a transect at each of three latitudes (45°05'N, 44°55'N, and 45°00'N) completed the definition of the distribution of variables; 3) a parachute drogue was followed for more than 24 hours to obtain a Lagrangean description; and 4) a box pattern was circuited several times in an effort to obtain a suspended mass balance determination. These latter stations also provided Eulerian time series at four stations. During the box pattern, we alternated between a fast and a slow mode every 24 hours. During the slow mode, we took optical and hydrographic profiles and collected water samples for analysis. During the fast mode, casts were made with a profiling current meter, circuiting the box in six hours. If there was time, optical profiles were taken but not water samples. The station locations and bathymetry are shown in Figure 9.

Particle size distributions were measured with a modified Coulter Counter interfaced to a Nuclear Data 2400 Multichannel Analyzer. Particle counts were accumulated in windows between particle volumes which were powers of two. The measurements encompassed the range from 32 to 131072 μm^3 particle volumes. Total particulate volume in the windows was computed from the average of the end volumes multiplied by the number of particles in the windows. Assuming a hyperbolic distribution (Bader, 1970), this computation gives a volume 3 to 8% that is too high depending on the logarithmic slope of the size distribution. Since the

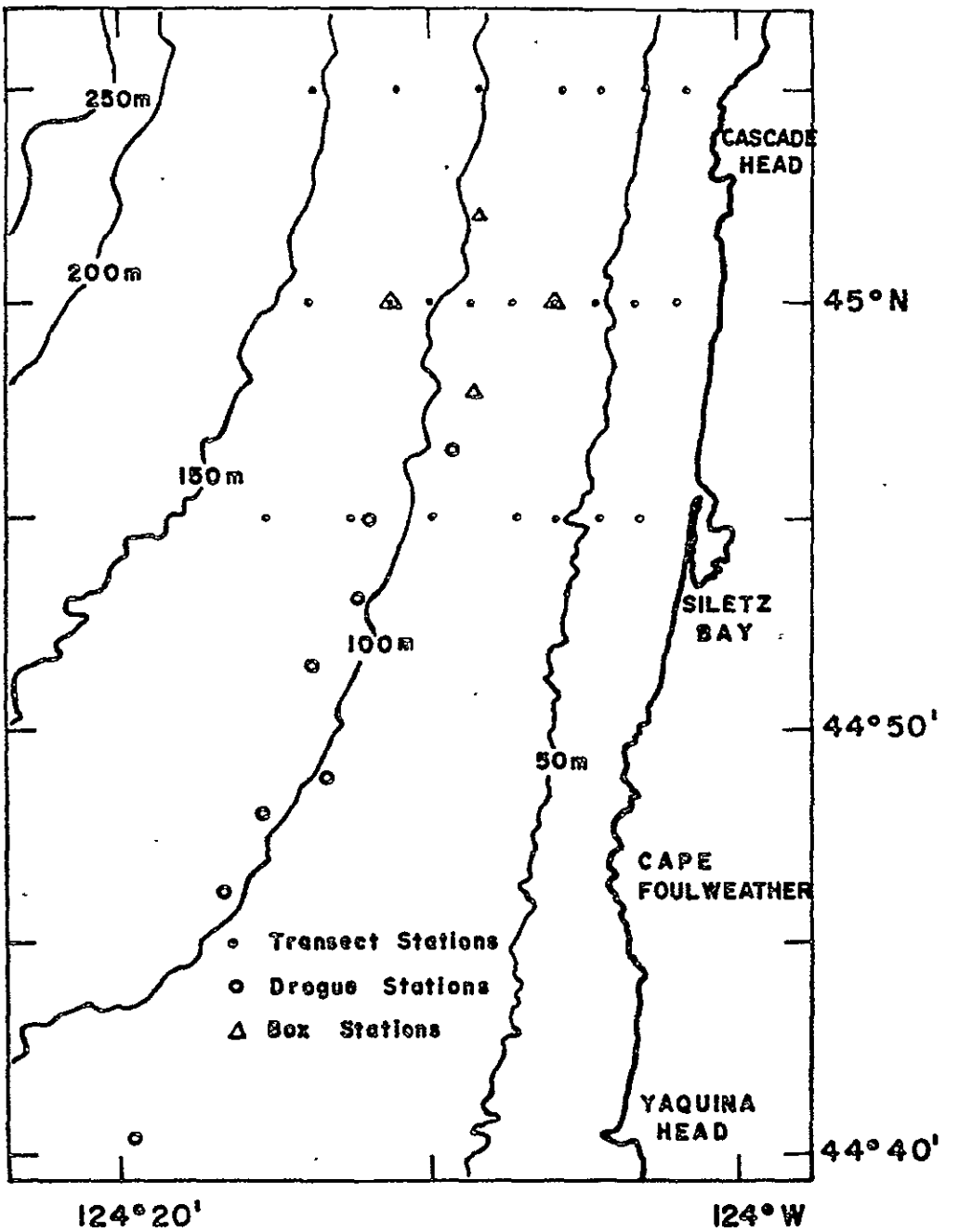

Figure 9. Station locations and bathymetry for cruise Y7408B of Oregon State University's R/V YAQUINA.

error in measurement may be as much and the error due to truncation at the small end is definitely greater, the computed volumes were not corrected. For many of our samples we have only the first six windows of data (of a possible twelve). Thus we will compute the log-log slope of the first six windows of the particle number concentration histogram and assume that it is equivalent to the slope of the cumulative size distribution as discussed in Section II.

Transmission of red light (660 nm) was measured *in situ* using a nephelometer developed by the Optical Oceanography group at Oregon State University. Red light was chosen because the absorption coefficient of "yellow substance" is negligible at the longer wavelengths (Jerlov, 1976). Thus the transmission is a measure of total particle attenuation and the known attenuation of pure seawater.

Transmission will frequently be used in this paper as a measure of particulate volume. Although we do have direct measurements of the particulate volume, transmission is sometimes preferred because it is measured continuously *in situ* instead of by discrete samples *in vitro*. We also believe that the precision of the transmission measurements are much better than the precision of the particle volume measurements. The regression: ln (volume) = 1.713 - 5.957 (Tr), where the suspended volume is in $10^6 \mu m^3 cm^{-3}$, and transmission (Tr) is expressed as a decimal, was derived from samples taken no deeper than 40 meters. The standard errors for the intercept and slope are 0.079 and 0.173 respectively, and the correlation coefficient is 0.915. It is more intuitive to show volume as a function of particulate attenuation C_p = -ln (Tr) -Cw where Cw is the attenuation coefficient of pure water.

Interpolation of a table in Jerlov (1976, pg. 52) gives a value for Cw of 0.324. This regression has an equally high correlation coefficient but predicts negative volumes within the range of transmissions observed. Both regressions are shown on Figure 10 along with the measured particulate volumes. The ln (volume) - Tr regression presented above shall be used in later calculations.

DATA

The first series of stations are three transects taken along the same line of latitude: 45°00' North. Figure 11 shows transmission, full logarithmic (log-log) slope of the particle size distributions and temperature for these transects. Minimum transmission is found near the surface, near shore. A subsurface tongue of low transmission extends offshore from the nearshore minimum. On the first and third transects there is a downward protuberance of the minimum at a distance of five to ten kilometers from shore. The particle size distributions show a definite front about 20 meters deep on all three transects with the lower slopes (larger particles more abundant) inshore. Temperature, in contrast, indicates very shallow fronts only loosely associated with the particle fronts. There is a strong thermocline between five and twenty meters depth. Beneath the thermocline there is a large area of homogeneous slopes. In the same area transmission varies greatly (45%-60%) and there is a temperature minimum.

Transmission, log-log slope, and temperature for transects at three different latitudes are shown in Figure 12. The surface layer shows in general, the same features as the transects of Figure 11, except the low slopes are confined closer to shore and the subsurface

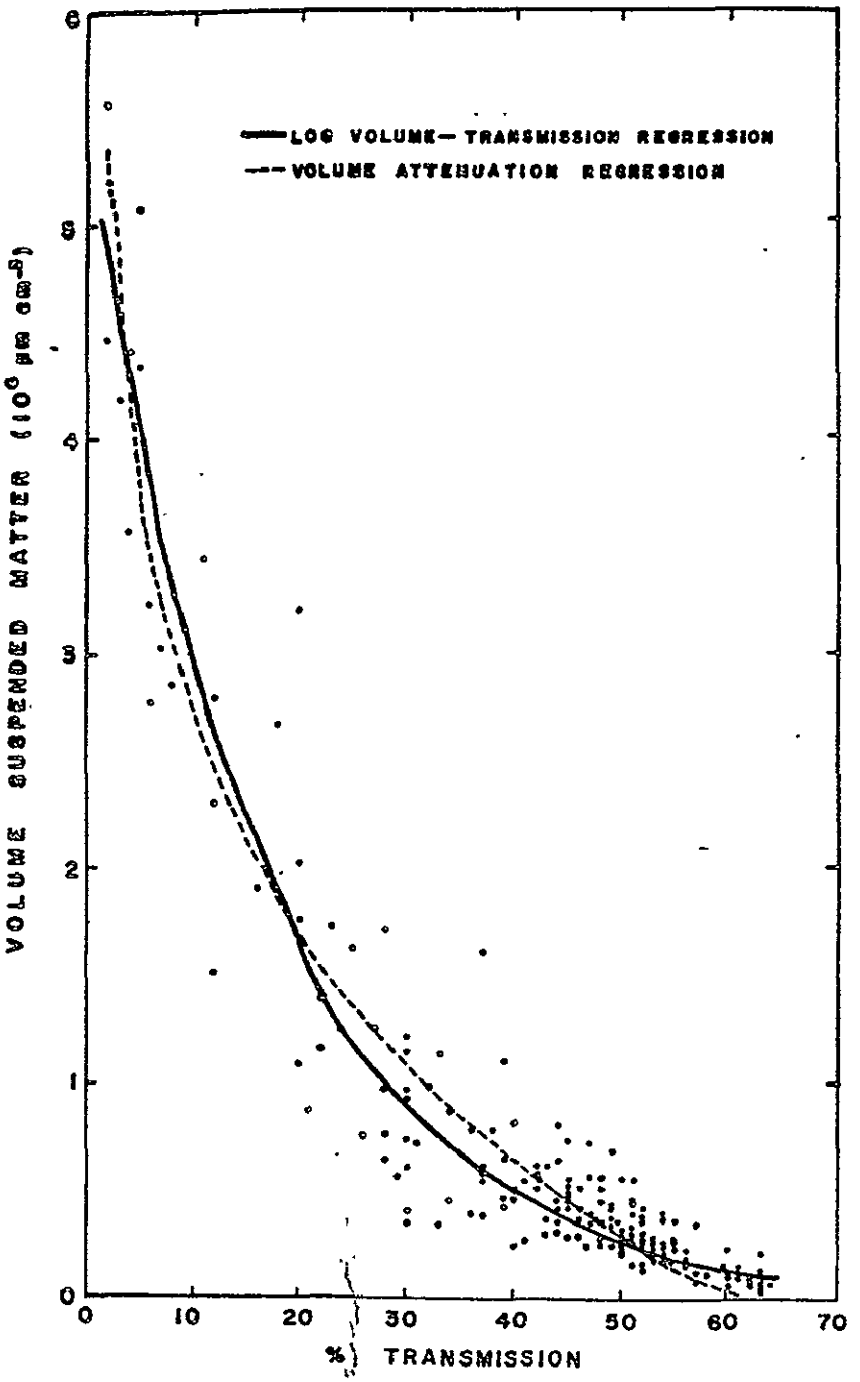

Figure 10. Volume of suspended matter versus light transmission (660 nm) for samples taken above 40 meters. Two regression curves, ln (volume) = 1.713 - 5.957 (Tr) and volume = -0.2420 + 1.536 (particulate attenuation), are shown.

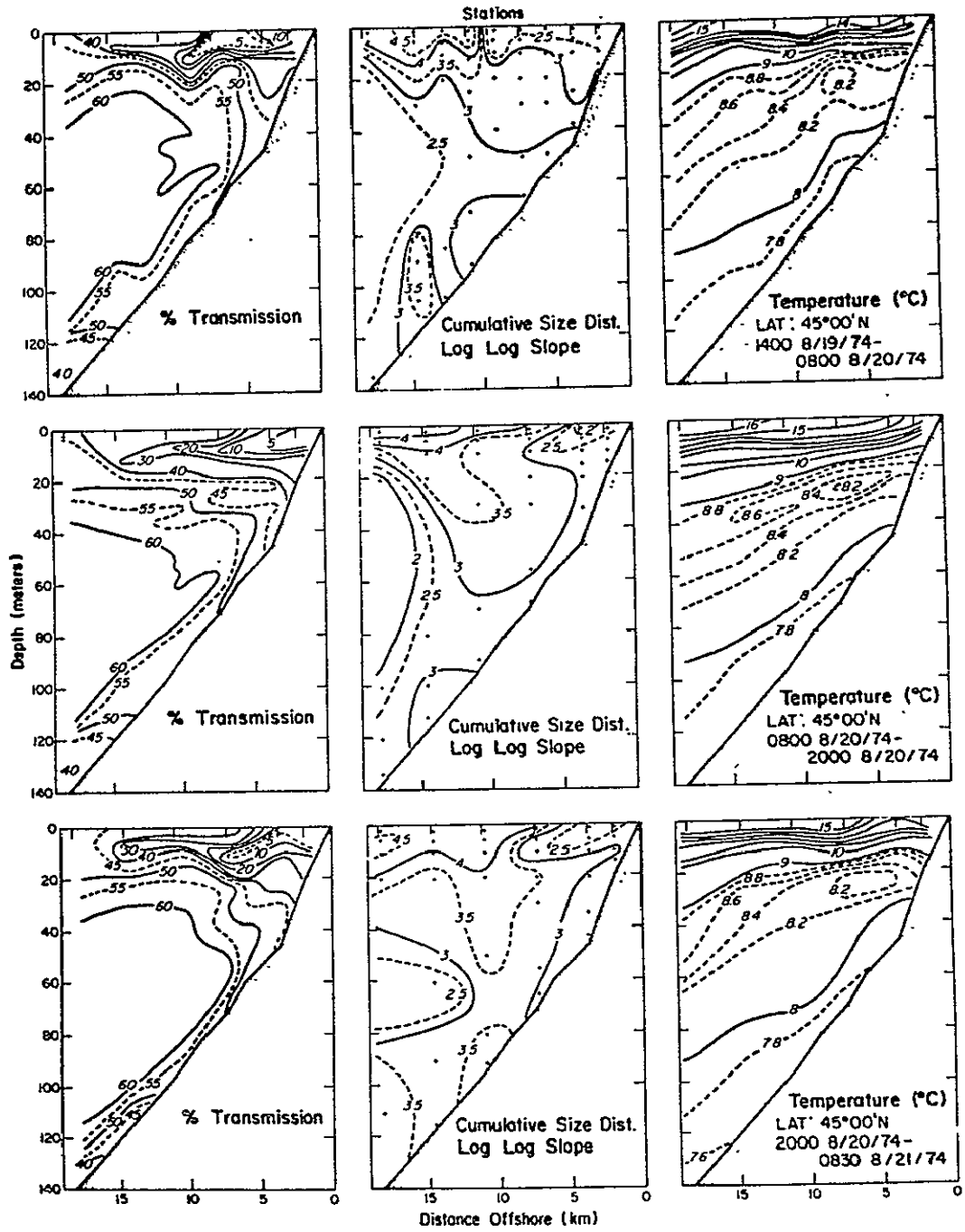

Figure 11. Transmission, log-log slopes of the particle size histograms and temperature for three consecutive transects at 45°00'N latitude off the Oregon coast.

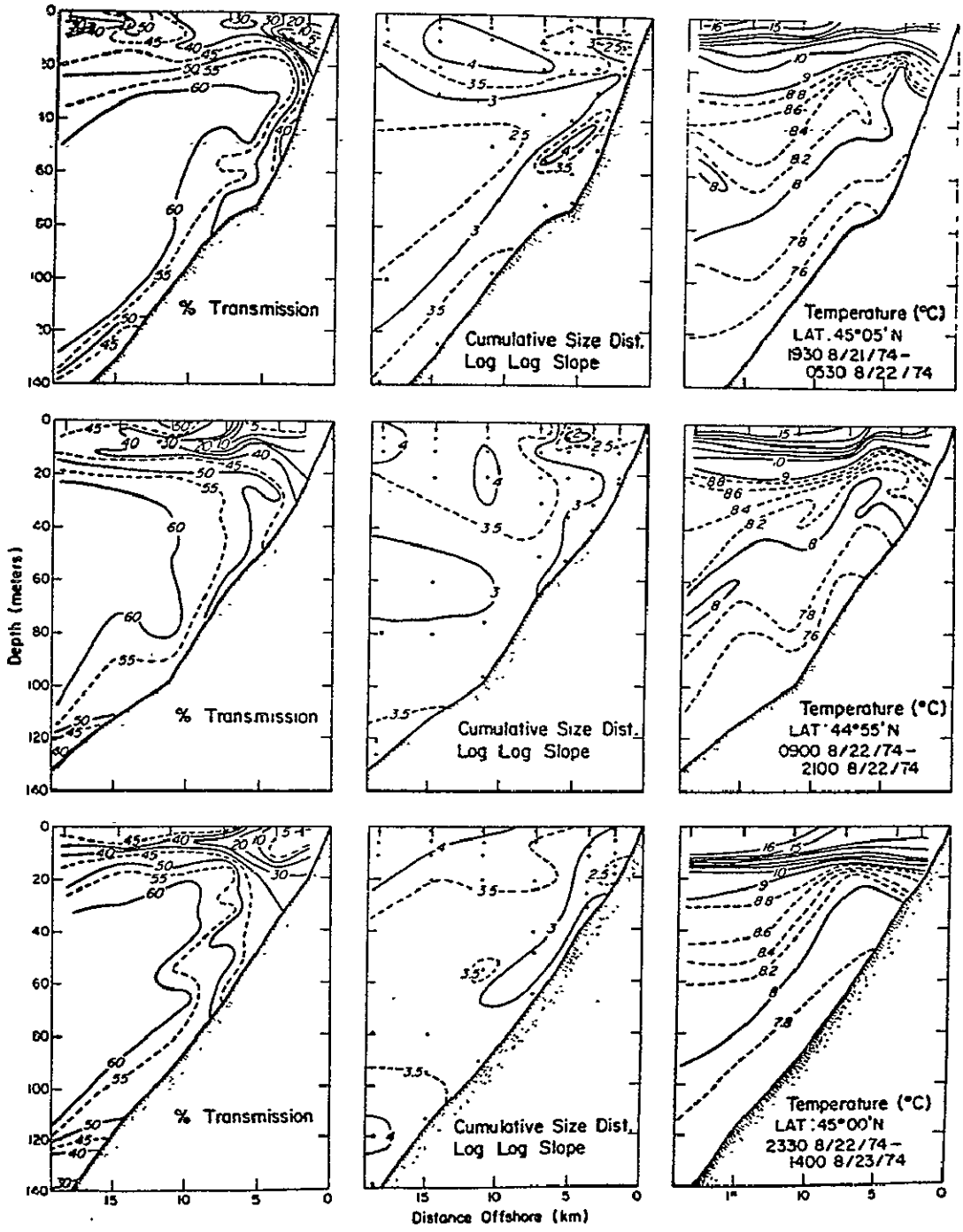

Figure 12. Transmission, log-log slopes of the particle size histograms and temperature for three transects at different latitudes off the Oregon coast.

minimum in transmission extends farther offshore. Below the thermocline the distribution of parameters has become more varied and more complex.

A better understanding of the differences denoted by changes in the log-log slope is given by examining the actual size distributions. Figure 13 shows the onshore-offshore variation at depths of 1 and 5 meters. The two types of size distribution are evident with the inshore (3.7 km), low slope type having one to two orders of magnitude higher concentrations of the largest particles than the type offshore of the front. At 7.4 km offshore, water with the high slope type (1m) rides on top water with the low slope type (5 m). Both types have a tendency to bulge upward at the small end, but this tendency decreases with a distance from shore and is much more noticeable at 5 meters than at 1 meter.

Changes in the particle size distributions with depth of three stations are shown in Figure 14. The slope of the size distributions change little with depth but the absolute concentration changes. The station nearest shore has lower slopes at all depths. One 60 meter sample is shown. It is an order of magnitude cleaner than the cleanest surface sample.

Nutrient and chlorophyll a data are presented in Figure 15. High values of both are restricted to a region very near shore. The region of high chlorophyll a is very similar to the region of low log-log slopes (Figure 12). Nutrient concentrations increase with depth but the contours slope much more than the isothermals do. The first transect has the lowest concentrations of nutrients near shore. It also has the most restricted region of low log-log slopes (Figure 12). Offshore both nutrients and chlorophyll a are at least an order of magnitude lower.

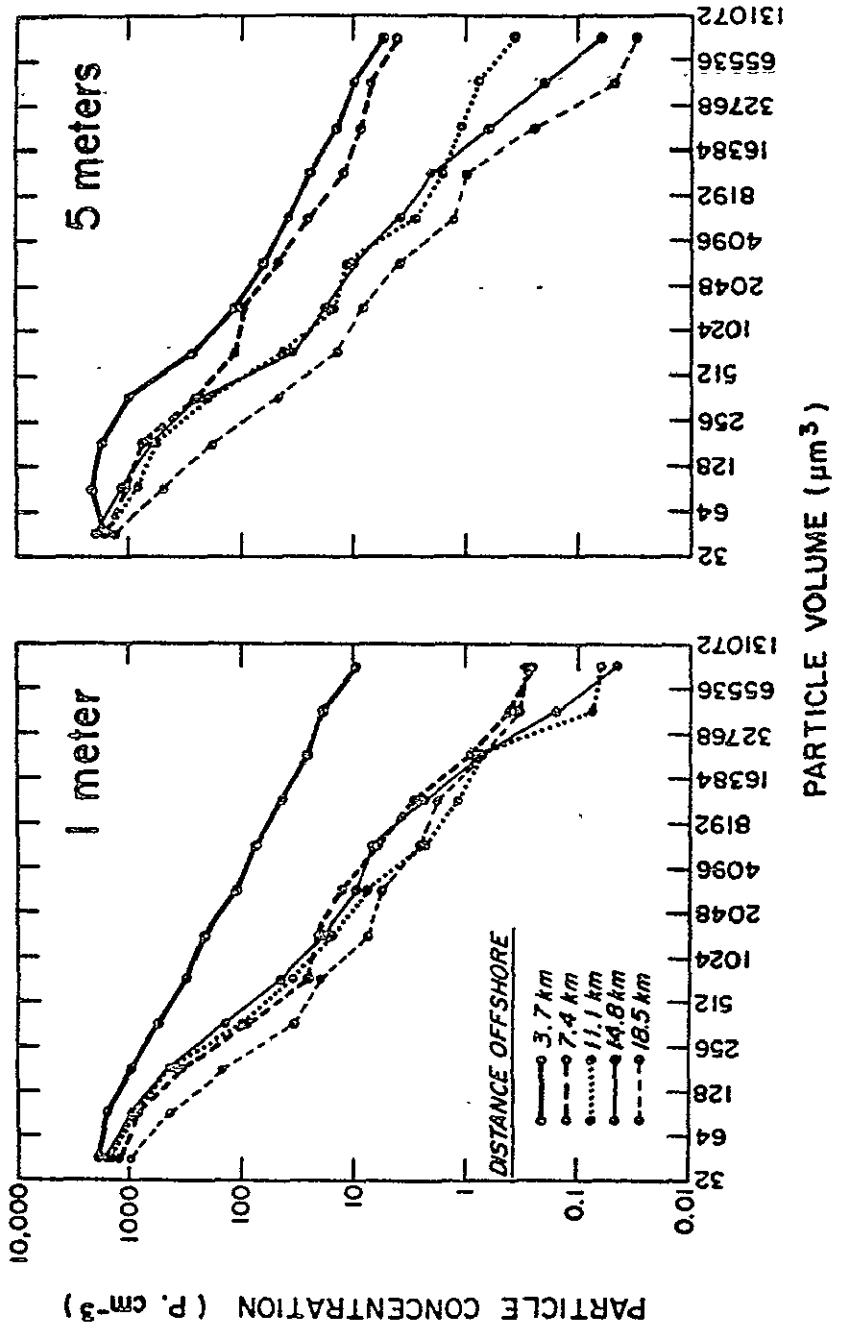

Figure 13. Particle size histograms for samples taken from 1 and 5 meter depths at varying distances from shore at 45°00'N latitude from 2000 PDT 8/20/74 to 0830 PDT 8/21/74.

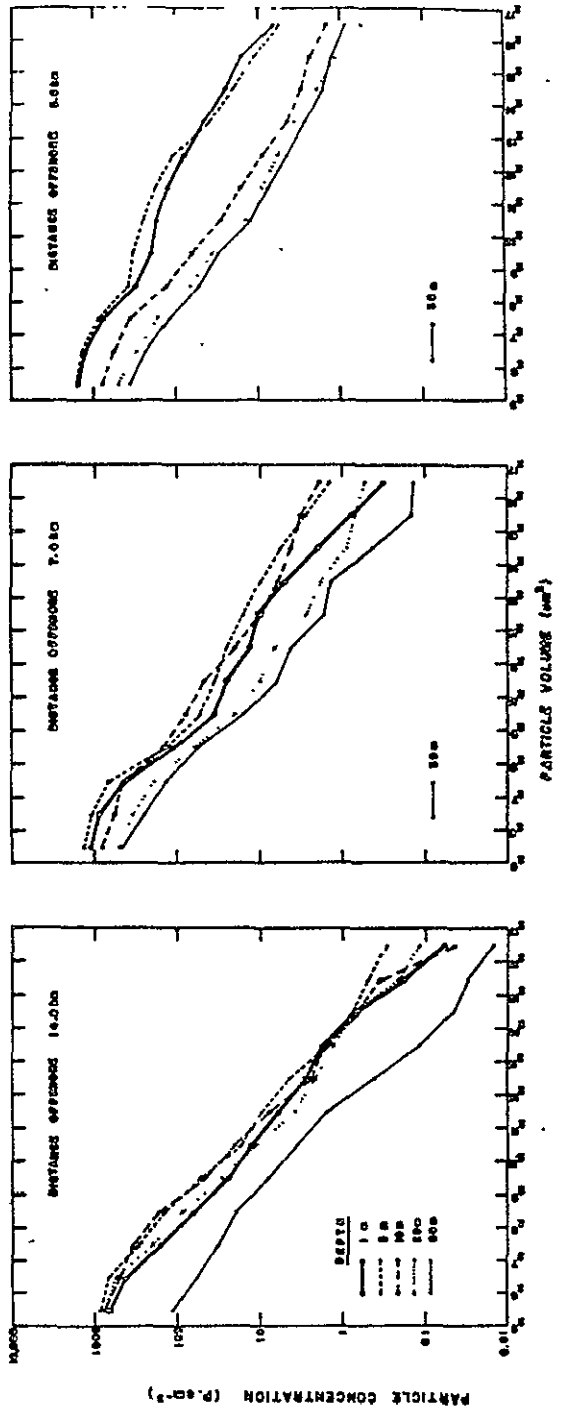

Figure 14. Particle size histograms for samples taken from 5.6, 7.4, and 14.8 km from shore at varying depths at 44°55'N from 0900 PDT 8/22/74 to 2100 PDT 8/22/74.

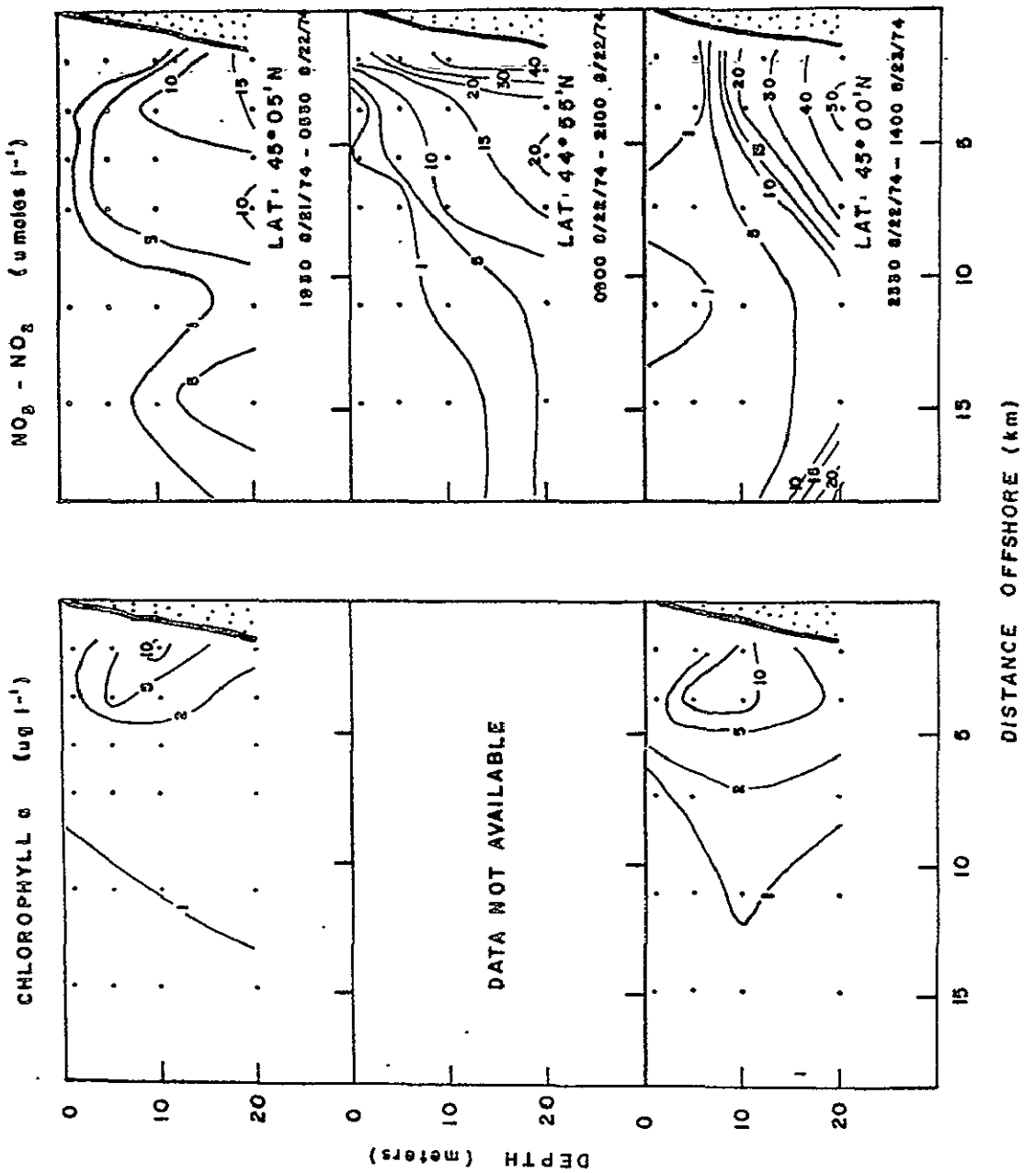

Figure 15. Chlorophyll a and nitrate-nitrite concentrations for three transects at different latitudes.

Figure 16 shows zooplankton biomass for the transects for which the data is available. Maximum values of biomass are also confined to the region very near shore. The offshore near surface water has almost two orders of magnitude less zooplankton biomass. This corresponds well with the two orders of magnitude difference in the large particles upon which it is assumed the zooplankton feed.

Lagrangian measurements were taken by the deployment of a parachute drogue. The parachute was tethered at a depth of five meters. Stations were taken about three hours apart while the ship followed the drogue closely. Figure 17 shows transmission, log-log slope and temperature for this series. Near the surface all three parameters vary little. There is no general trend towards more or less transmission. The bottom of the thermocline moves up and down and the transmission contours follow the same pattern. Transmission has a minimum at seven meters and the slopes of the size distributions are high similar to the situation offshore of the particle fronts in Figures 11 and 12. Note from Figure 9 that the drogue has approximately followed the bathymetry.

Eulerian time series of transmission and temperature for the north and south stations of the box pattern are shown in Figure 18. Log-log slopes are not shown since there were too few stations at which bottle samples were taken to draw meaninful contours. In general the samples taken show slopes less than 3 near the surface, greater than 3 near 20 meters depth and approximately 3 at the mid-depth transmission maximum. While these stations are in the same depth of water as the drogue stations, the lack of a near-surface minimum in turbidity indicates a profile similar to those inshore of the particle size

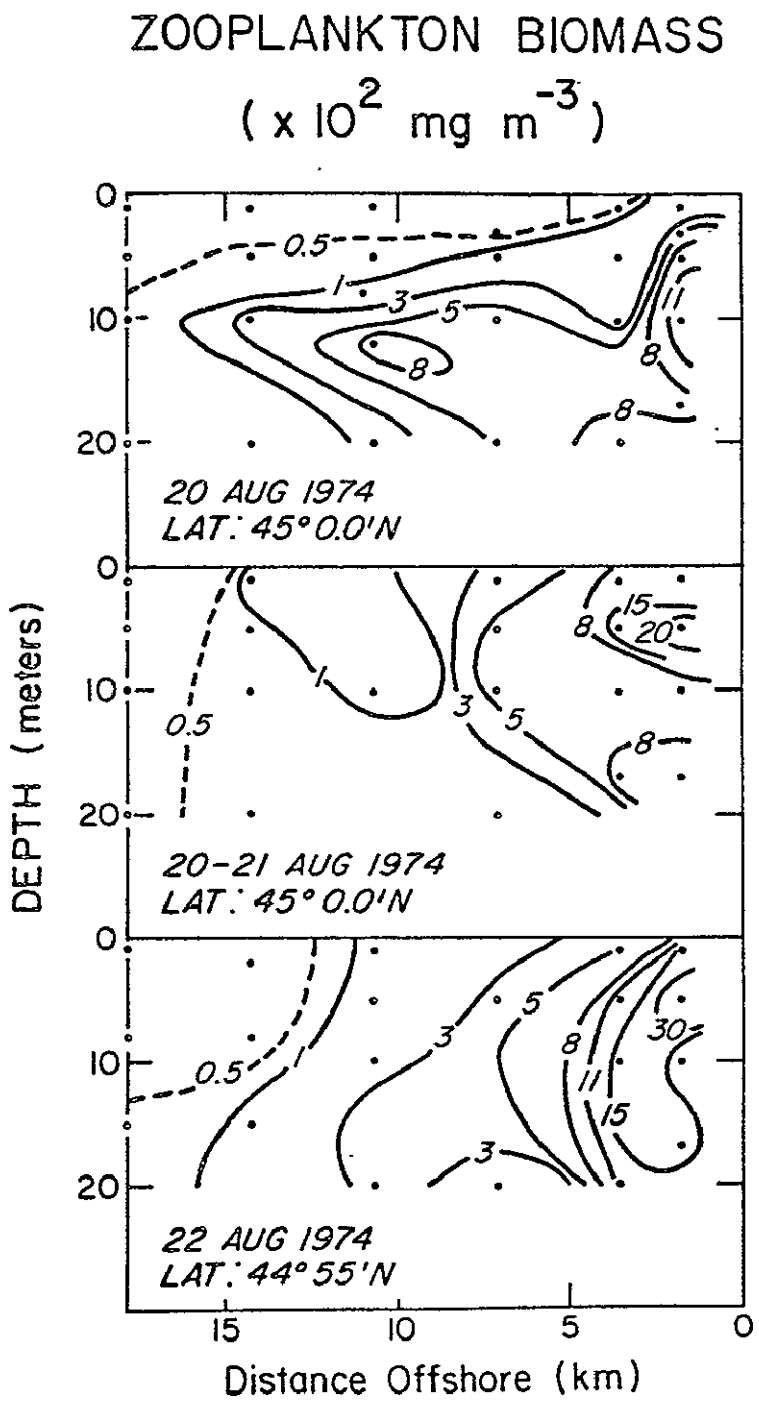

Figure 16. Zooplankton biomass for the three transects for which this data is available.

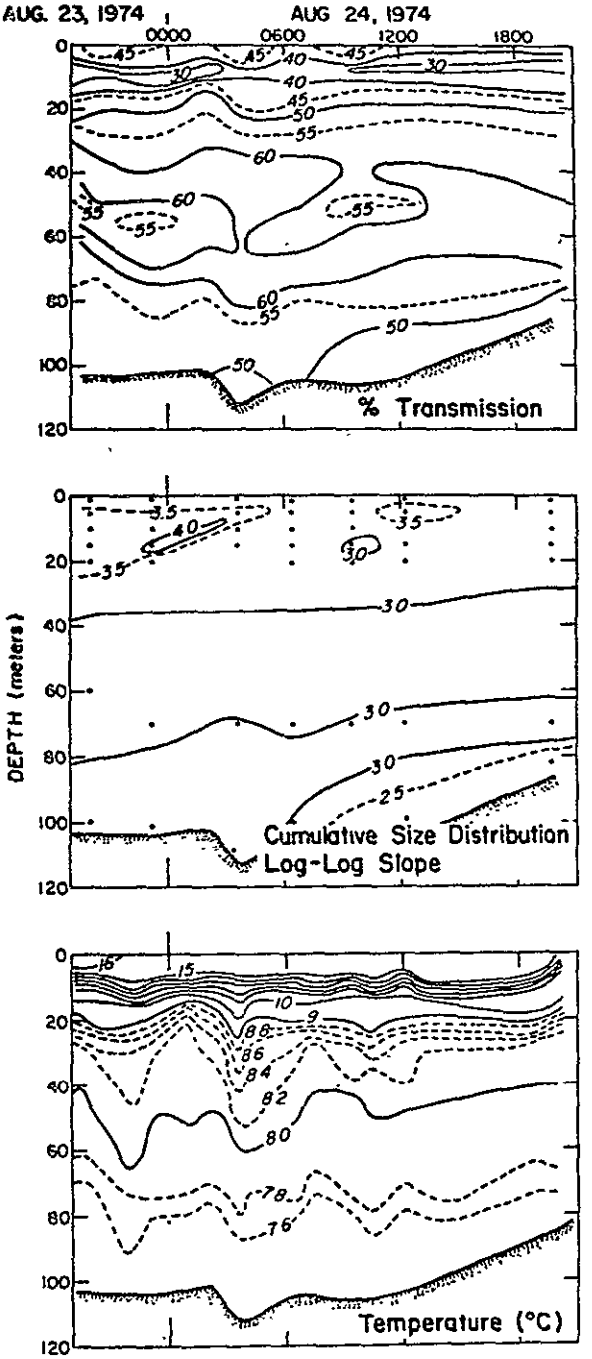

Figure 17. Light transmission, log-log slopes of the particle size histograms and temperature for stations taken while following a parachute drogue deployed at 5 meters depth.

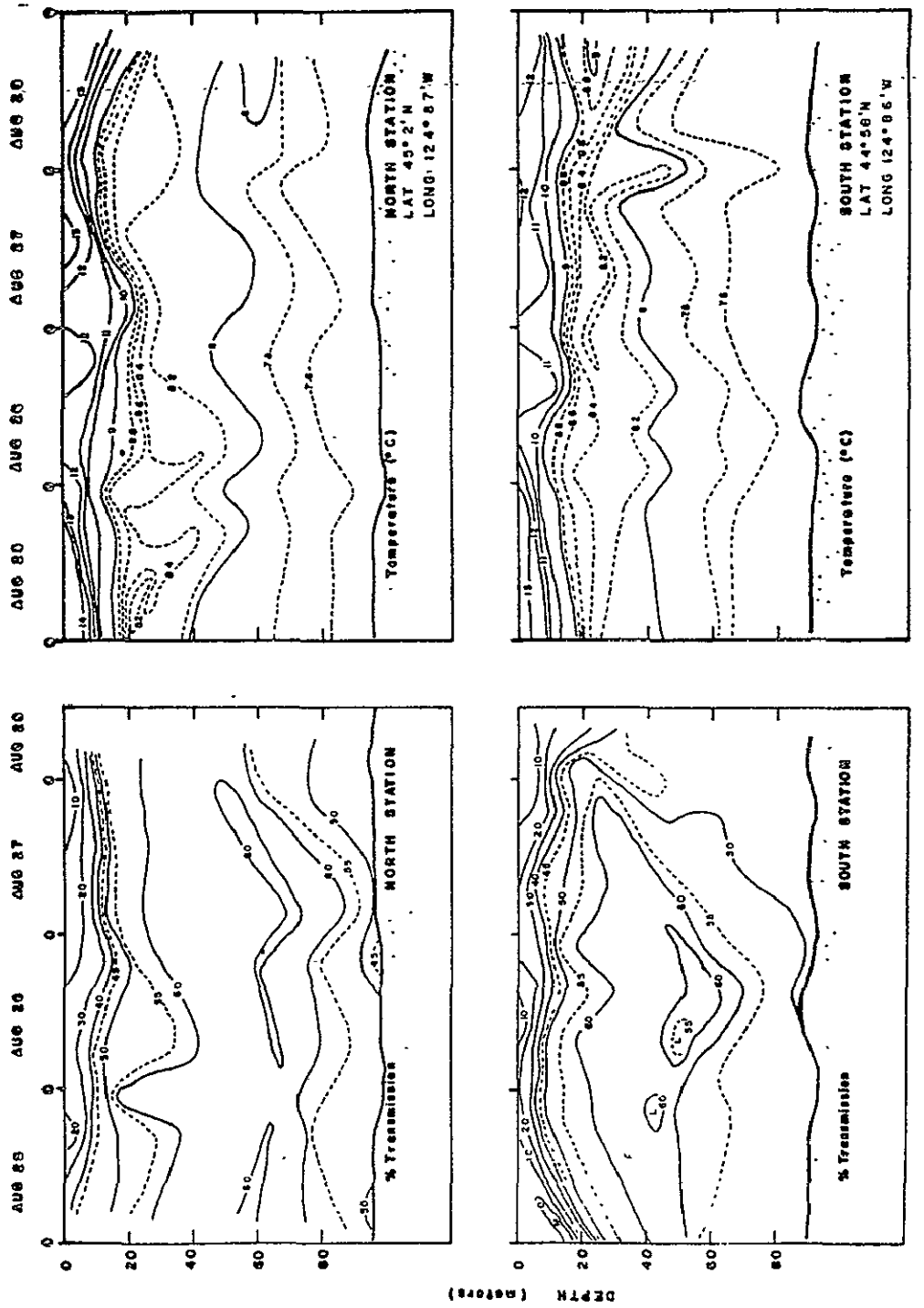

Figure 18. Light transmission and temperature for the north and south box stations.

distribution front. The low surface temperature also indicates the inshore water type. The mid-depth water is much clearer than is shown in the profiles inshore of the surface front. Both the north and south stations exhibit some patchiness, but there is no indication of a seven hour lag as would be predicted by the station locations and the north-south surface flow rate. Transmission decreases at both stations at the end of the time series, coinciding with a thickening of the bottom nepheloid layer. But a patch of turbid water found at the south station for two casts around noon August 26, does not show at all on the north station.

The temperature series show much similarity to each other, but the south station is a degree colder. While temperature shows patchiness similar to transmission, there is no obvious correlation (e.g., warm-turbid/cold-clear). The bottom boundary of the near-surface turbid layer is similar in shape to the thermocline. Occasionally there appears to be downwelling of warm water and an accompanying extension of low values of transmission into the mid-depths. The surface water at the end of both series is warmer than average, corresponding to the particle maximum and thicker bottom nepheloid layer. Some auxillary data for this cruise is presented in Appendix B.

DISCUSSION AND CONCLUSIONS

Inshore of the particle front, large numbers of large particles and broad humps in the distribution result in log-log slopes less than 3.0. Offshore of the front, the number of particles in the first three windows of the size distribution are only slightly lower than inshore, but larger particles drop in numbers rapidly giving high slopes. A

maximum in the particle size distribution is sometimes present at the second window. Just below the thermocline, both inshore and offshore, the number of particles decrease, the size distributions remains similar. The computed slopes are more moderate below the thermocline due to the more regular size distribution but still show a difference between the onshore and offshore types. The particle concentration at mid-depths offshore is an order of magnitude smaller than is found in the surface waters.

The two orders of magnitude difference in the number of large particles between samples from opposite sides of the front indicates that horizontal diffusion does not play an important role at the front. Although the smallest particles have similar concentrations, it is not likely that diffusion would be important for these and not for the larger particles. When nutrients are not depleted, the number of small particles may be greater offshore of the front than onshore (see Section III). The similarity between the particle and nutrient distributions suggest that nutrient concentration (combined with the light level) is the principal factor in determining the distribution of suspended mass. The positive correlation between zooplankton and phytoplankton indicates that grazing is not the controlling difference between the inshore and offshore water types. The front is thus an abutment of a nutrient poor and a nutrient-rich water mass, with the particle field in each determined independently.

The bottom of the surface turbid layer coincides with the bottom of the thermocline (Figures 11, 12, 17, 18). The isotherms do not remain at constant depth but are constantly moving up and down. From

this we see that there are vertical movements of water which are much greater than the settling rates of the particles and that the thickness of the surface turbid layer is highly dependent on these vertical displacements. As viewed from the air, this is likely to be the most important process occurring at the bottom of the turbid layer.

The large gradients of temperature and transmission below the surface mixed layer indicate upward vertical advection and low vertical eddy diffusivities (Zaneveld, 1972). There is little debate over the hypothesis of low diffusivity in the thermocline, but the role of settling needs further discussion. The solution of the vertical dispersion equation:

$$A \frac{\partial^2 P}{\partial z^2} - w \frac{\partial P}{\partial z} = 0 \quad \text{is} \quad p = C_1 e^{\frac{wz}{A}} + C_2$$

where P is the concentration of suspended particles (a function of size), A is the vertical eddy diffusivity, w is combined settling and advection, and C_1, C_2 are undetermined constants. If w is a function of the size of the particles, then one end of the size distribution will show greater relative changes with depth, thus changing the slopes of the size distribution. The region beneath the surface mixed layer is characterized by large changes in transmission but the log-log slopes are very homogeneous. We conclude that settling is relatively unimportant compared with advection of water masses. The gradient of turbidity beneath the thermocline appears to be neutral (not a function of size) dilution by the upwelling, deep, clean offshore water.

Offshore of the front, there is a sharp maximum in turbidity at the thermocline. It may not be clear from the figures, but the strip chart recorder shows a peak so sharp that the depth derivative of

transmission is not continuous at one point. This feature is not found inshore of the front. Expressing the particle dispersion equation as $\frac{\partial}{\partial z}\left(A \frac{\partial P}{\partial z} - wP\right) + T(z) = 0$ (Ichiye et al., 1972) where $T(z)$ is the sum of the horizontal transport and diffusion terms, integration gives:

$$A \frac{\partial P}{\partial z} - wP + \int_0^z T(z) = C \ .$$

C being a constant equal to $\left(A \frac{\partial P}{\partial z} - wP\right)$ evaluated at the surface. Solving for $\frac{\partial P}{\partial z}$ gives:

$$\frac{\partial P}{\partial z} = \frac{wP}{A} - \frac{\int_0^z T(z)}{A} + \frac{C}{A} \ .$$

If the dominant terms are the vertical advection and diffusion terms, then a sudden change of $\frac{\partial P}{\partial z}$ from a large positive number to a large negative number could only be accomplished by w changing sign at the same point that A becomes very small. Assuming that w is continuous (e.g., w must approach zero to change sign), we also know that A must approach zero faster than w and must reach zero at the same place. These are very stringent conditions, but the other terms are even less likely to meet them. One would expect the horizontal currents and gradients to be predominantly of one sign over the surface mixed layer and thus the $\int_0^z T(z)$ term would not go to zero at the particle maximum. Returning to the vertical terms, the coincidence of the minimums of diffusivity and settling rates may be reduced if we assume an active role (or natural selection) by the particulate matter. Smayda (1974) performed experiments on diatoms which showed an increase in sinking rates without loss of viability when the culture was subjected to low concentrations of alcohol. He also found that sinking rates increased with the age of the culture. Given that there is low nutrient

concentration in the surface layer, and low light conditions below the thermocline where nutrient concentrations are greater, phytoplankton may accumulate at the top of the thermocline (by adjustments of their density or by positive flotation mechanisms) to avail themselves of what nutrients may diffuse through. Thus, their settling velocities have been physiologically adjusted to zero just where the thermocline produces a minimum in turbulent diffusion. This does not mean the phytoplankton are neutrally buoyant since there may also be a slight upwelling through the thermocline. Onshore of the front there are ample nutrients so this process is not necessary.

The box stations were taken after about two days of consistent upwelling-favorable winds. As a result, the front has moved out of the region of study or dissipated entirely. The currents had a strong offshore component in the surface layer (Johnson, 1977). The resultant distribution of particulate matter was then consistent with the inshore water type out to the offshore box station (14.8) km). The temperature and transmission profiles reveal occasional lobes of surface water dropping into the mid-depth clean water. This may be taken as evidence of instabilities and is similar to the lobe in the first transect of Y7307D (Section III). Both transects of Section III were after about five days of consistent upwelling favorable winds. Earlier transects in the present study were during a period of alternating favorable and unfavorable winds. Thus between the two cruises, we may see a succession of phases of an upwelling cycle.

V. THE VERTICAL DISTRIBUTION OF PHYTOPLANKTON

The Equations

The dispersion equation for suspended particulates is:

$$\frac{\partial P}{\partial t} = \frac{\partial}{\partial x}\left(A_H \frac{\partial P}{\partial x}\right) + \frac{\partial}{\partial y}\left(A_H \frac{\partial P}{\partial y}\right) + \frac{\partial}{\partial z}\left(A_z \frac{\partial P}{\partial z}\right)$$

$$- \frac{\partial}{\partial x}(uP) - \frac{\partial}{\partial y}(vP) - \frac{\partial}{\partial z}((w - s)P) + R$$

where P is the amount of phytoplankton, A_H, A_z are the horizontal and vertical eddy diffusivities, u and v are horizontal current velocities, w is the vertical current velocity and s is the particle settling rate. R represents all the nonconservative processes (mainly biological and chemical). Since the vertical structure is fairly consistent on either side of the front and the evidence (Sections III and IV) indicates little interaction between the two water masses, the predominant processes creating the two different structures may be understood without considering the horizontal terms. Furthermore, the advection term can be expanded as follows:

$$\frac{\partial}{\partial z}((w - s)P) = (w - s)\frac{\partial P}{\partial z} + P\frac{\partial w}{\partial z}$$

assuming the settling rate to be constant. The vertical divergence term $\left(P \frac{\partial w}{\partial z}\right)$ will be balanced by the horizontal divergence terms in the full dispersion equation and thus should not be included in the vertical equations.

The high correlation between chlorophyll <u>a</u> and particulate volume indicates that most of the particles are phytoplankton; thus the nonconservative term R is important. The rate of increase of the

phytoplankton population is proportional to the amount of phytoplankton present.

$$\frac{\partial P}{\partial t} = VP$$

V is the constant of proportionality and is called the growth rate. V is related to the nutrient concentration in a manner described by the equation:

$$V = V_m \frac{N}{K_n + N}$$

where Vm is the maximum growth rate, N is the concentration of the limiting nutrient and K_n is the nutrient concentration that causes half the maximum growth rate (Eppley, Rogers and McCarthy, 1969). Growth is also influenced by the light intensity, so V will further be modified by a function L(z) to be presented later. Higher level trophic terms will be ignored. This can be justified, since we found that zooplankton correlated well with phytoplankton, thus the grazing will also be proportional to the phytoplankton population and will only adjust the maximum specific growth rate. Including two types of phytoplankton P_1, P_2 and their respective maximum specific growth rates V_{m1}, V_{m2}, half saturation constants K_{n1}, K_{n2}, and settling rates S_1, S_2, the total system of equations now becomes:

$$\frac{\partial P_1}{\partial t} = \frac{\partial}{\partial z}\left(A_z \frac{\partial P_1}{\partial z}\right) - (w - s_1)\frac{\partial P_1}{\partial z} + \frac{V_{m1} N P_1 L}{K_{n1} + N}$$

$$\frac{\partial P_2}{\partial t} = \frac{\partial}{\partial z}\left(A_z \frac{\partial P_2}{\partial z}\right) - (w - s_2)\frac{\partial P_2}{\partial z} + \frac{V_{m2} N P_1 L}{K_{n1} + N}$$

$$\frac{\partial N}{\partial t} = \frac{\partial}{\partial z}\left(A_z \frac{\partial N}{\partial z}\right) - w\frac{\partial N}{\partial z} - \frac{V_{m1} N P_1 L}{K_{n1} + N} - \frac{V_{m2} N P_2 L}{K_{n2} + N}$$

In order to make the models valid for more than one situation, the equations must be nondimensionalized. This is accomplished by making the following substitutions.

$t = t^*/V_{m2}$

$z = z^*(A_{zm}/V_{m2})^{1/2}$ where A_{zm} is the maximum eddy diffusivity

$A_z = A_z^* A_{zm}$

$N = N^* N_0$ where N_0 is the nutrient concentration at the base of the thermocline.

$w = w^*(A_{zm}V_{m2})^{1/2}$

$P_1 = P_1^* P_0$ where P_0 is an estimate of the maximum particulate nitrogen concentration in coastal waters.

$P_2 = P_2^* P_0$

$s = s^* (A_{zm} V_{m2})^{1/2}$

$V_{m1} = V_{m1}^* V_{m2}$

$V_{m2} = 1^* V_{m2}$

$K_m = K_{n1}^* N_0$

$K_{n2} = K_{n2}^* N_0$

Starred variables are nondimensional quantities. In this report time and space scales will be presented in dimensional form to correspond to the region of study and the choice of parameter values. It is a simple exercise, given the above equations, to make different estimates of the parameters and thus redefine the time and space scales. However, if one increases the space scale, the light functions and diffusivity function are spread out to greater depths. This is equivalent to assuming clearer water and a deeper thermocline. These changes are all very compatible, though, since a larger space scale would imply a

region further offshore where clearer water and a deeper thermocline are to be expected.

Dropping the stars and simplification gives the following non-dimensional equations.

$$\frac{\partial P_1}{\partial t} = \frac{\partial}{\partial z}\left(A_z \frac{\partial P_1}{\partial z}\right) - (w - s_1)\frac{\partial P_1}{\partial z} + \frac{V_{m1} N P_1 L}{V_{m2}(K_{n1}+N)}$$

$$\frac{\partial P_2}{\partial t} = \frac{\partial}{\partial z}\left(A_z \frac{\partial P_2}{\partial z}\right) - (w - s_2)\frac{\partial P_2}{\partial z} + \frac{N P_2 L}{K_{n2}+N}$$

$$\frac{\partial N}{\partial t} = \frac{\partial}{\partial z}\left(A_z \frac{\partial N}{\partial z}\right) - w\frac{\partial N}{\partial z} - \frac{V_{m1} P_0 N P_1 L}{V_{m2} N_0 (K_{n1}+N)} - \frac{P_0 N P_2 L}{N_0 (K_{n2}+N)}$$

The Parameters

A commonly used value of vertical eddy diffusivity of suspended matter is 1 $cm^2\ sec^{-1}$ (Ichiye, Bassin, and Harris, 1972; O'Brien and Wroblewski, 1973a). This is the value that will be assigned to A_{zm}. Values for the maximum specific uptake of nitrate (V_m) are usually near $10^{-5}\ sec^{-1}$ (O'Brien and Wroblewski, 1973b; MacIsaac and Dugdale, 1969). In less favorable regions, Mac Isaac and Dugdale (1969) found V_m values more than an order of magnitude less. If we accept the stated values for A_{zm} and V_{m2}, then the depth increment for the model becomes one meter and the time increment fifteen minutes.

Smayda (1971) found sinking rates of about 2×10^{-4} cm sec^{-1} for healthy phytoplankton of less than 10 μm diameter and about 5×10^{-4} cm sec^{-1} for healthy cells of 20 μm diameter. These values shall be used for s_1 and s_2 respectively. We have not taken into account the fact that phytoplankton could increase their settling velocities without loss of viability when placed in an unfavorable environment (Smayda,

1974). This could, however, play a role in the creation of a maximum at the thermocline when the surface waters are depleted of nutrients.

The light function L has been digitized directly from Yentch, (1963, curve III, Fig. 1) which was computed by combining Jerlov's (1951) data on coastal transparency and the photosynthesis-light relationships from Ryther (1956). Two effects that have been left out to keep the model simple are self shading and species specific light reactions. Self shading should decrease the differences in concentration from one model to the next but may enhance the differences in vertical structure.

The parameter P_0/N_0 enters into the nondimensional equation to keep both nutrients and phytoplankton (nondimensional) of order 1. The concentration of nitrate at 20 meters is 20 - 30 μg-at NO_3 l^{-1} which is equivalent to 280-420 μg N l^{-1}. Measurements of particulate nitrogen during a cruise off Oregon in late July 1973 indicate a maximum value of about 100 μg N l^{-1}. Therefore, P_0/N_0 shall be assigned the value 0.3.

MacIsaac and Dugdale (1969) found twice to ten times higher V_m values in eutrophic regions than in oligotrophic regions. The region under study in this report has tremendous contrasts of nutrient concentrations but is also characterized by rapid changes in the order of several days. So the smaller value will be used to obtain 0.5 for V_{m1}/V_{m2}. This reflects a shorter past history at any given nutrient concentration.

Epply et al. (1969) report values of K_n for nitrate of 1-10 μg-at l^{-1} for large phytoplankton and 0.1-1.4 for small phytoplankton. Since the present study is in a very nutrient rich region, the larger

values may be more appropriate. This results in nondimensional values of 0.05 and 0.4 for K_{n1} and K_{n2} respectively.

Using mixing length theory, Neumann and Pierson (1966) find the eddy diffusivity $A = \overline{\rho \xi_z \ell}$ where ξ_z is the vertical component of turbulent motion and ℓ is the mixing length. They also give the work done against buoyant forces by

$$W_B = g\rho\xi_z\ell \frac{1}{\rho}\frac{\partial\rho}{\partial z}$$

and

$$W_B = g\rho\xi_z\ell \frac{1}{\rho}\frac{\partial\rho}{\partial z} = g\frac{A}{\rho}\frac{\partial\rho}{\partial z}$$

where g is the acceleration of gravity and ρ is the fluid density. Assuming the available energy to be constant we find that A is inversely proportional to the vertical density gradient. Two typical density profiles from the August 1974 cruise are shown in Figure 19 along with the computed relative eddy diffusivities. One was taken offshore of the particle front and one was inshore. The gradients are almost identical in the two profiles although the absolute values are much different. The profile of diffusivity (which will be included in the models) consists of a broad region of low diffusivity between the high values near the surface and below the thermocline. Nutrients will be assumed to have the same eddy diffusivity coefficients as particles. There is little literature on diffusivities of nutrients, but there is some information of diffusivity of salt which is also a dissolved substance. Bowden (1975) gives examples of computations resulting in eddy diffusivities for salt of 0.4-4.0 $cm^2\ sec^{-1}$. This is compatible with the above assumption. Figure 19 also shows the relationship of the vertical particle distribution to the thermocline for both cases.

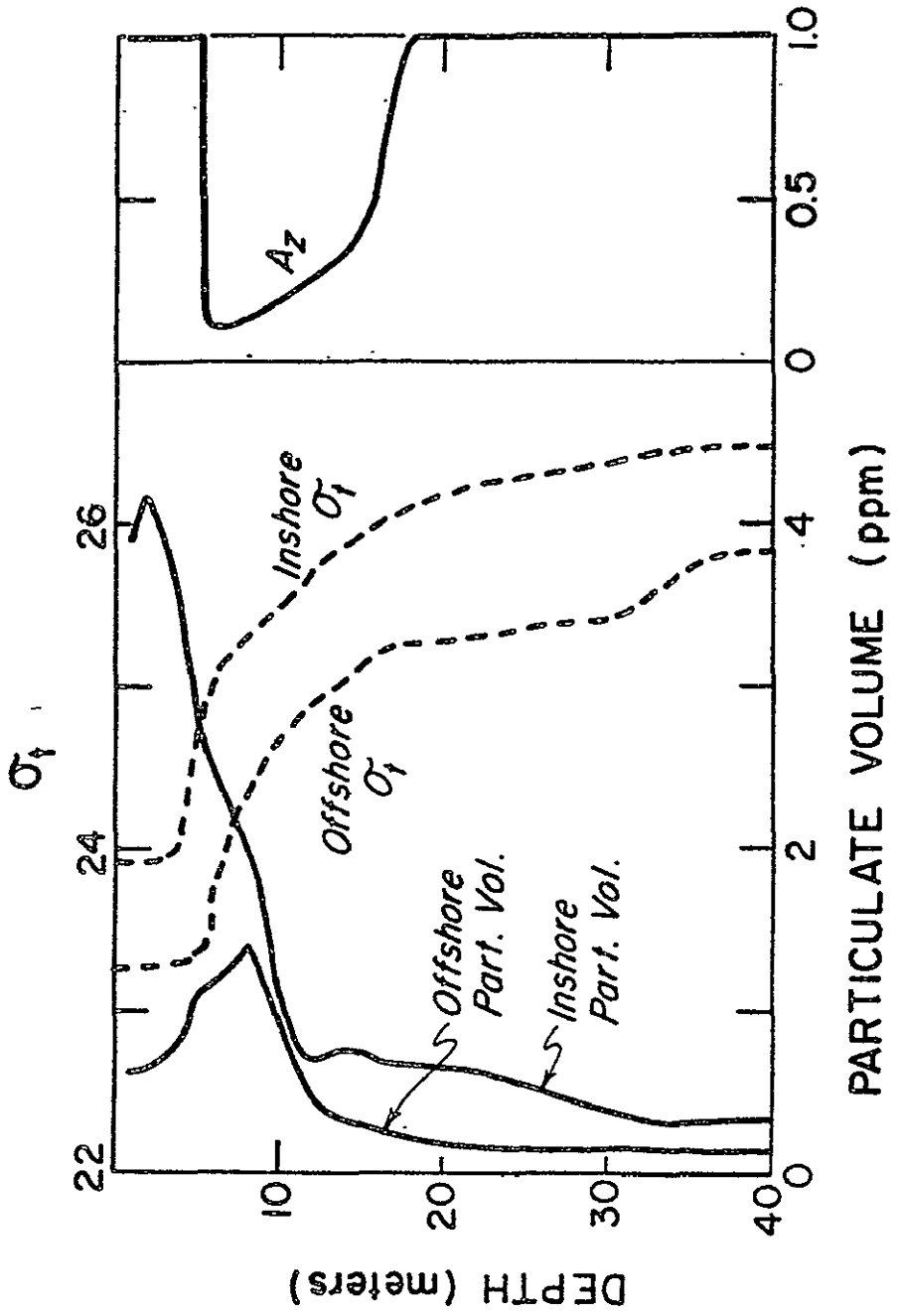

Figure 19. Particulate volume (computed from light transmission values) and density for typical stations inshore and offshore of the particle front. To the side is the derived relative eddy diffusivity.

The difference equation that will be used in the model of phytoplankton is:

$$P_{t+1,z} = P_{t,z} - w\frac{T}{H}(P_{t,z+1} - P_{t,z}) - s\frac{T}{H}(P_{t,z} - P_{t,z-1}) + A_z\frac{T}{H^2}(P_{t,z+1} - P_{t,z}) - A_{z+1}\frac{T}{H^2}(P_{t,z} - T_{t,z-1}) + \frac{V_m NL}{K_n+N}\ T\ P_{t,z}$$

with a time increment T of 900 sec. and a depth increment H of 100 cm.

The simple method of evaluating stability given by Acton (1970) will be used to evaluate the difference equation above. Assuming all values $P_{t,z}$ at time t have errors of size $\varepsilon_{t,z}$, the error in $P_{t+1,z}$ can be computed as follows:

$$\varepsilon_{t+1,z} = \varepsilon_{t,z}\left(1 + w\frac{T}{H} - s\frac{T}{H} - A_z\frac{T}{H^2} - A_{z+1}\frac{T}{H^2} + \frac{V_m NL_T}{K_n+N}\right) + \varepsilon_{t,z-1}\left(s\frac{T}{H} + A_{z+1}\frac{T}{H^2}\right) + \varepsilon_{t,z+1}\left(A_z\frac{T}{H^2} - w\frac{T}{H}\right)$$

Since the coefficients of $\varepsilon_{t,z}$, $\varepsilon_{t,z+1}$ and $\varepsilon_{t,z-1}$ are always positive, the worst case occurs when $\varepsilon_{t,z}$, $\varepsilon_{t,z-1}$ and $\varepsilon_{t,z+1}$ all have the same sign. Assuming the ε's are equal and substituting the maximum value for $\frac{V_m NL_T}{K_n+N}$, the worst case simplifies to:

$$\varepsilon_{t+1} = \left(1 + \frac{V_m NL_T}{K_n+N}\right)\varepsilon_t = 1.0054\ \varepsilon_t$$

This is greater than the critical value (1.0) but the 800 iterations amplify the error by a factor of only $1.0054^{800} \cong 74$. The best case at the depth of maximum production occurs when $\varepsilon_{t,z-1}$ and $\varepsilon_{t,z+1}$ equal $-\varepsilon_{t,z}$.

$$\varepsilon_{t+1,z} = (1 + 2w\frac{T}{H} - 2s\frac{T}{H} - 2A_z\frac{T}{H^2} - 2A_{z+1}\frac{T}{H^2} + \frac{V_m N L_T}{K_n+N})\varepsilon_{t,z}$$

Choosing the most negative values for all the terms gives

$$\varepsilon_{t+1,z} = (1. - 0.027 - 0.009 - 0.18 - 0.k8 + 0.0054)\varepsilon_{t,z} = 0.6094\ \varepsilon_{t,z}$$

In the average case errors would be damped, thus there is reason to believe the model will be stable.

A practical test of stability became apparent in developing the model. Nonstable systems produced negative values of P at the base of the pycnocline where the second derivative of P was very large and the magnitude of P was small. In the final version, P fell smoothly to the small values at the base of the pycnocline.

The Models

The models will cover the top 40 meters of the water column. Particles and nutrients will be constrained to have a zero gradient at the bottom boundary. The top boundary condition states that there is no flux of particles or nutrients across the top surface. Values of P_1, P_2, w and N are assigned to the middle of one meter increments. Diffusivities are given for the edges of the increments. The time increment is 15 minutes and the maximum duration 200 hours. The Fortran program for the models is listed in Appendix C.

The first model will attempt to describe the vertical distribution of particles found offshore of the color front during the August 1974 cruise (Section IV). That situation was characterized by low nutrient concentrations in the surface water. From the low nutrients and high temperatures we might assume that there was only weak upwelling. Thus

the velocity field will be defined as follows: 10^{-3} cm sec^{-1} upwelling from 20 m to 40 m depth and linearly increasing from zero at the surface to 10^{-3} cm sec^{-1} at 20 meters.

The starting conditions and the development of the vertical structure of nutrients and the two types of phytoplankton are shown in Figure 20. Both kinds of particles (P_1 shall be considered to represent small particles and P_2 large particles although they are defined only by settling rate and nutrient uptake dynamics) develop a maximum in the region of low eddy diffusivity. The depth of this maximum does not change significantly during its development. The maximum of the product of the light and nutrient factors for each kind of particle occurs at the same depth as the maxima of P_1 and P_2. For P_2 this is almost the point that settling and advection balance. Settling and advection balance for P_1 four meters above the maximum of P_1. Both maxima are in the upper half of the pycnocline similar to the placement of the offshore maximum, Figure 19. Very near the surface there is a slight decrease with time in the large particles but an increase in the numbers of small particles. The nutrient concentration has almost achieved steady state.

The next effort will model conditions inshore of the particle front. The distribution of parameters suggests a more vigorous upwelling especially very near the shore. Nutrient concentrations are high. The assigned values of the upwelling velocities are exactly ten times those used in the previous profile. Figure 21 shows the results of this model. The particle gradient at the surface is small, but the turbid layer is very shallow with a strong gradient beneath it. The maximum has risen until it is almost at the surface. The

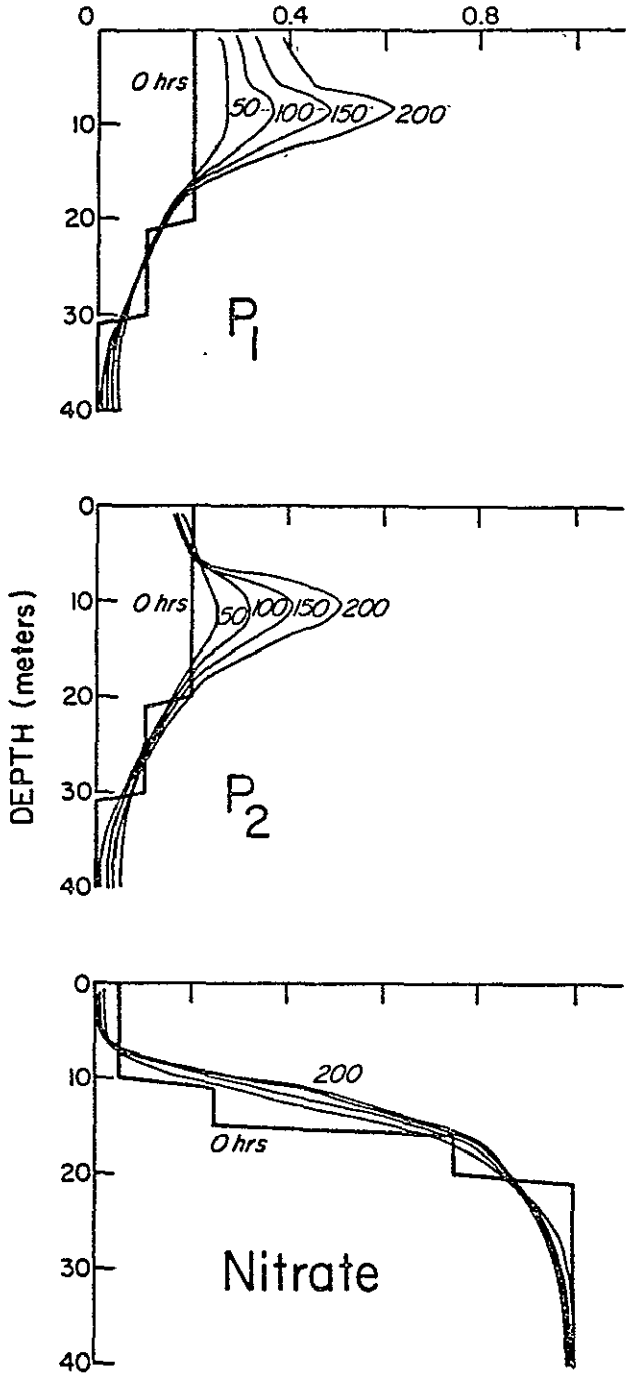

Figure 20. The development of the vertical structure of the two types of phytoplankton and nitrate (all in nondimensional units) for the low-nutrient, mild upwelling model.

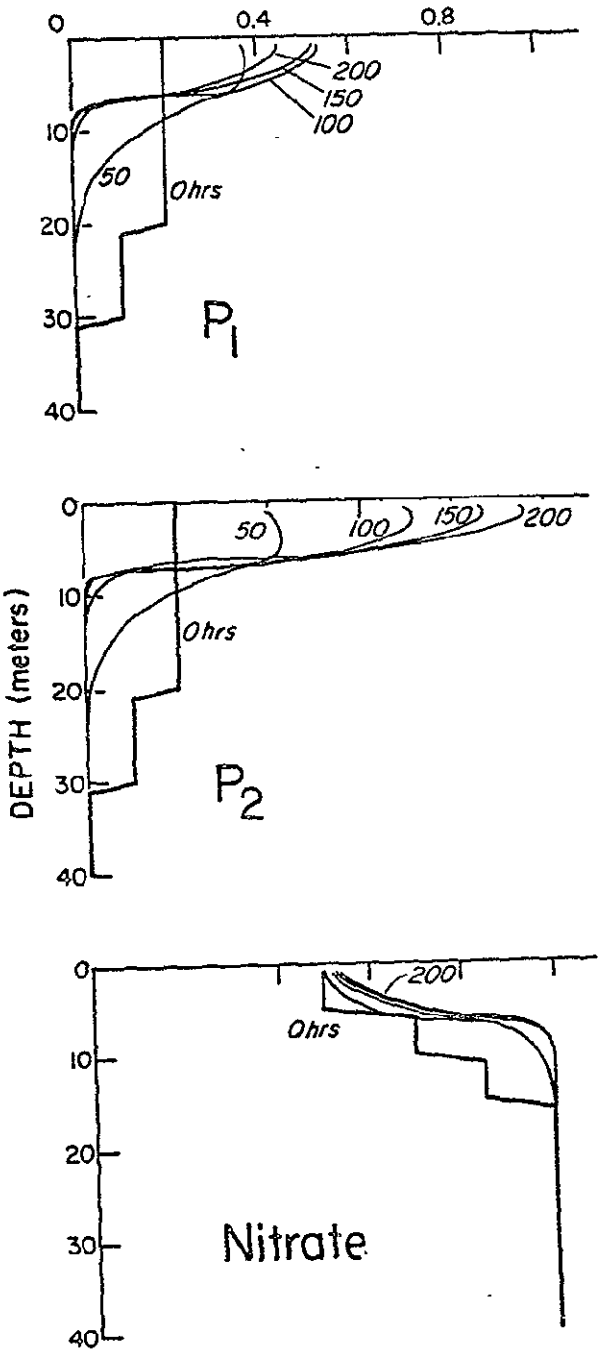

Figure 21. The development of the vertical structure of the two types of phytoplankton and nitrate (all in nondimensional units) for the high nutrient, strong upwelling model.

large particles (P_2) have increased in numbers the most. Settling and advection balance at a depth of less than one meter. Production is maximized at three meters. The small particles are decreasing because they cannot maintain themselves against the divergence caused by the strong upwelling. Again the nutrient concentration is near steady state but at a much higher concentration.

As conditions in the upwelling region can change very quickly, a model has been included which is a combination of the previous two (i.e. high nutrients and low vertical advection). The results are shown in Figure 22. The concentrations increase very rapidly and the maxima display a large increase in depth. Nutrients quickly change to a profile similar to the first model. The surface waters are predominated by small particles and the pycnocline by large particles.

In Figure 23, the model data is summarized and compared with the experimental data of Section IV. Models 1 and 2 are qualitatively similar to the offshore and inshore average profiles of Figure 23a. The results of the models (Figure 23b) are shown in nondimensional units. The dimensional units are determined by the parameters N_0 and P_0/N_0. P_0/N_0 was assigned the value 0.3 to make P_0 = 1.0 equivalent (in units $\mu gN\ell^{-1}$) to the maximum particle concentration found inshore of the front when N_0 was 30 μmoles ℓ^{-1}. Model 2 overestimates the surface concentrations by about 40%. Offshore of the front, the nitrate concentrations at 20 meters is about 10 μmoles ℓ^{-1}, P_0/N_0 is the same so a P_0 of 1.0 is now equivalent to 1.3 ppm by volume and again the model overestimates by 40%. The model curves have the correct shape and are in the right proportion to each other when the dimensionalizing factors are taken into account. The lack of a grazing term may account

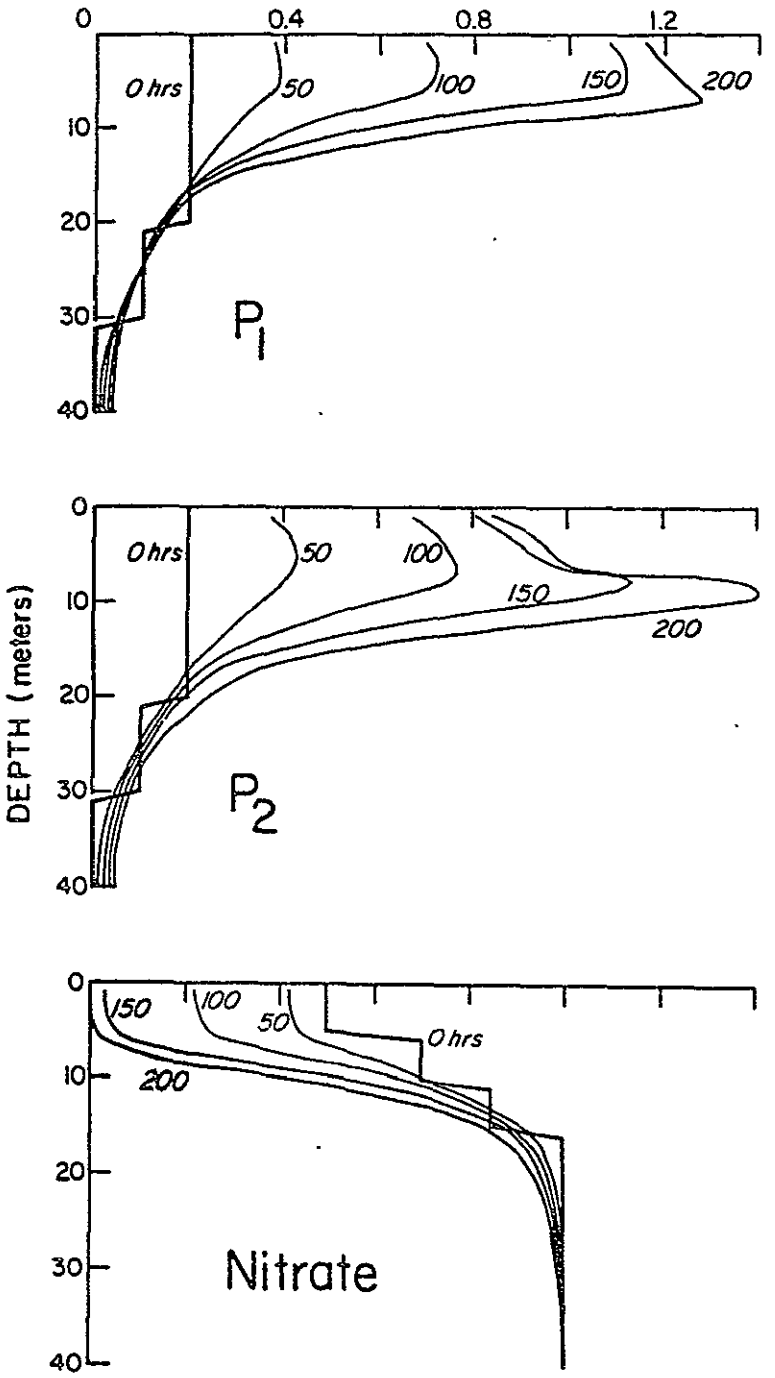

Figure 22. The development of the vertical structure of the two types of phytoplankton and nitrate (all in nondimensional units) for the high-nutrient, mild upwelling model.

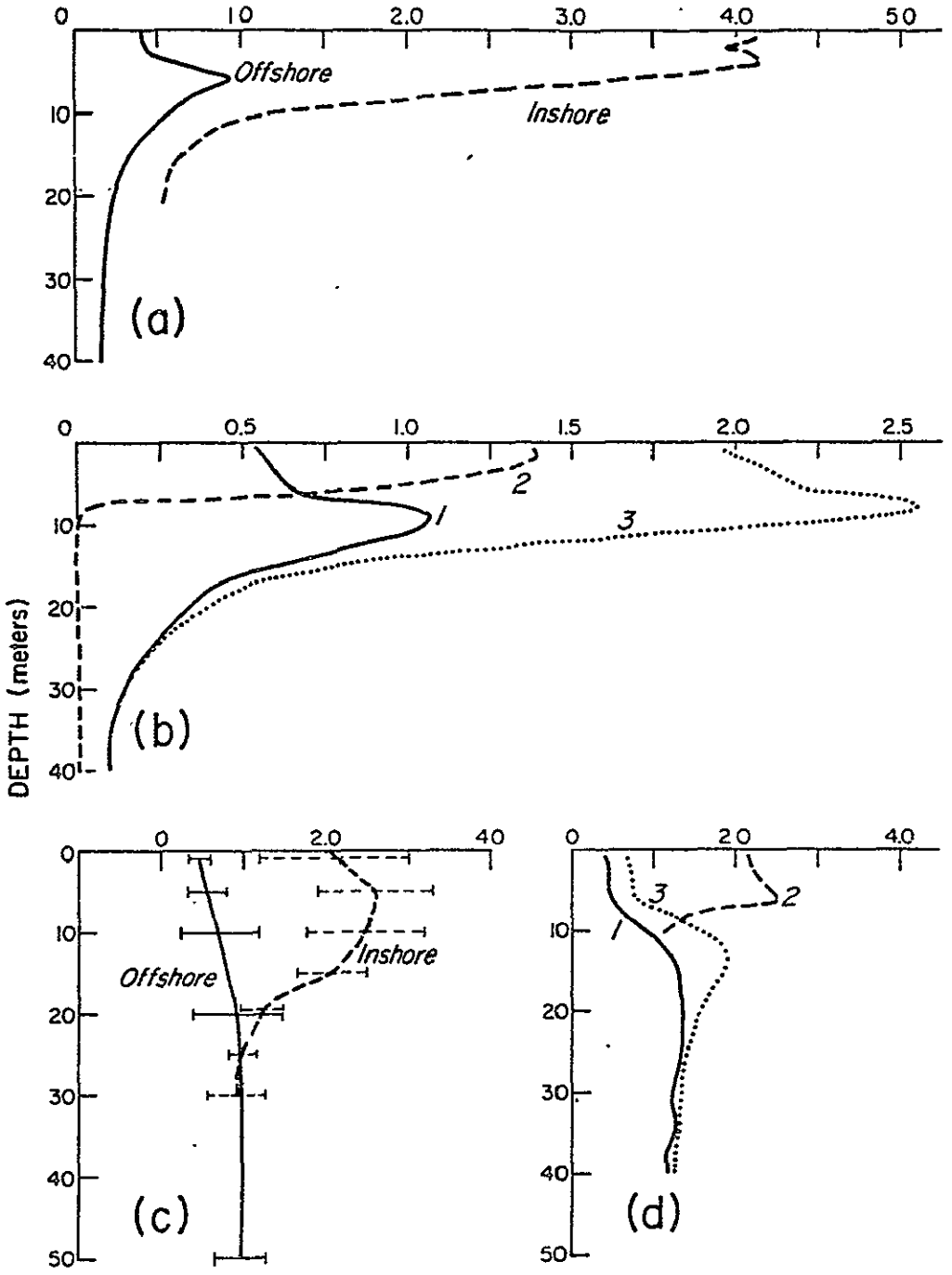

Figure 23. A comparison of the observed and the obtained vertical distributions.

a. The average suspended particulate volume (ppm) computed from light transmission measurements inshore and offshore of the particle front.
b. The sum of P_1 and P_2 for the three models (nondimensional).
c. The average and the 95% confidence intervals for the average of the ratio of large to small particles by volume.
d. The ratios of P_2 to P_1 for the three models.

for the overestimazion. Changing N_0 from model to model also changes the nutrient half saturation constants. In this way, allowance is made not only for species difference but to differences due to conditioning.

Figures 23c and d compare the relative numbers of large and small particles. The experimental data is computed by dividing the volume concentration of particles between 16 and 60 μm diameter by the volume concentration of particles between 3.5 and 16 μm diameter. The model results are simply P_2/P_1. Only a qualitative agreement was expected since the size separations and the assignments of settling velocities and growth rates are somewhat arbitrary. However, numerical agreement is present also.

Sensitivity Analysis

Sensitivity analysis was performed by varying the parameters by 30% and observing the change in the model results. Model 1 was used for that purpose because it had the most structure and thus should be the most sensitive. The results were normalized so that if a 30% change in a parameter produced a 30% change in the model, the resultant statistic would be 1.0. The sensitivity was calculated at 1, 20 and 40 meters depth and at the particle maximum which was at 7-9 meters for the small particles and at 9-11 meters for the large particles. The results are shown in Table IV. None of the coefficients are greater than 1.0 and most are less than 0.5 which is encouraging evidence of the model's lack of sensitivity to the parameter values. P_2 is more sensitive than P_1. This correlates with Malone's (1971) field measurements that indicate that large phytoplankton are more sensitive to their

Table IV. Sensitivity Coefficients for Various Model Parameters

Depth	$\frac{A_z}{P_1}\frac{\partial P_1}{\partial A_z}$	$\frac{A_z}{P_2}\frac{\partial P_2}{\partial A_z}$	$\frac{V_{m1}}{P_1}\frac{\partial P_1}{\partial V_{m1}}$	$\frac{V_{m1}}{P_2}\frac{\partial P_2}{\partial V_{m1}}$	$\frac{V_{m2}}{P_1}\frac{\partial P_2}{\partial V_{m2}}$	$\frac{V_{m2}}{P_2}\frac{\partial P_2}{\partial V_{m2}}$	$\frac{w}{P_1}\frac{\partial P_1}{\partial w}$	$\frac{w}{P_2}\frac{\partial P_2}{\partial w}$
1	.45	.43	.20	-.28	-.20	.33	.30	.26
Particle max	-.09	-.12	.85	-.20	-.13	.90	.09	.16
20	.11	-.02	.54	-.02	0.0	.67	-.54	-.43
40	.95	.77	.08	0.0	0.0	.07	-.56	-.58

Depth	$\frac{K_{n1}}{P_1}\frac{\partial P_1}{\partial K_{n1}}$	$\frac{K_{n1}}{P_2}\frac{\partial P_2}{K_{n1}}$	$\frac{K_{n2}}{P_1}\frac{\partial P_1}{\partial K_{n2}}$	$\frac{K_{n2}}{P_2}\frac{\partial P_2}{\partial K_{n2}}$
1	-.16	.17	.21	-.36
Particle max	-.27	.06	.12	-.64
20	-.07	0.0	0.0	-.34
40	0.0	0.0	0.0	0.0

environment. The eddy diffusivity has the most effect at the surface and at 40 meters while the maximum specific growth rates have a large effect at the particle maximum and at 20 meters. The effect on the size distributions can be determined by taking the difference of the sensitivity coefficients for P_1 and P_2. The biological terms, V_m and K_n have a large effect on the size distribution while the diffusivity has a significant effect only at 40 meters. The sensitivity of the relative vertical structure can be determined by the difference between the coefficients at 1 meter and at the maximum. The vertical structure of P_1 and P_2 are most affected by their respective growth rates followed by eddy diffusivity. But the change of the total suspended volume $P_1 + P_2$ is most affected by the eddy diffusivity. Thus the magnitude of the features and the particle size distributions are most sensitive to the biological terms while the shape of the vertical distribution is largely a function of the vertical structure of the eddy diffusivity

Discussion

The three models reveal the trends that may occur when upwelling of a given intensity is maintained for several days. Under mild upwelling, a sharp maximum in suspended volume will form at or move to the top of the thermocline. This is the result of a rapidly decreasing light function and a rapidly increasing nutrient concentration producing maximum growth in this region. The depth at which the sinking and advection rates balance also occurs in this region but not necessarily at the same depth as the maximum. There may also be adaptations

(Smayda; 1970, 1974) by the phytoplankton to make their sinking rates balance advection at these desirable depths. This would accentuate the maximum. Relative particle size decreases at the surface under mild upwelling conditions but the concentration may increase or decrease depending on the nutrient concentration at the start. Nutrients are soon depleted in the surface waters.

In the case of strong upwelling, nutrients become plentiful in the euphotic zone and the maximum particle concentration moves to the surface. Larger phytoplankton become prevalent. The upwelling of clean water decreases the thickness of the turbid layer. The surface concentrations would be even higher if the surface waters were not being constantly diluted by the upwelled water. If upwelling velocities were even greater, the surface concentrations may even decrease with time.

Ignored as a consequence of using a one-dimensional model is the effect of horizontal fluxes of nutrients and particles. In a two cell circulation, a downwelling region exists next to the upwelling region. It is easy to imagine that the nutrient rich upwelled water is advected to a place where there is no upwelling and the consequent growth is not obscured by dilution. Thus one cannot take the results of these few one-dimensional models and apply them independently to various locations. However, if one keeps in mind the concepts of conservation of matter, these models may help make sense of two-dimensional distributions. A two-dimensional model has been developed, but due to the larger computer times involved, funds ran out before meaningful results could be obtained. The preliminary results (200 iterations instead of 800) look encouraging, however, in that the observed features of the Oregon transects (Section IV) were beginning to form.

The given models provide a qualitative or first order quantitative prediction of vertical profiles in the Oregon region. Inclusion of grazing and self-shading terms may improve the model, but having only first order approximations of the many parameters makes one wonder if it would be worth the extra cost.

VI. DETERMINING CIRCULATION BY REMOTELY MONITORING THE DISTRIBUTION OF PARTICULATES

The inverse problem (determining current patterns from successive measurements of ocean color spectra) is not easily solved. From observations of natural patchiness in two upwelling regions (Beers, Stevenson, Epply and Brookes, 1971; Pearcy and Keene, 1974), one finds that the salient features do not move with the currents but merely define boundaries of current systems and eddies. The solution of the problem then requires some knowledge of the current patterns and biological dynamics in the region. Since color fronts do not necessarily indicate that there is also a temperature front, infrared measurements may add more information.

Method: Conservation of Water Mass

Ignoring the depth limitations of remote ocean color spectra measurements, a method of estimating the two dimensional (vertical and onshore-offshore) flow pattern from the distribution of parameters in the ocean will be presented. The first assumption is that nearshore and just offshore of the particle front, horizontal processes other than the divergence already included in the vertical model can be ignored. Thus, at these points, we can compare the observed vertical profile with the results of our vertical model and determine an order of magnitude for upwelling velocities. The second assumption is that the two-dimensional conservation of mass equation, $\frac{\partial w}{\partial z} + \frac{\partial u}{\partial x} = 0$, holds. Stevenson, Garvine and Wyatt (1974) show a large component of the surface current perpendicular to the front. This component increases in magnitude and

increases relative to the component parallel to the front with distance from shore until it becomes too close to the front to measure current velocities with surface drogues. This supports (at the order of approximation we are interested in) the otherwise dubious idea of two-dimensional conservation of mass.

Guessing the rate of upwelling through the thermocline W, assuming the vertical velocity of the water at the surface to be zero, and knowing the depth of the mixed layer D, one can calculate $\frac{\partial w}{\partial z} = \frac{W}{D}$ and thus obtain $\frac{\partial u}{\partial x}$ by the conservation equation. Applying the boundary conditions of no onshore-offshore flow at the coast and at the particle fronts yields a distribution of average offshore flow in the surface layer. There is usually a strong gradient of velocity in the mixed layer (Huyer, 1976; Johnson, 1977), so the velocity at the surface may be about twice the average flow of the mixed layer.

It only remains to estimate W. If there is a sharp subsurface maximum, W is small perhaps of order 10^{-3} cm sec^{-1}. W is large (10^{-2} cm sec^{-1}) if there is a near surface maximum and W is very large (2.0-3.0 x 10^{-2} cm sec^{-1}) if the surface maximum is very shallow or the entire surface layer is very clean. A thickening of the surface layer offshore of a high upwelling region indicates reduced upwelling, and a downward protuberance at the front indicates downwelling. With these assumptions, the onshore-offshore flow can be approximated.

Examples

The first transect of the July 1973 cruise (Figure 6) shows a near surface maximum at all points except at the station farthest from shore. There is a shallow turbid layer at stations one and four and

a very deep turbid layer at stations two and three. This suggests that there is maximum upwelling at stations one and four and downwelling at stations two and three. This conclusion is supported by the presence of a temperature front between stations two and four. At station six there is a near surface maximum consisting of mostly small particles. The predominance of small particles in a surface maximum has not been predicted by any of our models. An explanation is that due to recent past history the seed population was much larger for the small particles than for the large ones. This is supported by the higher temperatures offshore of the front suggesting that strong upwelling just recently started there.

We have assumed strong upwelling at the coast. A value of $w = 2.0 \times 10^{-2}$ cm sec^{-1} is often reported in the literature as mentioned several times previously. There is no thermocline at station one but the turbid layer is about 20 m thick. From this one obtains 1 cm sec^{-1} km^{-1} as the increase with distance offshore (gradient) of the offshore flow. The particle front is at about 5 km from shore, so the offshore flow increases to 2.5 cm sec^{-1} and then decreases back to zero due to downwelling inshore of the front. The surface current may be the order of 5 cm sec^{-1}. Offshore of the front, there also seems to be strong upwelling, the thermocline is about ten meters deep, resulting in a 2.0 cm sec^{-1} km^{-1} gradient of offshore flow. Thus, at ten km from shore, the average offshore flow may approach 10 cm sec^{-1} and the surface flow 20 cm sec^{-1}. Farther offshore the situation is unclear.

The second transect (Figure 7) is much simpler. The turbid layer is shallowest at the station nearest shore and increases in thickness and concentration with distance from shore. The maximum is always at

the surface and is dominated by the large particles. The maximum upwelling is thus at the shore and the phytoplankton grow on the nutrient-rich water as they are carried offshore. The offshore gradient of concentration is not monotonic enough to calculate the offshore transport from a specific growth rate. This may be due to longshore variation and the predominate longshore motion.

The shallow turbid layer seems to persist out to 7 km from shore. The thermocline depth is about 10 m. Using the same method results in final offshore velocities of 14 cm sec^{-1}. Surface velocities may approach 30 cm sec^{-1}. This is compatible with the profile of offshore velocity given by Huyer (1976) on July 12, 1976, two weeks before this transect.

The profiles in Section IV are similar to each other. The features move onshore and offshore but do not change much. This may reflect tidal motions or periodic changes in upwelling-downwelling at the coast corresponding to the periodic wind velocities (Johnson, 1977). There is a definite particle front but only a very shallow temperature front. The turbid layer is often thicker just inshore of the front than farther offshore. The large particles and near surface maximum indicate strong upwelling near the coast. The thickening of the turbid layer towards the particle front indicates slight downwelling. Offshore of the front upwelling seems to be weak as indicated by the subsurface maximum and the predominance of small particles. The temperatures during this cruise are higher than those of the previous year (Section III) because the upwelling winds are periodic instead of steady as was the case then. Inshore of the front, the offshore flow would be similar to that determined for the transect of Figure 6.

Offshore, however, the vertical velocities are low and to even predict a direction of flow may be risky as the data of Stevenson, Garvine and Wyatt (1974) show onshore motion at the surface offshore of a similar front.

There is no current data in the surface layer during any of the above transects. However, during the box experiment of the August 1974 cruise (Figure 18), Johnson (1977) reports strong upwelling and offshore velocities of the order 10 cm sec^{-1}. Figure 18 shows a surface maximum of turbidity at all stations during this experiment. The particle size distributions had low slopes as reported in Section IV. This implies a relatively greater number of large particles. Thus what little current data we do have does not conflict with the conclusions of the above method.

Future Experiments

Any future experiments must include surface current data to evaluate the results of the models. The profiling current meter may not be adequate since it is time consuming and the readings above 10 meters depth may be influenced by the presence of the ship. A better choice may be lines of near surface current meter strings. Lines two minutes of latitude apart with strings at 2, 4, 6 and 8 nautical miles from shore and current meters at 2, 7, 12 and 17 meters depth may even provide enough resolution to do mass balance calculations assuming the surface of the water is motionless (averaged over a tidal cycle).

Uptake rates of nitrogen can be determined by suspending the innoculated samples at the depth at which they are taken. Thin bottles should be used so that the ultraviolet light is not cut out. This

would also provide a chance to use both thick and thin bottles to examine the effect of ultraviolet light. The incubation takes some time so it will not be possible to do this while making a rapid transect. Rapid transects are necessary to get a synoptic picture of the distribution of parameters and to maximize the usefulness of brief airplane overflights.

Many parameters are needed as input to models. Measurements should be made for as many as possible of the following: particulate nitrogen, nitrate ammonia, zooplankton biomass, chlorophyll a, phaeophytin, and irradiance. Water density, light transmission, and particle size measurements are absolutely necessary. It would be helpful if the particle measurements were supplemented by microscopic analysis and percent organic matter determinations. Aerial color and infrared photography would reveal the orientation and movement of particle fronts and the temperature field.

The following is a rough draft of a cruise plan for such an experiment:

1) Deploy near-surface current meter strings at 2, 4, 6 and 8 NM from shore at 44° 59' N and at 45° 01' N. The current meters should be at 5, 10, 15 and 20 m depth.

2) Make four rapid transects of 45° 00' N with stations 1, 2, 3, 4, 5, 6, 8 and 10 NM from shore. If a station is not being completed every hour, station 10 and/or 5 may be omitted. Airplane overflights should coincide with the middle stations of two of the transects.

3) Assuming upwelling is evident, deploy a parachute drogue inshore of front at 44° 58' N. Keep the ship as close as possible

to the drogue and take stations every 90 minutes until drogue merges with a front or reaches 10 NM from shore or 48 hours have elapsed.

4) Make anchor station 2 NM from shore at 45° 00' N. Deploy another ship 1 NM downcurrent. Take stations from both ships every two hours for 48 hours.

5) Make four rapid transects of 45° 00' N.

6) Retrieve current meters.

Such an experiment would provide the data necessary to make more extensive numerical modeling worthwhile. Several additions to the model are worth evaluating. First, the model should be extended to two or three dimensions. Furthermore, the effects of grazing, self shading, species specific light-photosynthesis relationships and diurnal variations need to be evaluated.

With the ample surface current measurements and the wide area synoptic pictures from the airplane overflight, combined with ample ground truth data, the heating of a water parcel and the growth of its accompanying phytoplankton may be monitored as the parcel moves with the surface currents. This information can be compared to the predictions of the model and perhaps the reasons for the discrepancies can be found. All this could then be used to develop a more definitive method of determining surface current patterns from successive measurements from an airborne vehicle.

BIBLIOGRAPHY

Acton, F. S. 1970. Numerical methods that work. Harper and Row. New York. 541 pp.

Anderson, G. C. 1969. Subsurface chlorophyll maximum in the northeast Pacific Ocean. Limnol. Oceanogr. 14:386-391.

Bader, H. 1970. The hyperbolic distribution of particle sizes. J. Geophys. Res. 75:2823-2830.

Beers, J. R., M. R. Stevenson, R. W. Eppley and E. R. Brooks. 1971. Plankton populations and upwelling off the coast of Peru, June 1969. Fish. Bull. 69:859-876.

Bowden, K. F. 1975. Currents and mixing in the ocean. In: Chemical Oceanography. Vol. 1. Editors: J. P. Riley and G. Skirrow. pp. 43-72. Academic Press, London.

Carder, K. L., G. F. Beardsley, Jr. and H. Pak. 1971. Particle size distributions in the eastern equatorial Pacific. J. Geophys. Res. 76:5070-5077.

Eittreim, S., P. E. Biscaye and A. L. Gordon. 1973. Comments on paper by T. Ichiye, N. J. Bassin and J. E. Harris 'Diffusivity of suspended matter in the Caribbean Sea'. J. Geophys. Res. 78:6401-6403.

Eppley, R. W., J. N. Rogers and J. J. McCarthy. 1969. Half-saturation constants for uptake of nitrate and ammonium by marine phytoplankton. Limnol. Oceanogr. 14:912-920.

Hecky, R. E. and P. Kilham. 1974. Comment on 'Environmental control of phytoplankton cell size'. Limnol. Oceanogr. 19:361-365.

Huyer, A. 1974. Observations of the coastal upwelling region off Oregon during 1972. Ph.D. Thesis. Oregon State University. 149 pp.

_____. 1976. A comparison of upwelling events in two locations: Oregon and Northwest Africa. J. Mar. Res. 34:531-546.

Ichiye, T., N. J. Bassin and J. E. Harris. 1972. Diffusivity of suspended matter in the Caribbean Sea. J. Geophys. Res. 77: 6576-6588.

Jerlov, N. G. 1951. Optical studies of ocean waters. Reports of the Swedish Deep-Sea Expedition. 3:1-59.

_____. 1976. Marine Optics. Elsevier Scientific Publishing Company. Amsterdam. 231 pp.

Johnson, D. R. 1977. Determining vertical velocities during upwelling off the Oregon coast. Deep-Sea Res. 24:171-180.

Kamykowski, D. 1974. Possible interactions between phytoplankton and semidiurnal internal tides. J. Mar. Res. 32:67-89.

Kitchen, J. C., D. Menzies, H. Pak and J. R. V. Zaneveld. 1975. Particle size distribution in a region of coastal upwelling analyzed by characteristic vectors. Limnol. Oceanogr. 20:775-783.

Kopelevich, O. V. and V. I. Burenkov. 1972. Statistical characteristics of the light scattering functions of sea water. In: Optics of the Ocean and the Atmosphere. Nauka. Leningrad.

MacIsaac, J. J. and R. C. Dugdale. 1969. The kinetics of nitrate and ammonia uptake by natural populations of marine phytoplankton. Deep-Sea Res. 16:45-57.

Malone, T. C. 1971. The relative importance of nanoplankton and netplankton as primary producers in the California current system. Fish. Bull. 69:799-820.

Mooers, C. N. K., C. A. Collins and R. L. Smith. 1976. The dynamic structure of the frontal zone in the coastal upwelling region off Oregon. J. Phys. Ocean. 6:3-21.

Mueller, J. L. 1973. The influence of phytoplankton on ocean color spectral. Ph.D. Thesis. Oregon State University. 239 pp.

_____. 1976. Ocean color spectra measured off the Oregon coast: characteristic vectors. Appl. Optics. 15:394-402.

Neumann, G. and W. J. Pierson, Jr. 1966. Principles of physical oceanography. Prentice-Hall. Englewood Cliffs. 545 pp.

O'Brien, J. J. and J. S. Wroblewski. 1973a. On advection in phytoplankton models. J. Theor. Biol. 38:197-202.

_____ and _____. 1973b. A simulation of the mesoscale distribution of the lower marine trophic levels off west Florida. Inv. Pesq. 37:193-244.

Okubo, A. 1971. Oceanic diffusion diagrams. Deep-Sea Res. 18:789-802.

Pak, H., G. F. Beardsley, Jr. and R. L. Smith. 1970. An optical and hydrographic study of a temperature inversion off Oregon during upwelling. J. Geophys. Res. 75:629-636.

Parsons, T. R. 1969. The use of particle size spectra in determining the structure of a plankton community. J. Oceanogr. Soc. Jap. 25:6-15.

Parsons, T. R. and M. Takahashi. 1973. Environmental control of phytoplankton cell size. Limnol. Oceanogr. 18:511-515.

Pattullo, J. and W. Denner. 1965. Processes affecting seawater characteristics along the Oregon coast. Limnol. Oceanogr. 10:443-450.

Pearcy, W. G. and D. F. Keene. 1974. Remote sensing of water color and sea surface temperatures off the Oregon coast. Limnol. Oceanogr. 19:573-583.

Riley, G. A. 1963. Theory of food-chain relations in the ocean. In: The Sea. Vol. 2. Editor: M. N. Hill. pp. 438-463. Interscience. New York.

Ryther, J. H. 1956. Photosynthesis in the ocean as a function of light intensity. Limnol. Oceanogr. 1:61-70.

Semina, H. J. 1972. The size of phytoplankton cells in the Pacific Ocean. Int. Rev. Gesamten Hydrobiol. 57:177-205.

Sheldon, R. W. and T. R. Parsons. 1967. A practical manual on the use of the Coulter Counter in marine science. Coulter Electronics Sales Co. Canada. 66 pp.

Simonds, J. L. 1963. Application of characteristic vector analysis to photographic and optical response data. J. Opt. Soc. Am. 53:968-974.

Smayda, T. J. 1970. The suspension and sinking of phytoplankton in the sea. Oceanogr. Marine Biol. Ann. Rev. 8:353-414.

_____. 1971. Normal and accelerated sinking of phytoplankton in the sea. Marine Geol. 11:105-122.

_____. 1974. Some experiments on the sinking characteristics of two freshwater diatoms. Limnol. Oceanogr. 19:628-635.

Stevenson, M. R., R. W. Garvine and B. Wyatt. 1974. Lagrangian measurements in a coastal upwelling zone off Oregon. J. Phys. Oceanogr. 4:321-336.

Thompson, J. D. 1974. The coastal upwelling cycle on a beta-plane: hydrodynamics and themodynamics. Ph.D. Thesis. Florida State University. 141 pp.

Wroblewski, J. S. 1976. A model of the spatial structure and productivity of phytoplankton populations during variable upwelling off the coast of Oregon. Technical Report. Mesoscale-Air-Sea Interaction Group, Florida State University, Tallahassee, 116 pp.

Wroblewski, J. S. and J. J. O'Brien. 1976. A spatial model of phytoplankton patchiness. Mar. Biol. 35:161-175.

Wroblewski, J. S., J. J. O'Brien and T. Platt. 1975. On the physical and biological scales of phytoplankton patchiness in the ocean. Mém. Soc. r. Sci. Liège. 7:43-57.

Yentsch, C. S. 1963. Primary production. Oceanogr. Mar. Biol. Ann. Rev. 1:157-175.

Zaneveld, J. R. V. 1972. Optical and hydrographic observations of the Cromwell Current between 92° 00' W and the Galapagos Islands. Ph.D. Thesis. Oregon State University. 87 pp.

Zaneveld, J. R. V. and H. Pak. 1973. Method for the determination of the index of refraction of particles suspended in the ocean. J. Opt. Soc. Am. 63:321-324.

APPENDICES

APPENDIX A

FORTRAN Program for Characteristic Vector Analysis

```
      PROGRAM KHRV
      DIMENSION X(12,204),AV(12),XN(12,204),XX(12,12),V(12)
      DIMENSION D(12),W(12)Y(204)
C
C     READ AND COMPUTE AVERAGE OF LOG CONCENTRATION
C
      DO 1 I=1,12
1     AV(I)=0.
      DO 2 J=1,204
      READ(7,1001)(X(I,J),I=1,12)
      DO 99 IZ-1,12
99    X(IZ,J)=ALOG(X(IZ,J))
      DO 3 K=1,12
3     AV(K)=AV(K)+X(K,J)
2     CONTINUE
      DO 4 L=1,12
4     AV(L)=AV(L)/204.
      WRITE(61,1002)AV
C
C     COMPUTE VARIANCE-COVARIANCE MATRIX
C
      DO 5 M=1,204
      DO 6 MM=1,12
6     XN(MM,M)=X(MM,M)-AV(MM)
5     CONTINUE
      DO 7 N=1,12
      DO 8 N1=1,12
      XX(N,N1)=0.
      DO 9 N2=1,204
9     XX(N,N1)=XX(N,N1)+XN(N,N2)*XN(N1,N2)
8     CONTINUE
7     CONTINUE
C
C     COMPUTE AND PRINT THE TRACE
C
      TR=0.
      DO 10 IA=1,12
10    TR=TR+XX(IA,IA)
      WRITE(61,1003)TR
C
C     COMPUTE FIRST TWO CHARACTERISTIC VECTORS
C
      DO 11 JA=1,2
C
C     INITIAL GUESS
C
      DO 12 KA=1,12
12    V(KA)=1.
```

```
C
C     RECURSIVE LOOP
C
      DO 13 LA=1,15
      DO 14 MA=1,12
      D(MA)=0.
      DO 15 IB=1,12
15    D(MA)=D(MA)+V(IB)*XX(IB,MA)
14    CONTINUE
      G=ABS(D(1))
      DO 16 JB=1,12
16    IF(ABS(D(JB)).GT.G)G=ABS(D(JB))
      DO 17 KB=1,12
17    V(KB)=D(KB)/G
      WRITE(61,1002)V
13    CONTINUE
C
C     NORMALIZE SUM OF SQUARES = ROOT
C
      SQ=0.
      DO 18 LB=1,12
18    SQ=SQ+V(LB)*V(LB)
      DO 19 MB=1,12
      V(MB)=SQRT(ABS(G/SQ))*V(MB)
19    W(MB)=V(MB)/G
C
C     COMPUTE WEIGHTING FACTORS
C
      DO 20 IC=1,204
      Y(IC)=0.
      DO 21 JC=1,12
21    Y(IC)=Y(IC)+W(JC)*XN(JC,IC)
20    CONTINUE
C
C     WRITE VECTOR, ROOT AND WEIGHTING FACTORS
C
      WRITE(61,1002)V,G
      WRITE(1,1004)Y
      WRITE(61,1005)
C
C     REMOVE VARIANCE DUE TO FIRST VECTOR
C
      DO 22 KC=1,12
      DO 23 LC=1,12
23    XX(KC,LC)=XX(KC,LC)-V(KC)*V(LC)
22    CONTINUE
11    CONTINUE
      CALL EXIT
1001  FORMAT(/6E13.4/6E13.4)
1002  FORMAT(5E13.4)
1003  FORMAT(5X,'TRACE',E13.4)
1004  FORMAT(6E13.4)
1005  FORMAT(' ')
      END
```

APPENDIX B

Supplementary Data

Additional data from the August 1974 cruise is presented here. Particulate volume concentration was measured by an electronic particle sizer interfaced to a Nuclear Data 2400 Multichannel Analyzer. The measurements encompassed the size range from 32 to 131072 μm^3 particle volumes. Light scattering at 45° (B45) was measured with a Brice-Phoenix Photometer with a mercury lamp and a 546 nm filter. Particulate attenuation (C) was calculated by taking the negative natural logarithm of transmission (660 NM) and subtracting the attenuation (0.324) of pure seawater (Jerlov, 1976). B45/C was plotted as an indication of the index of refraction of the particles. It is also affected by the slope of the particle size distribution.

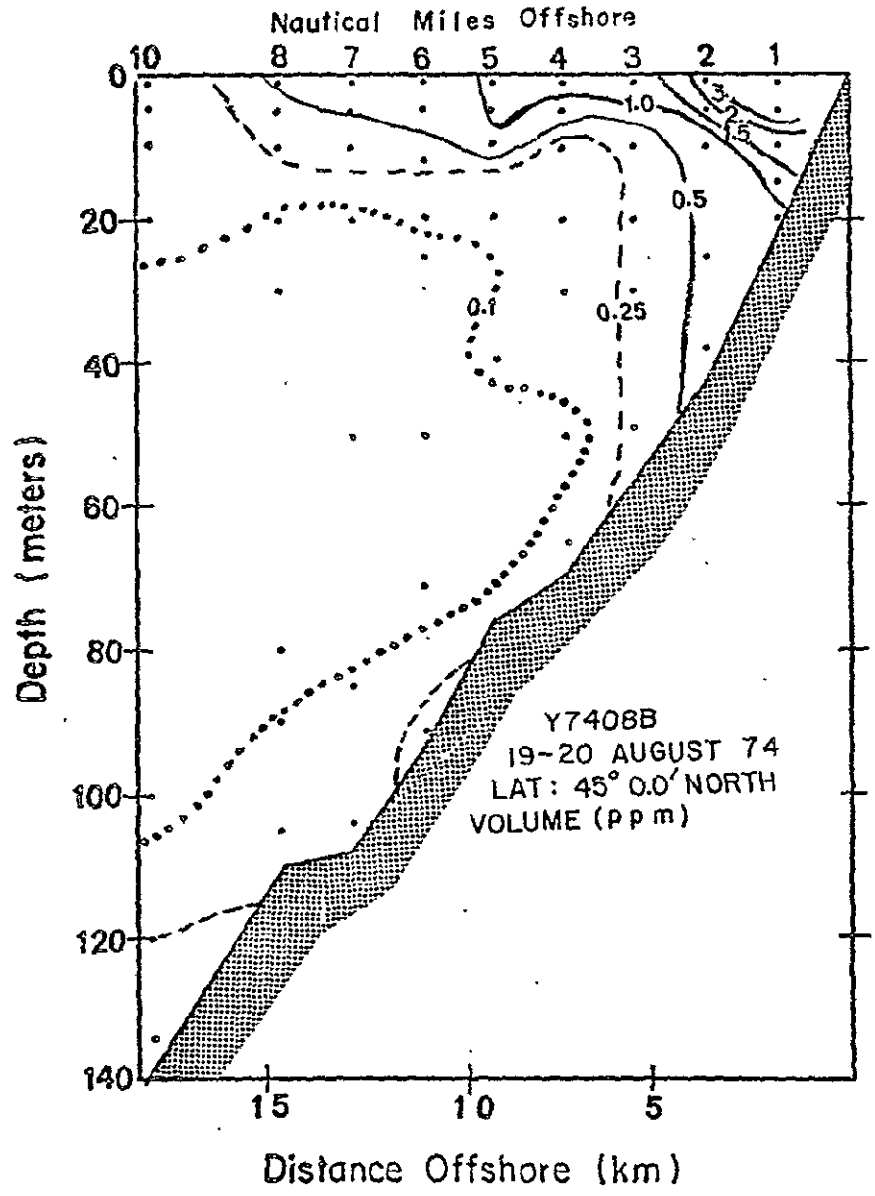

Figure 24. The distribution of particulate volume concentration along a transect during 19-20 August 1974.

ORIGINAL PAGE IS
OF POOR QUALITY

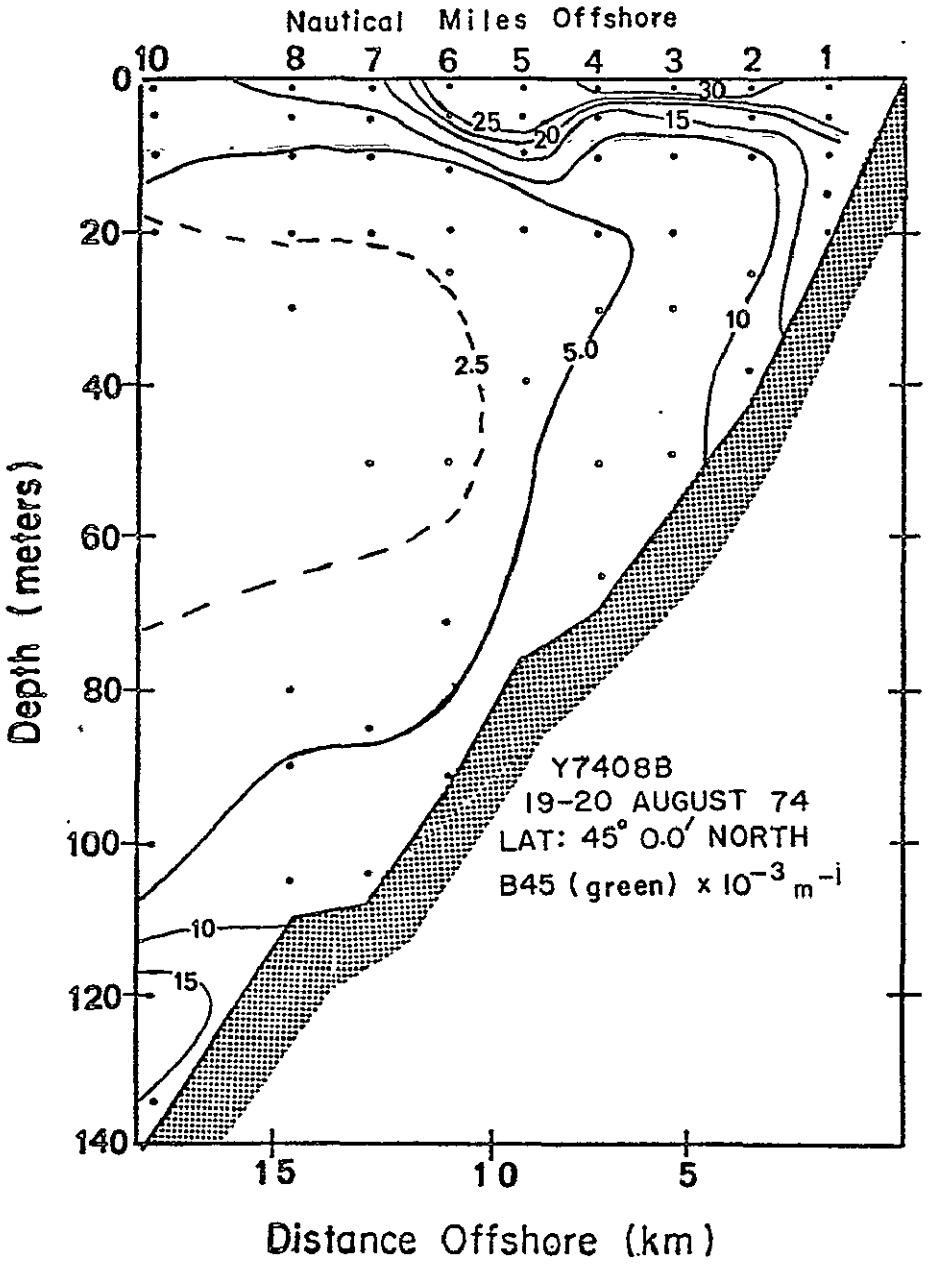

Figure 25 The distribution of light scattering (546 nm) at 45° (β45) from the forward direction along a transect during 19-20 August 1974.

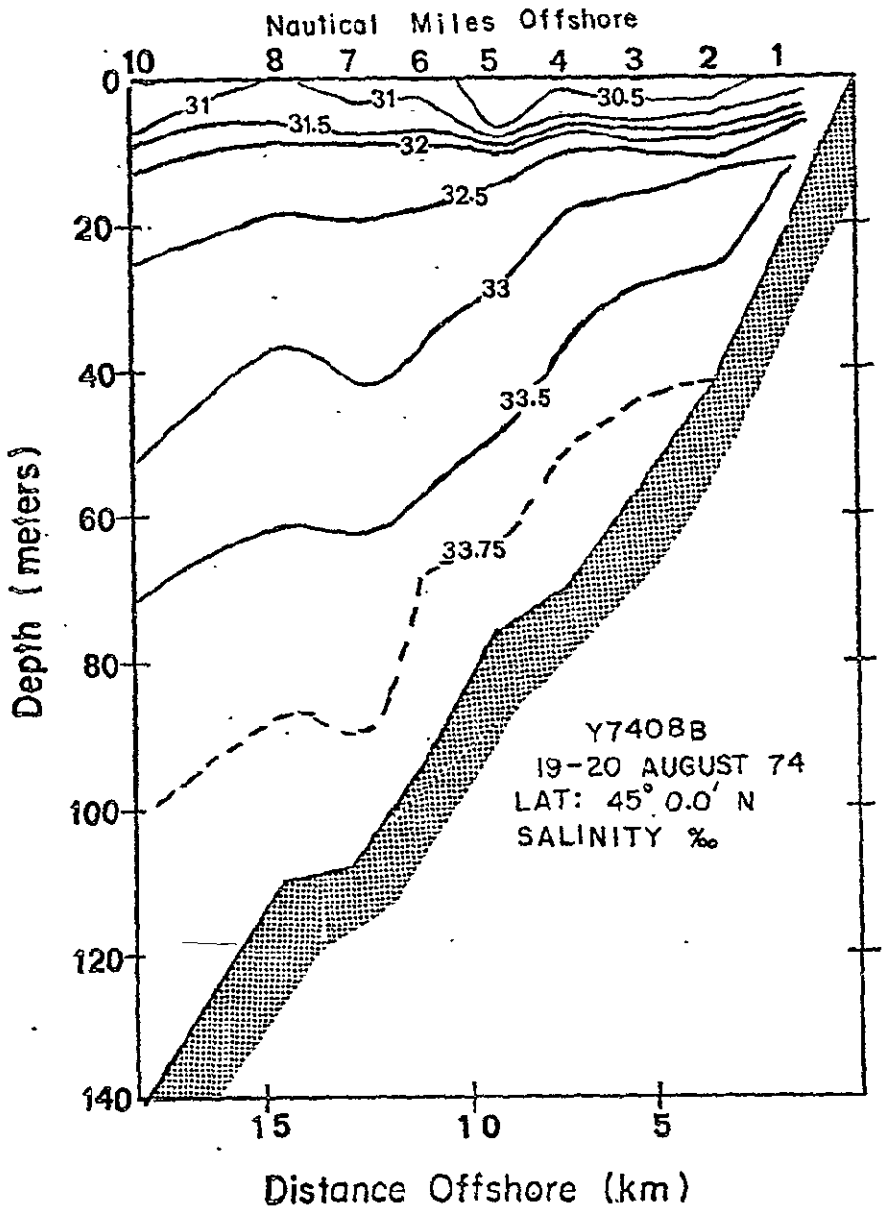

Figure 26 The distribution of salinity along a transect during 19-20 August 1974.

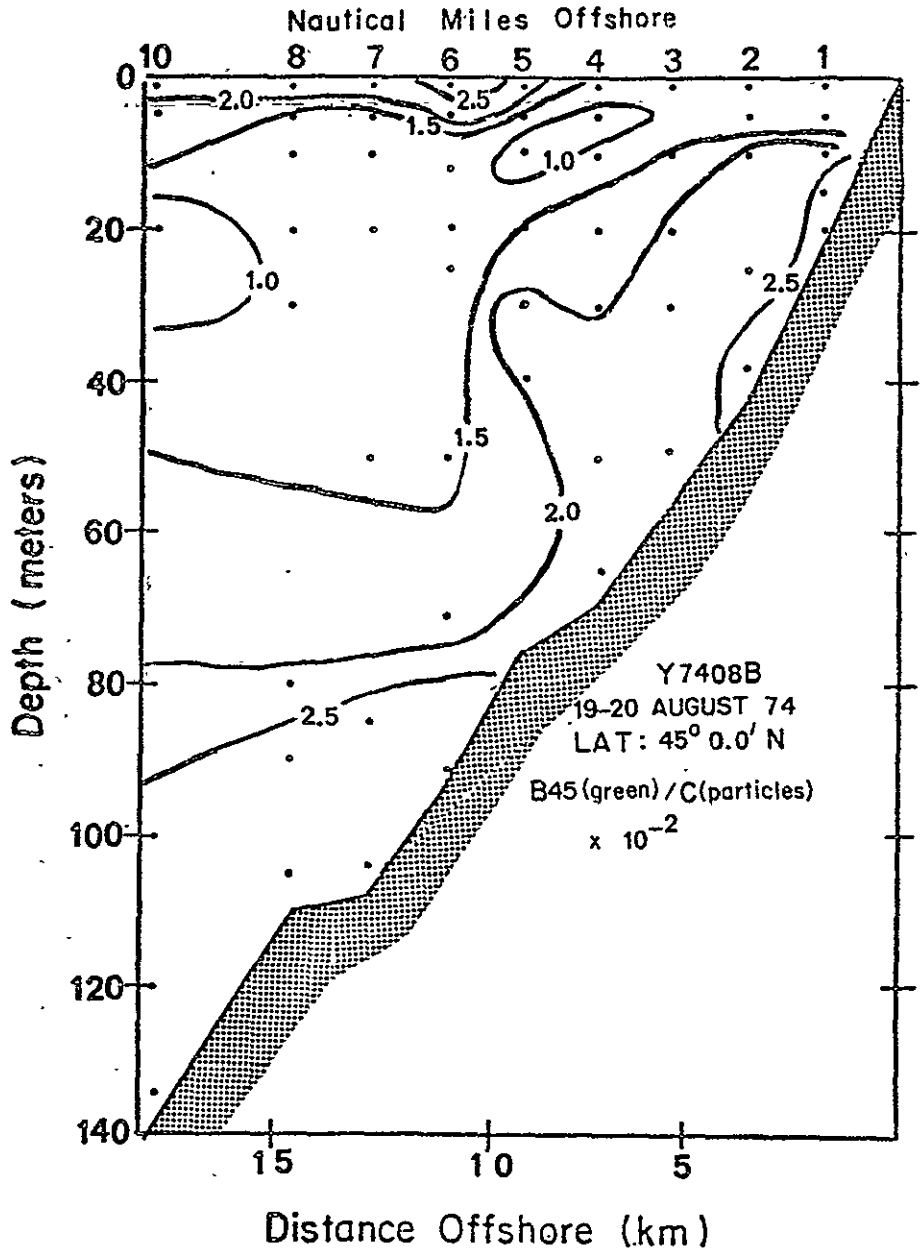

Figure 27 The distribution of the ratio of light scattering (546 nm) at 45° (β45) to the attenuation (C) of light (660 nm) due to suspended particles along a transect during 19-20 August 1974.

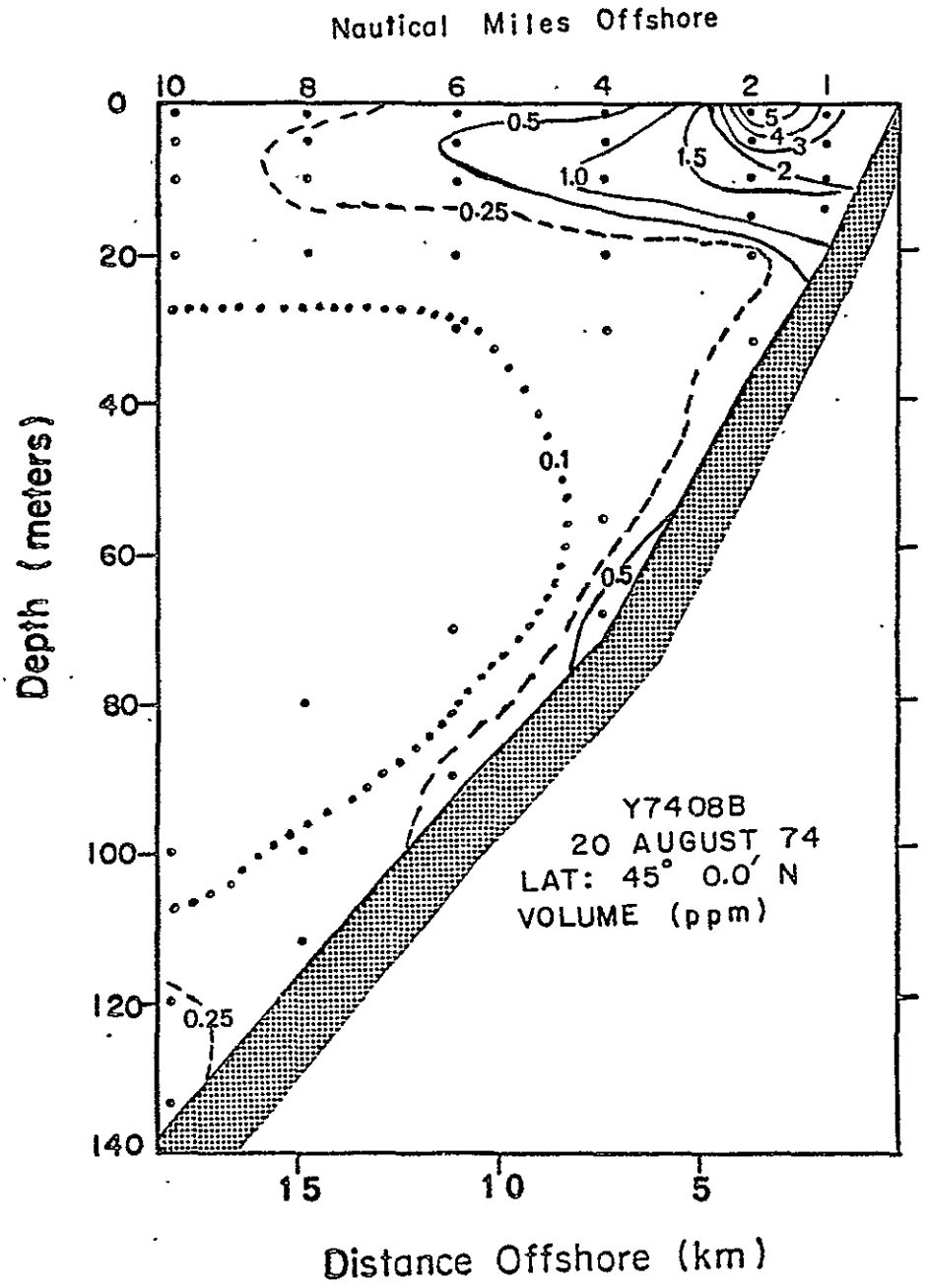

Figure 28 The distribution of particulate volume concentration along a transect during 20 August 1974.

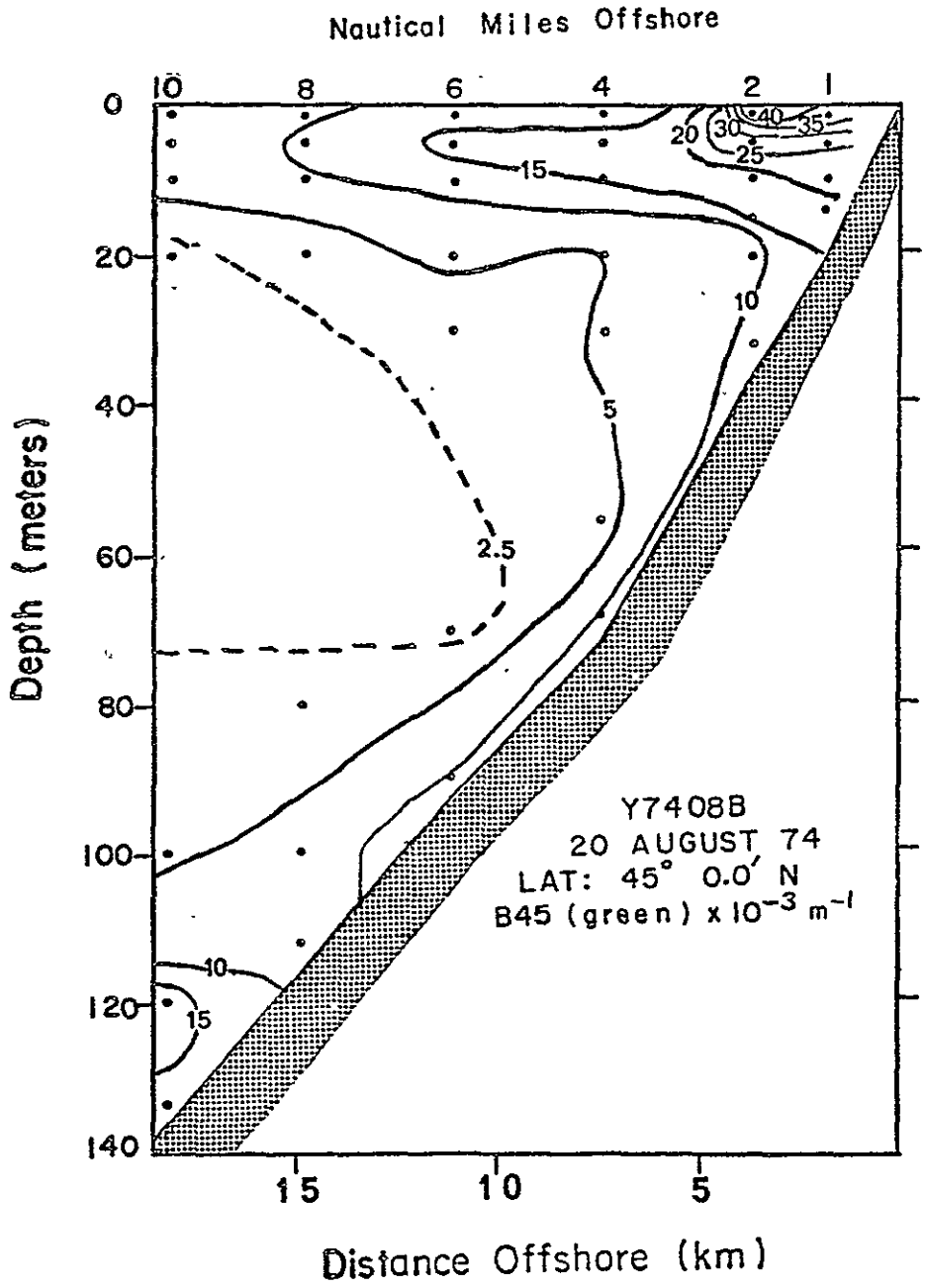

Figure 29 The distribution of light scattering (546 nm) at 45° (β45) from the forward direction along a transect during 20 August 1974.

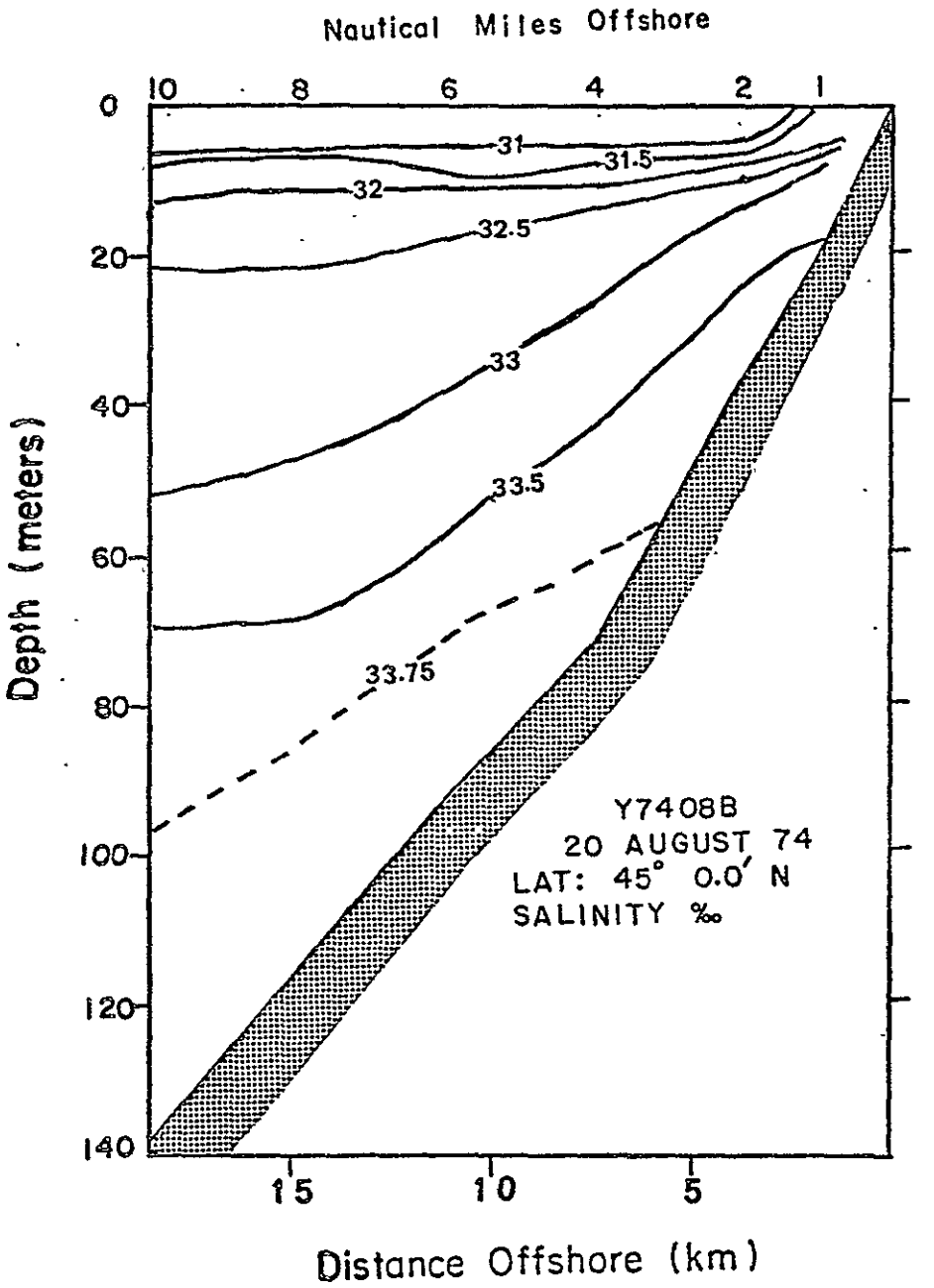

Figure 30 The distribution of salinity along a transect during 20 August 1974.

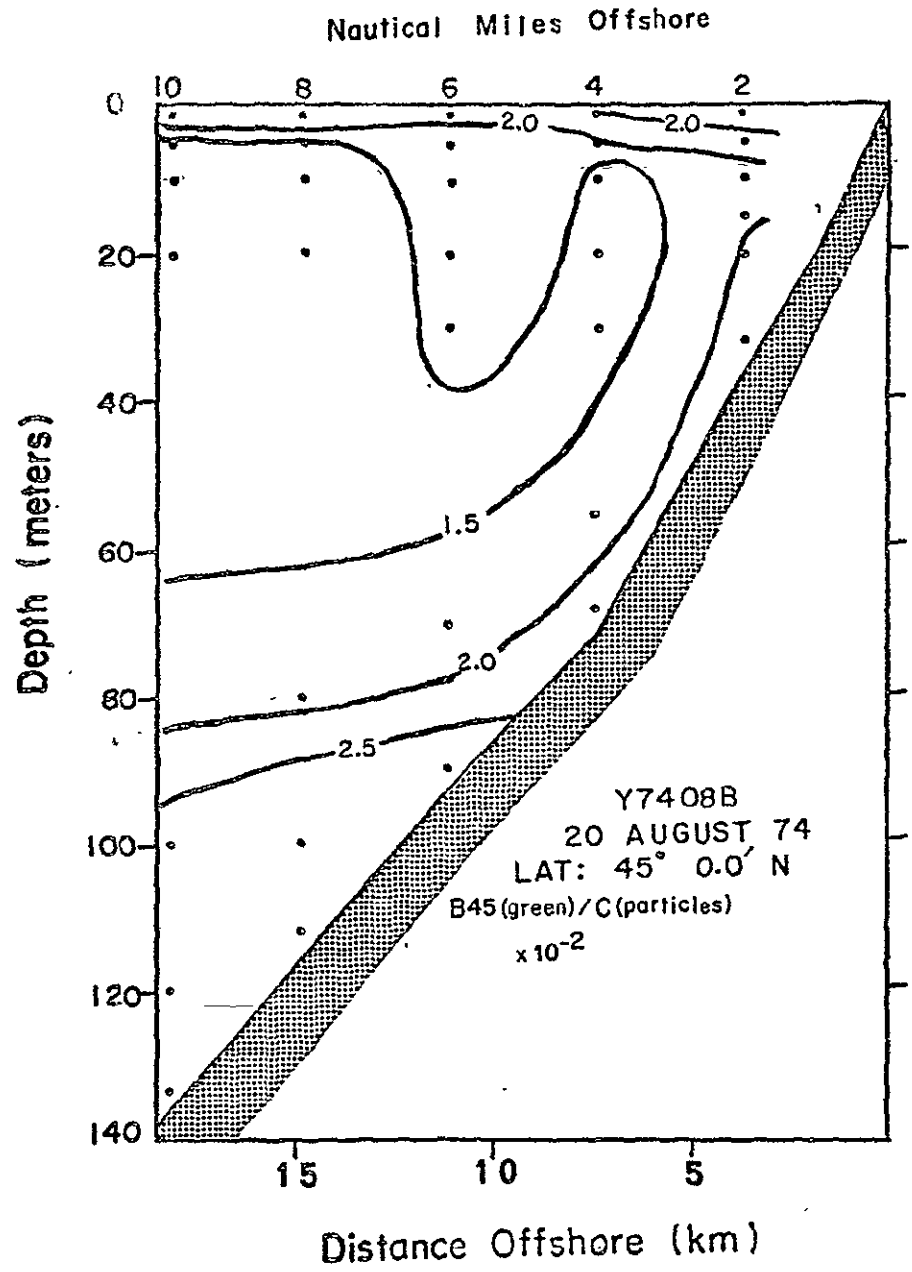

Figure 31 The distribution of the ratio of light scattering (546 nm) at 45° (β45) to the attenuation (C) of light (660 nm) due to suspended particles along a transect during 20 August 1974.

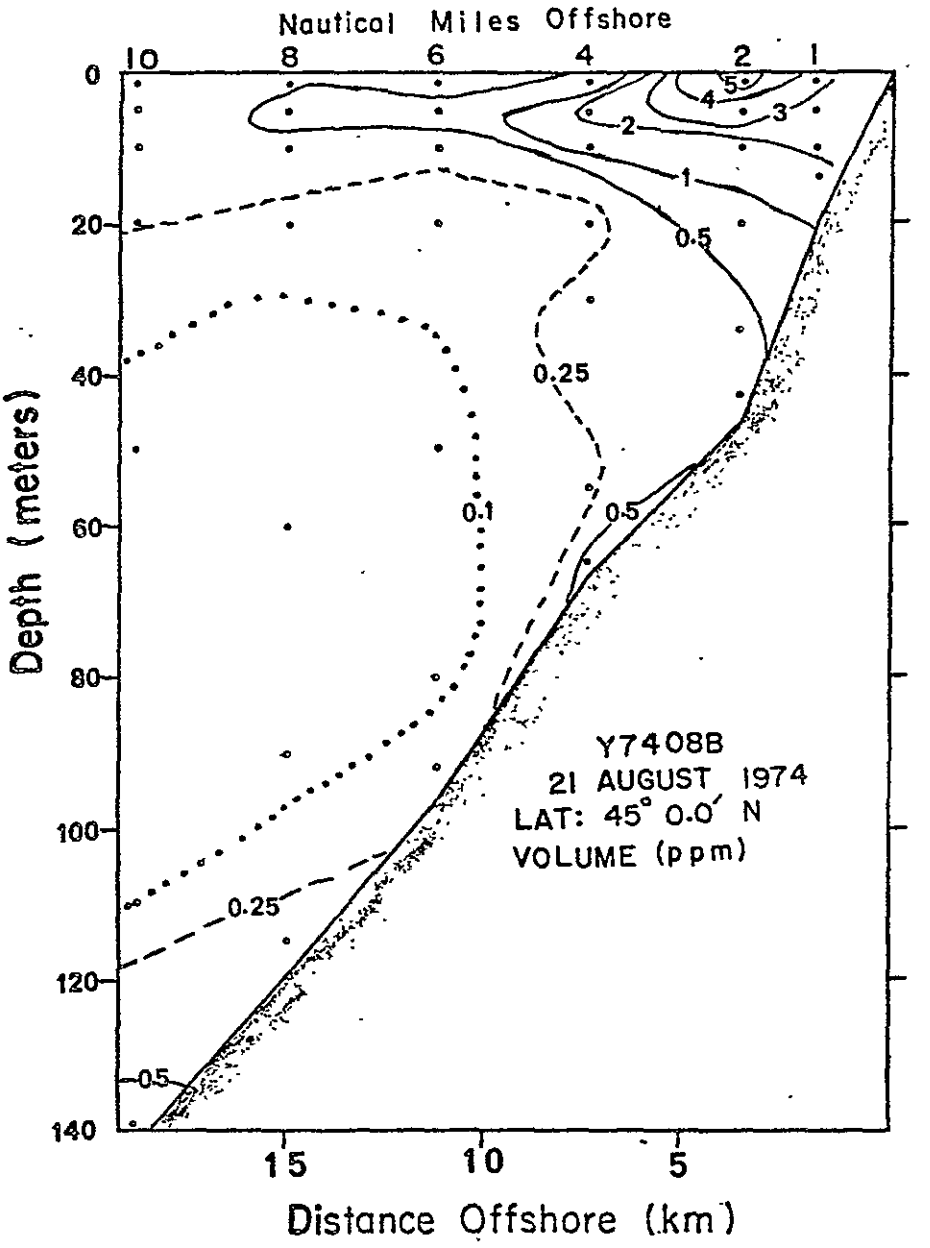

Figure 32 The distribution of particulate volume concentration along a transect during 21 August 1974.

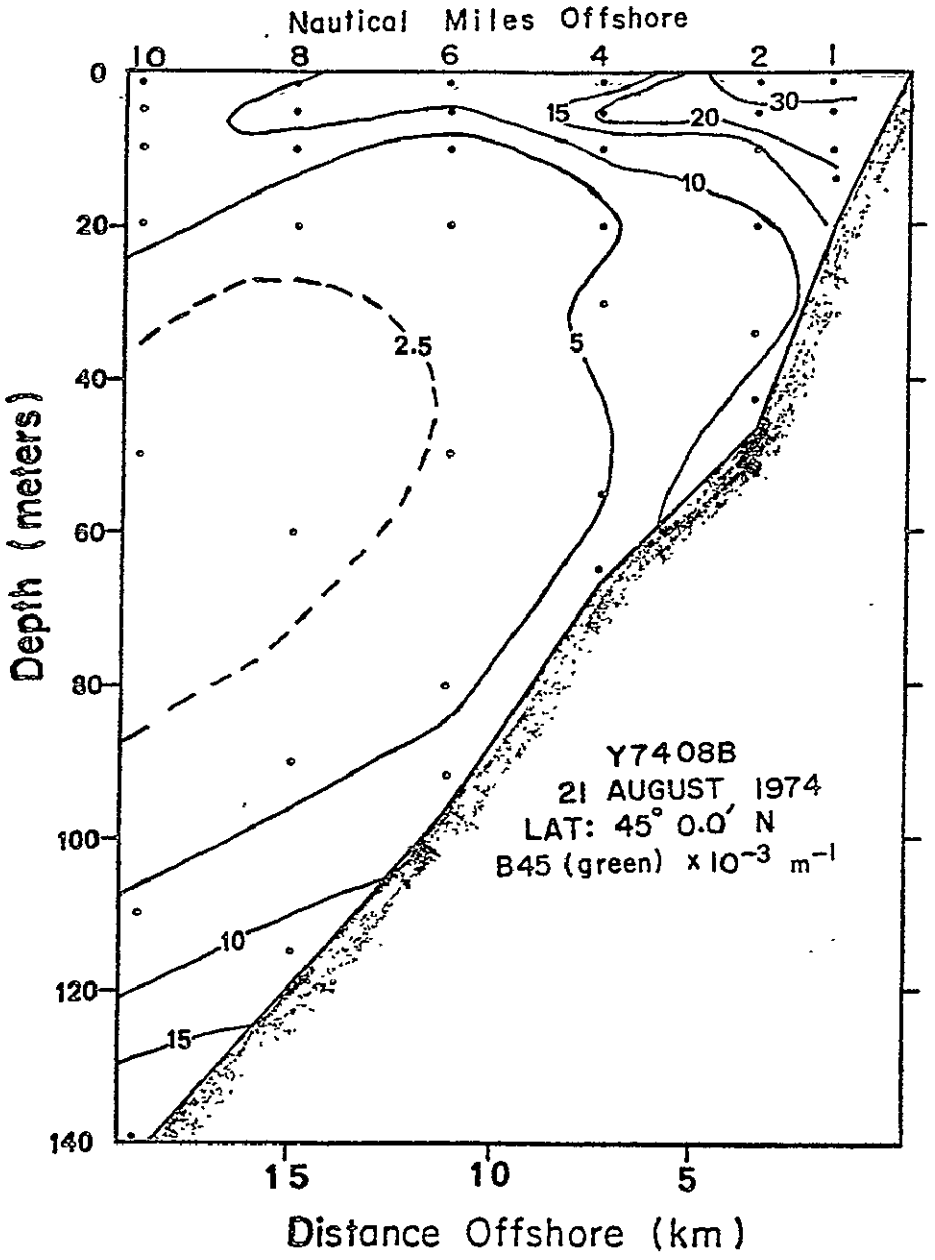

Figure 33 The distribution of light scattering (546 nm) at 45° ($\beta 45$) from the forward direction along a transect during 21 August 1974.

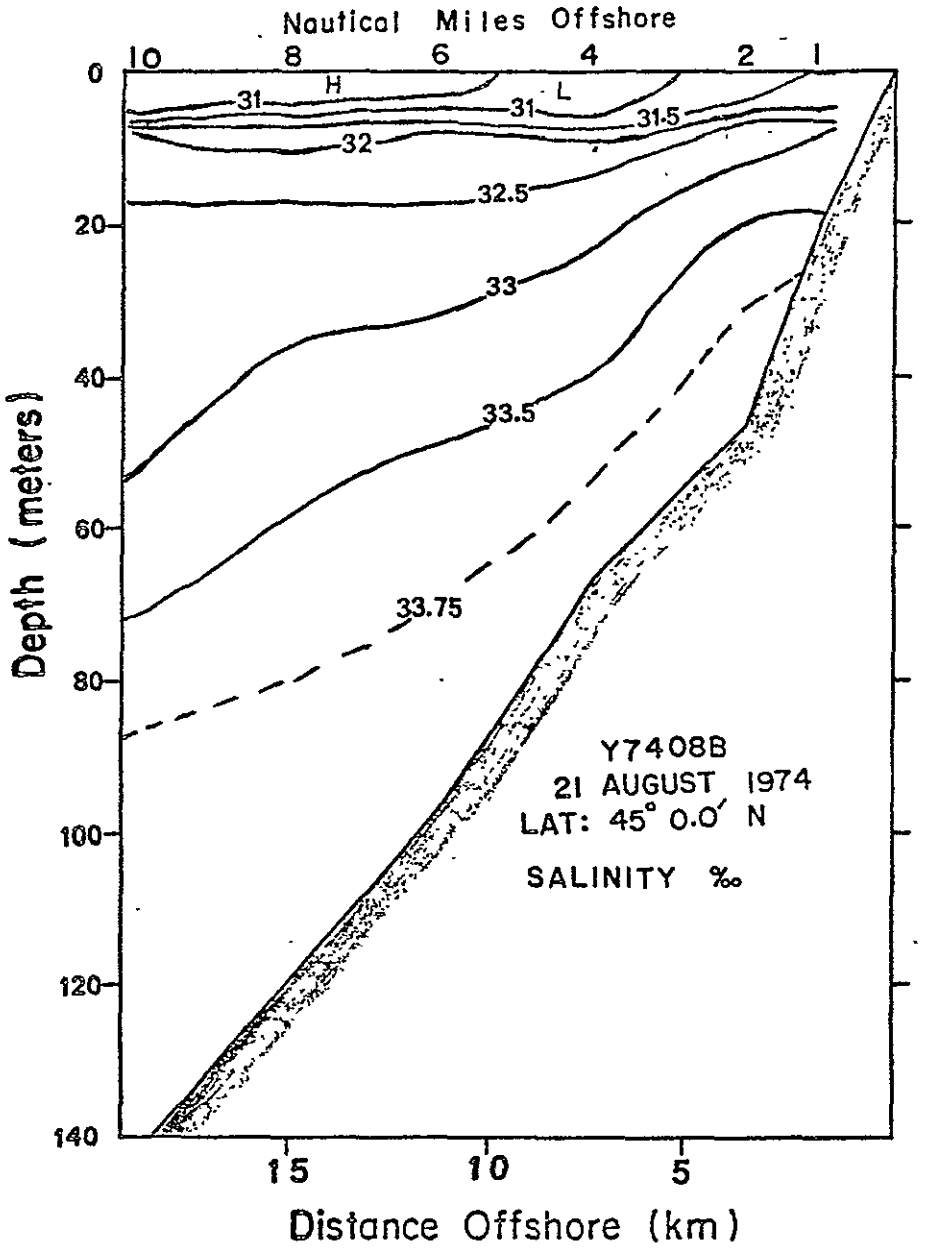

Figure 34 The distribution of salinity along a transect during 21 August 1974.

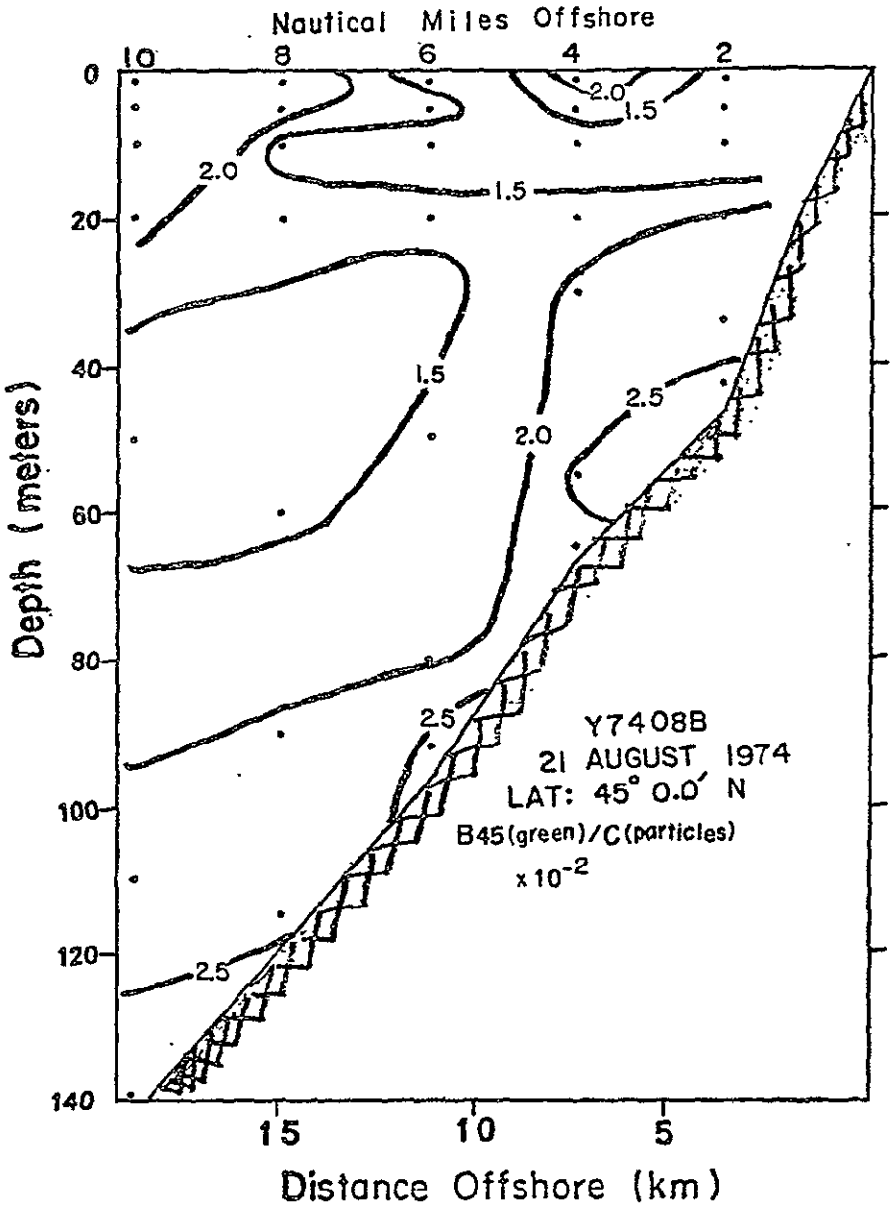

Figure 35 The distribution of the ratio of light scattering (546 nm) at 45° (β45) to the attenuation (C) of light (660 nm) due to suspended particles along a transect during 21 August 1974.

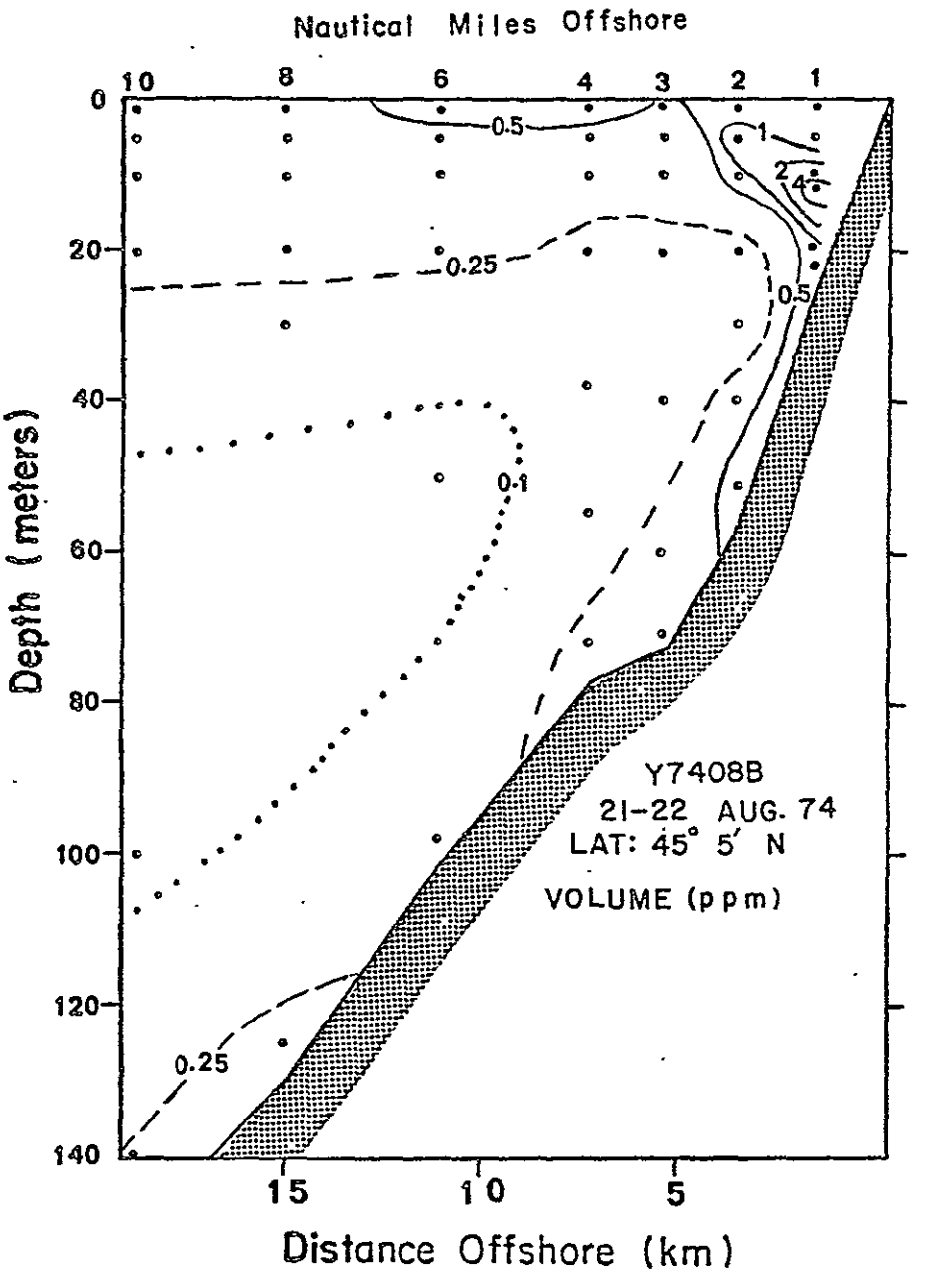

Figure 36 The distribution of particulate volume concentration along a transect during 21-22 August 1974.

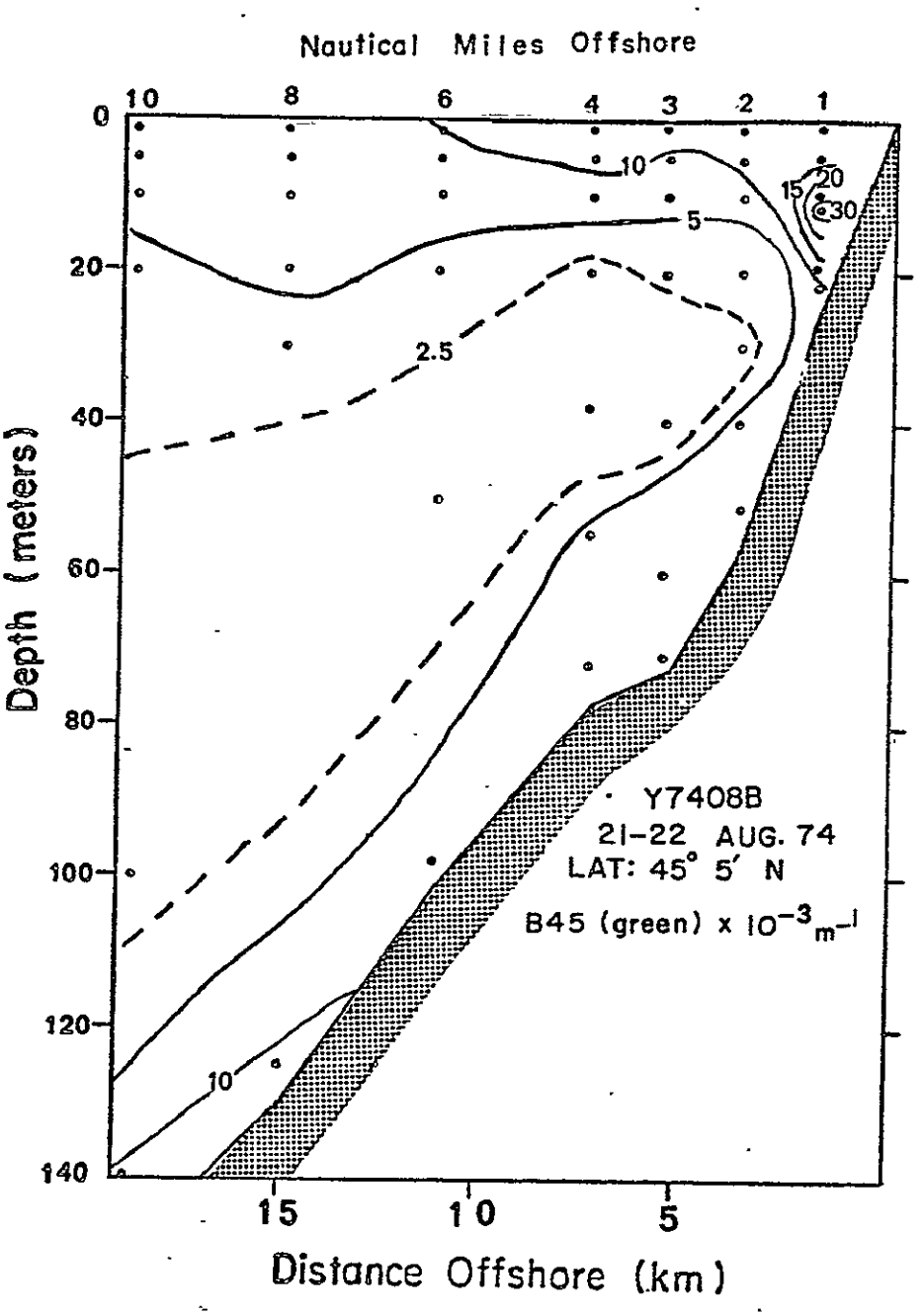

Figure 37 The distribution of light scattering (546 nm) at 45° (β45) from the forward direction along a transect during 21-22 August 1974.

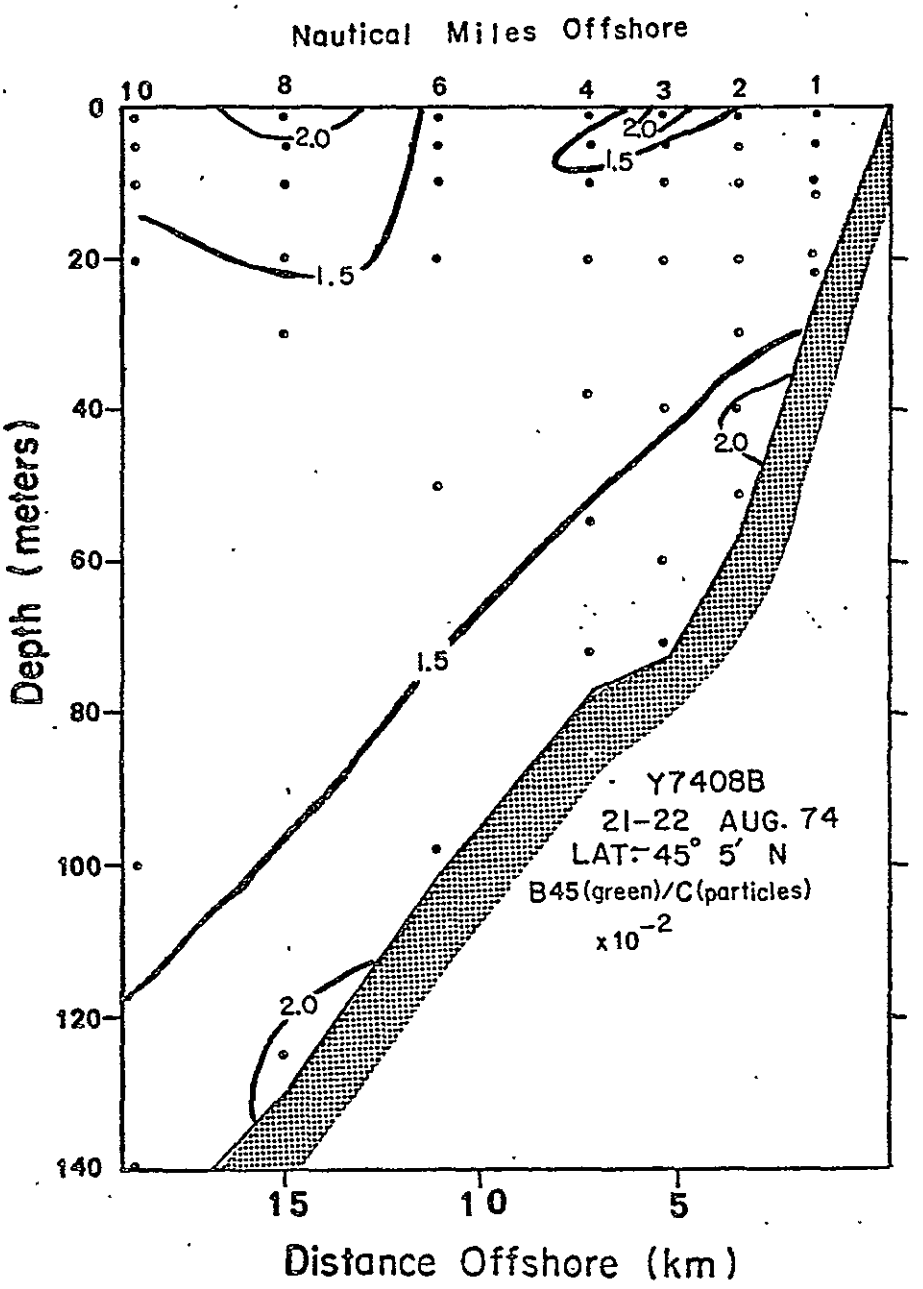

Figure 38 The distribution of the ratio of light scattering (546 nm) at 45° (β45) to the attenuation (C) of light (660 nm) due to suspended particles along a transect during 21-22 August 1974.

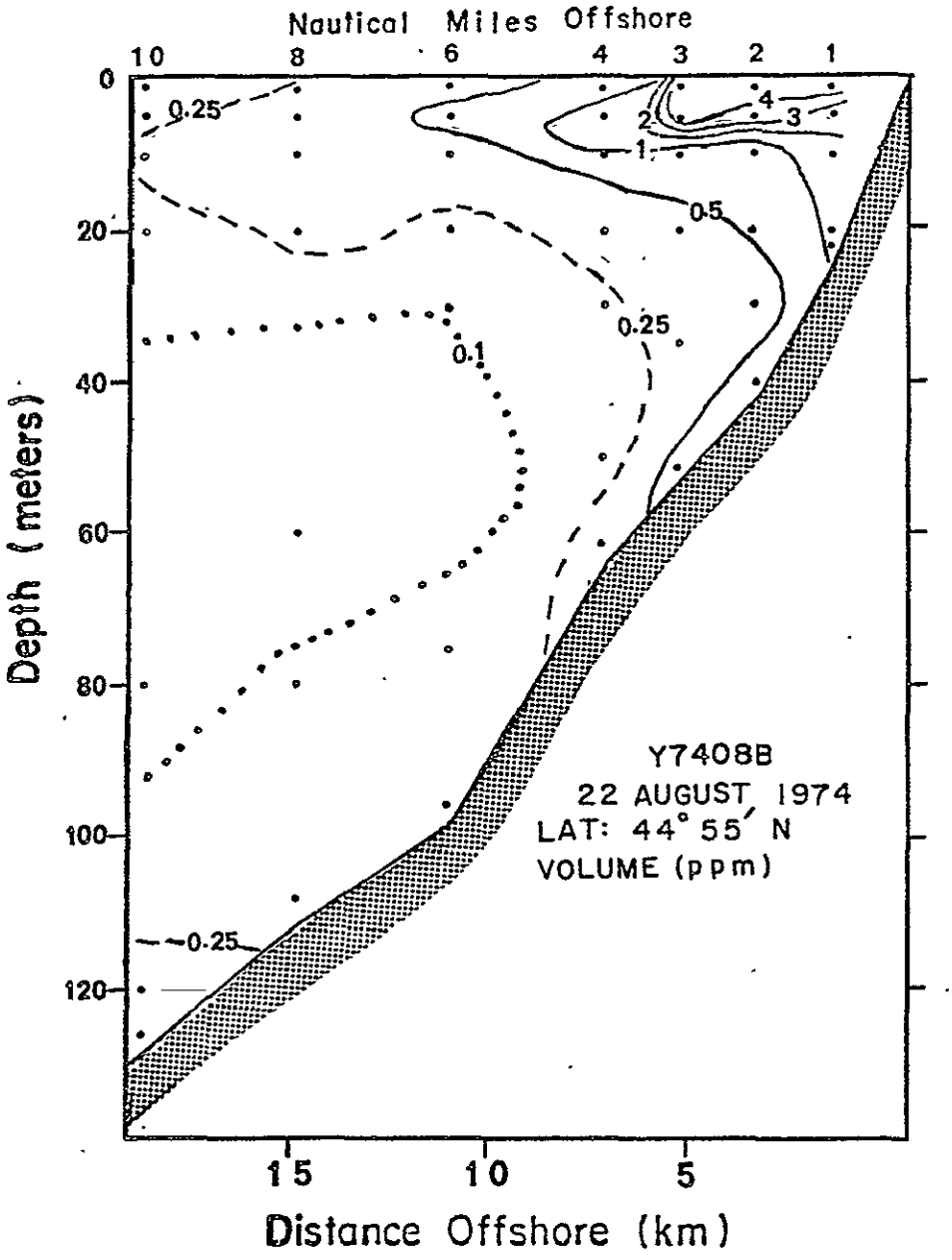

Figure 39 The distribution of particulate volume concentration along a transect during 22 August 1974.

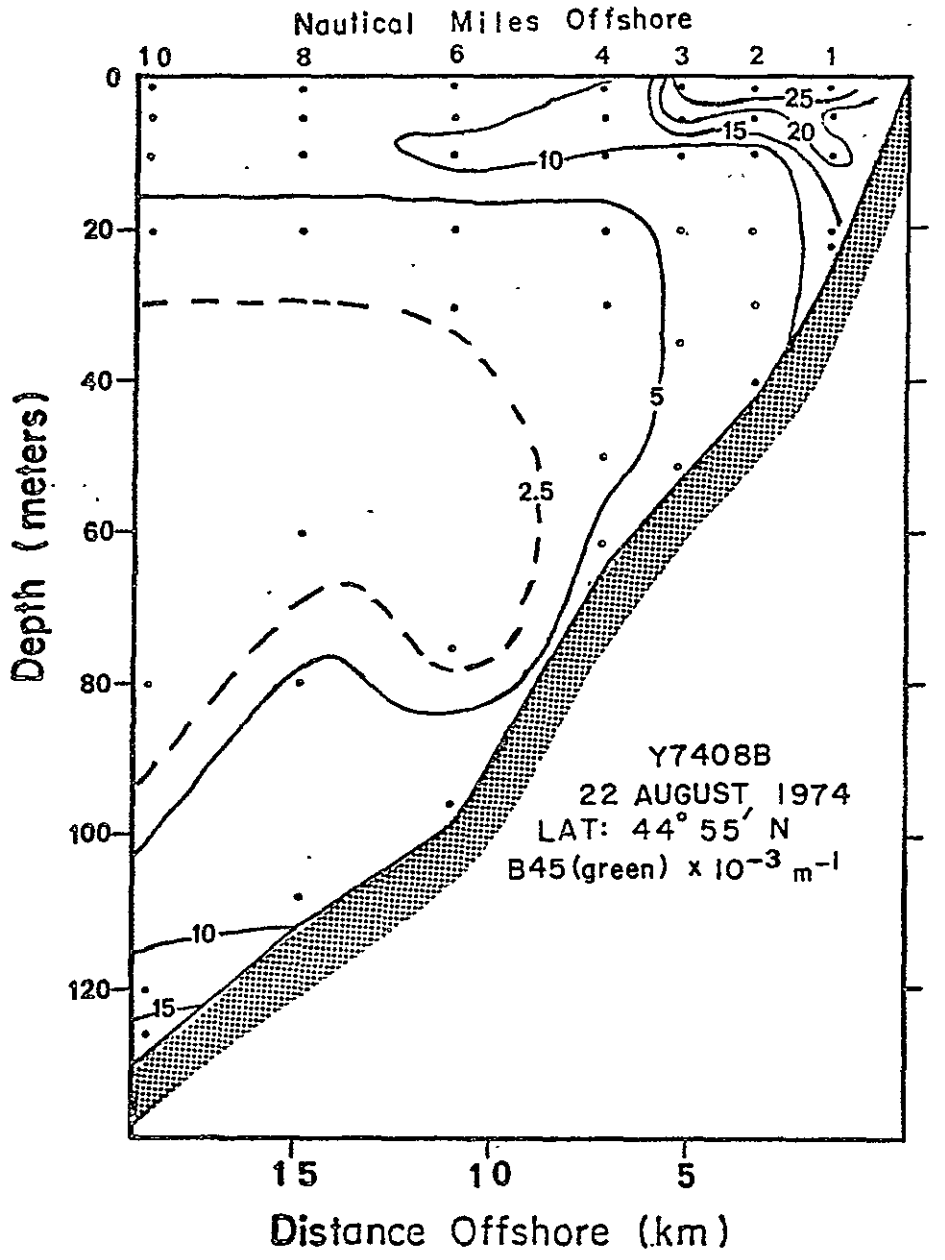

Figure 40 The distribution of light scattering (546 nm) at 45° (β45) from the forward direction along a transect during 22 August 1974.

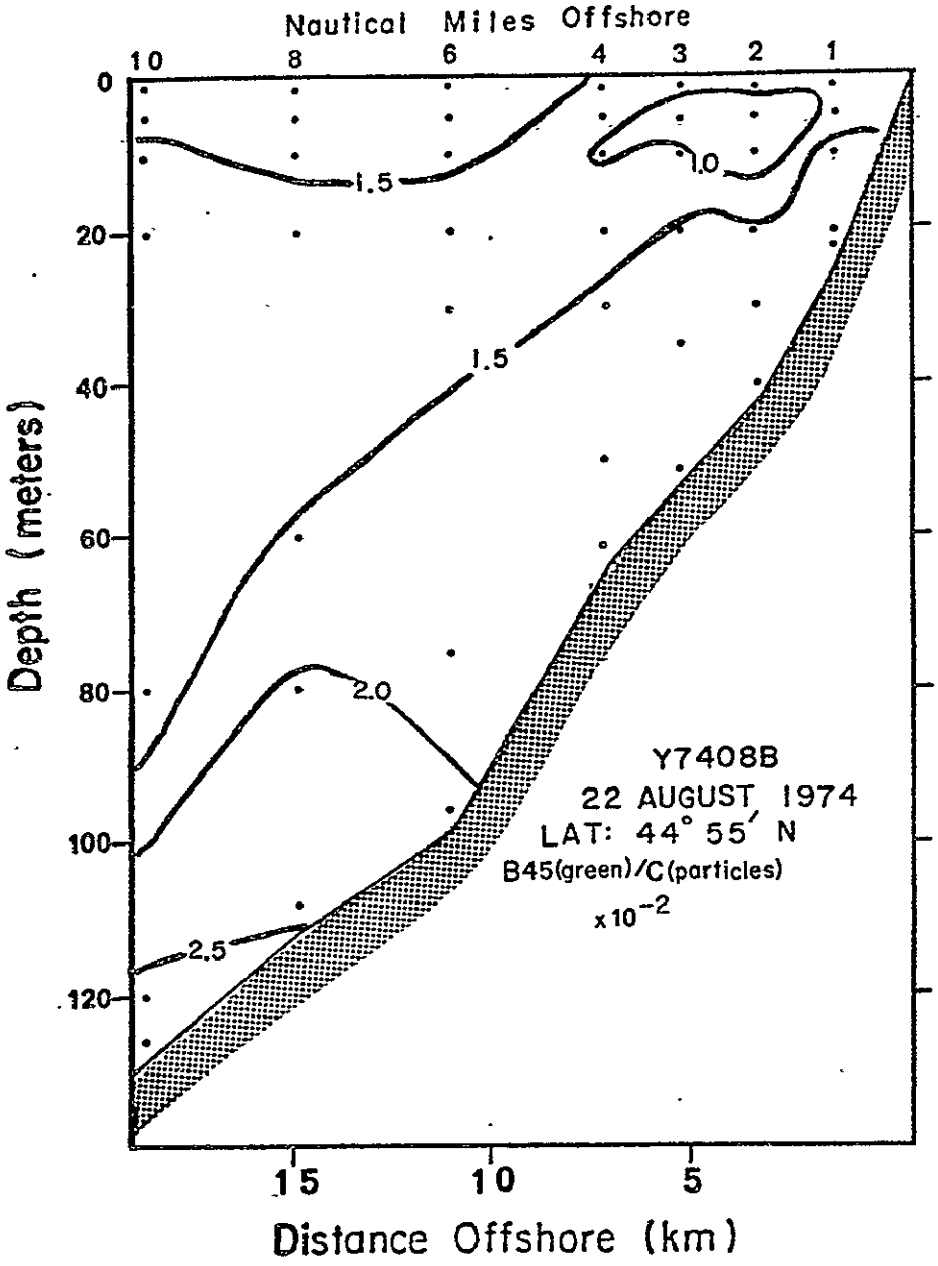

Figure 41 The distribution of the ratio of light scattering (546 nm) at 45° (β45) to the attenuation (C) of light (660 nm) due to suspended particles along a transect during 22 August 1974.

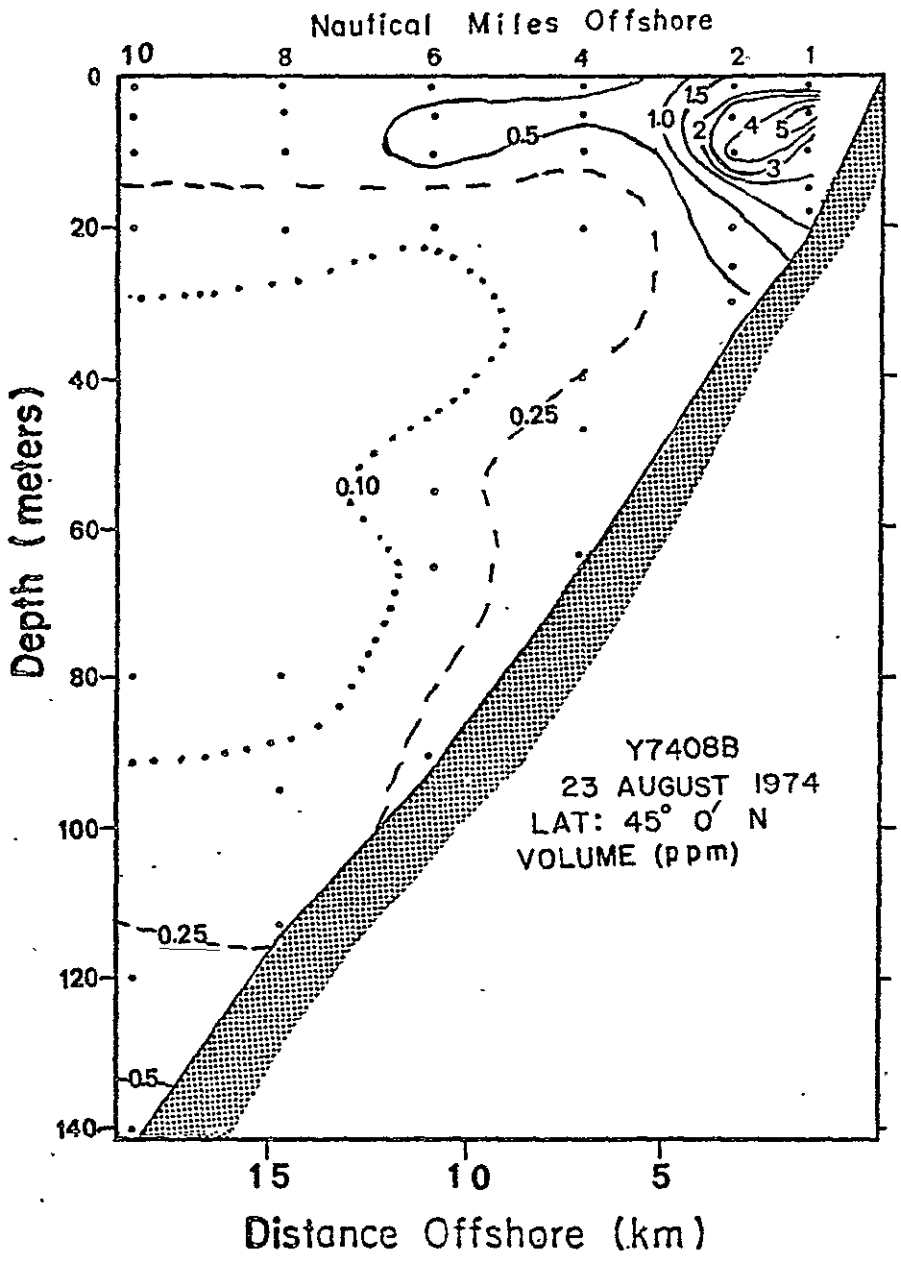

Figure 42 The distribution of particulate volume concentration along a transect during 23 August 1974.

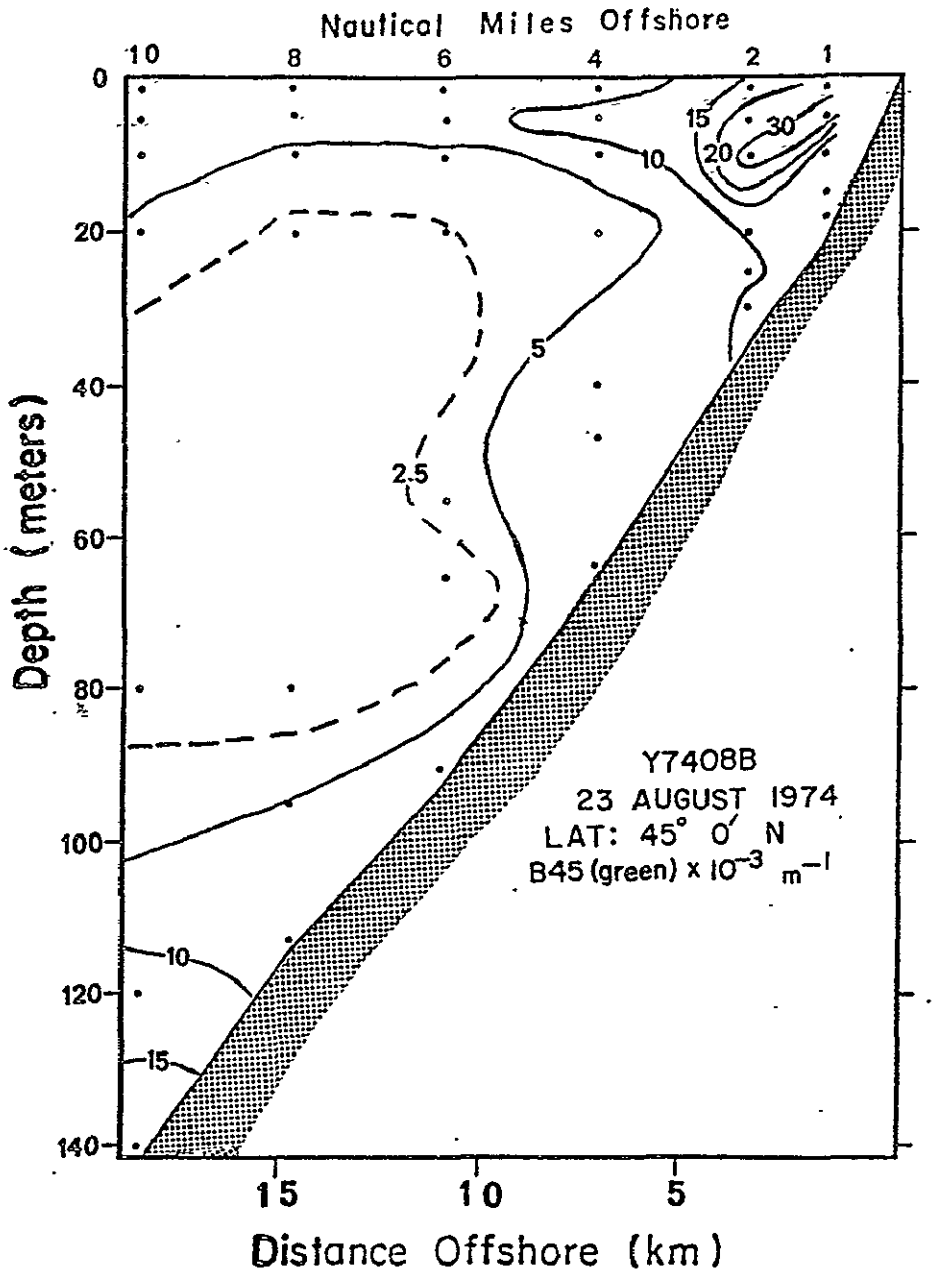

Figure 43 The distribution of light scattering (546 nm) at 45° (β45) from the forward direction along a transect during 23 August 1974.

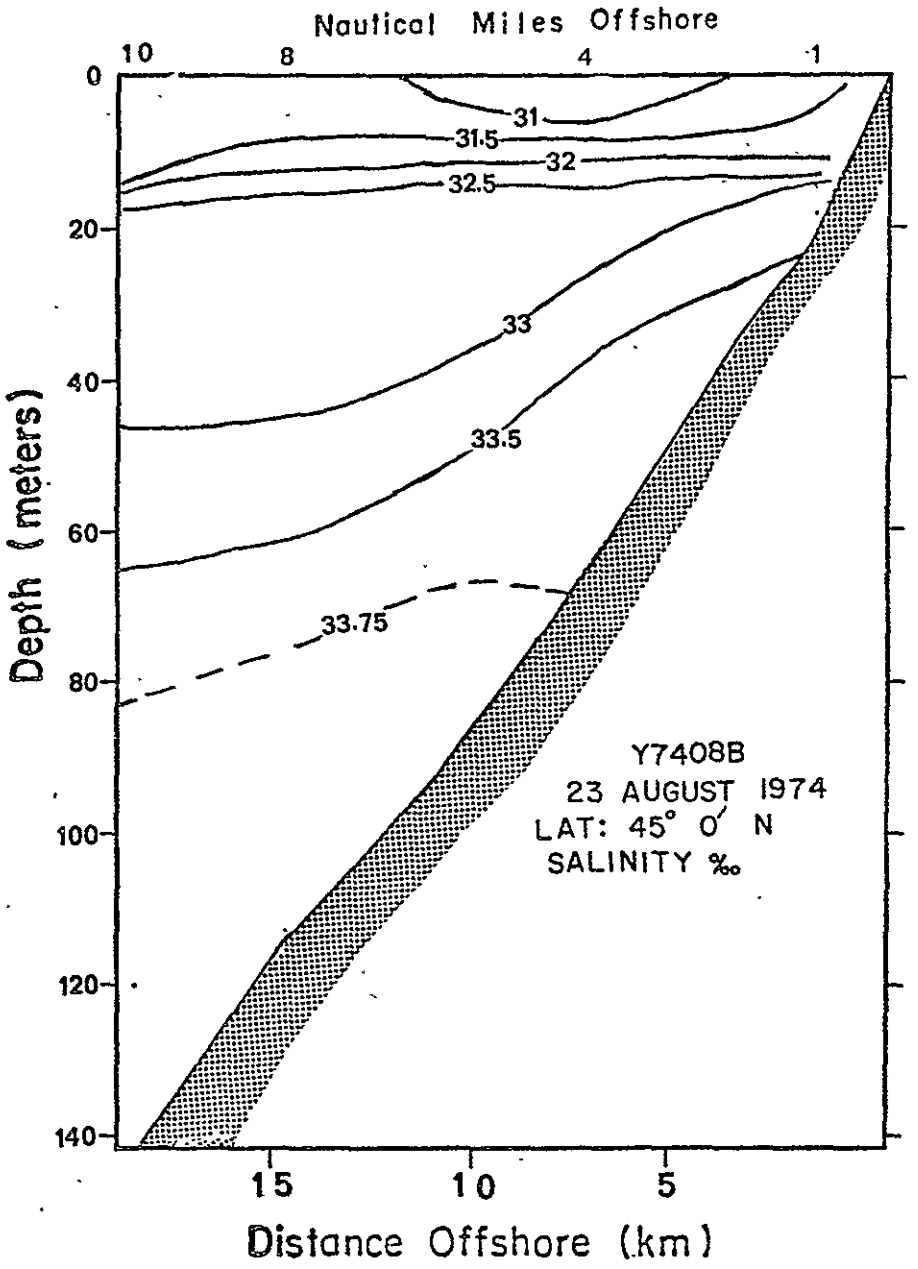

Figure 44 The distribution of salinity along a transect during 23 August 1974

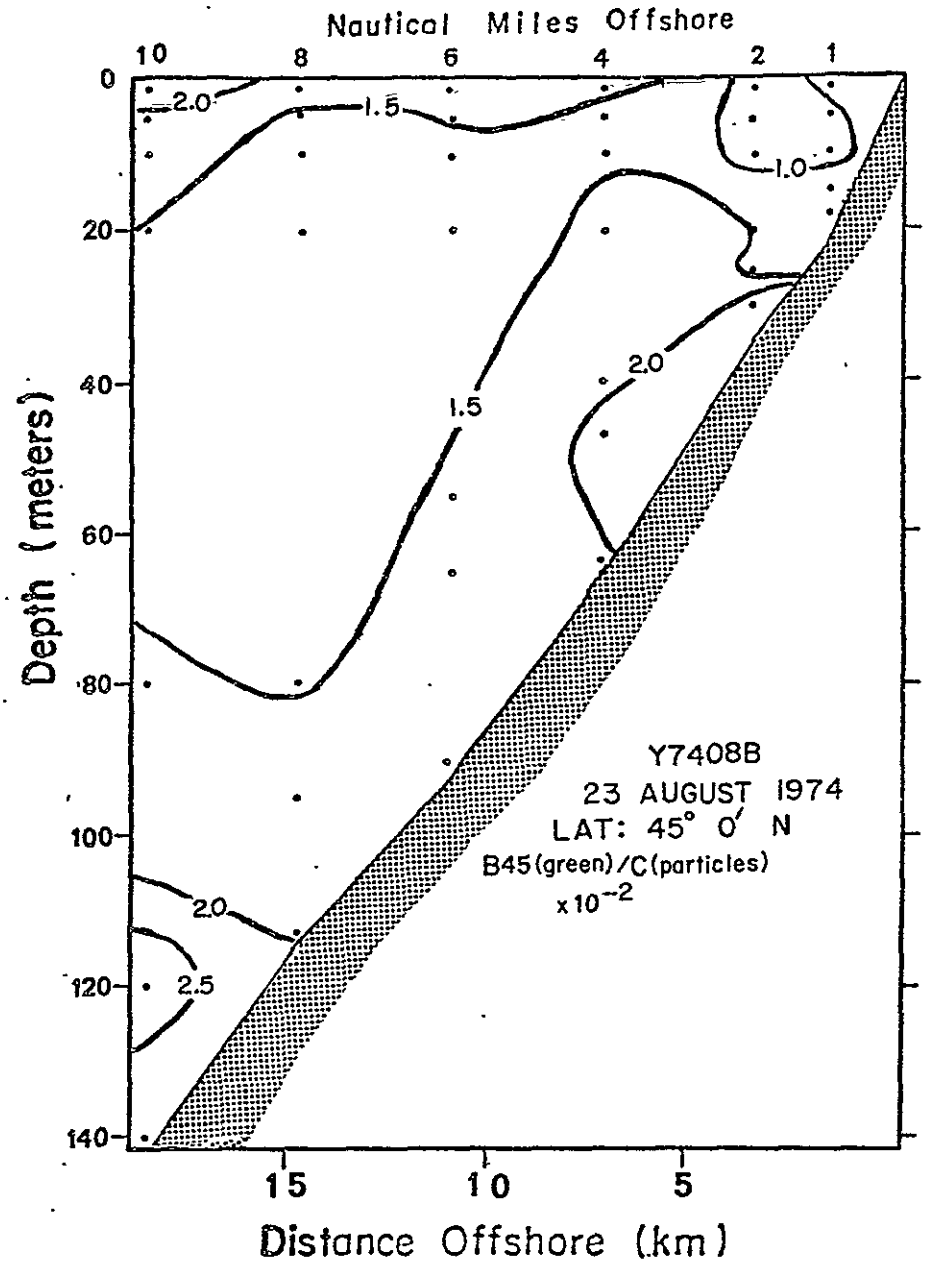

Figure 45 The distribution of the ratio of light scattering (546 nm) at 45° (ß45) to the attenuation (C) of light (660 nm) due to suspended particles along a transect during 23 August 1974.

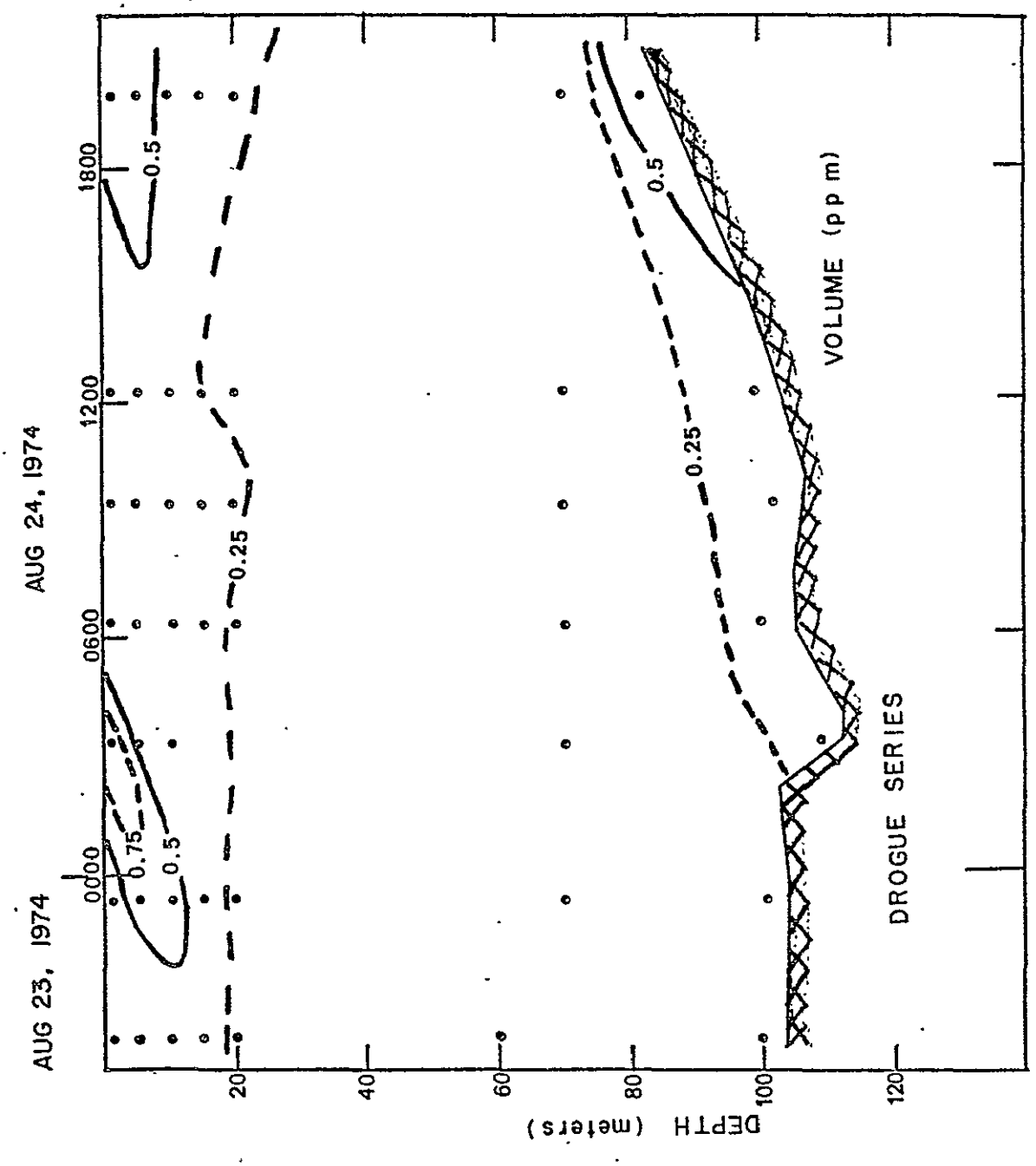

Figure 46 The time change of particulate volume concentration while following a drogue deployed at 5 meters depth.

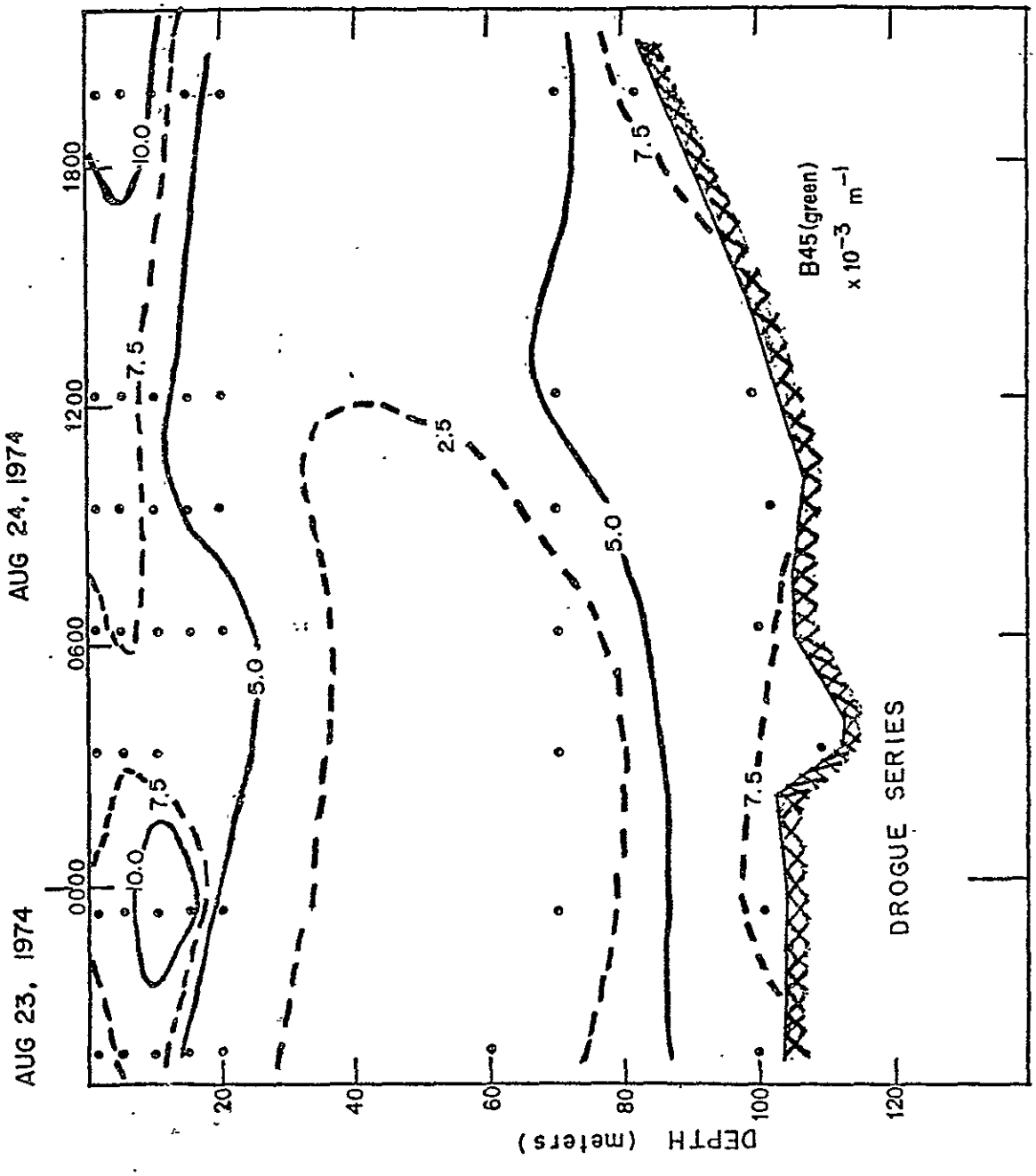

Figure 47 The time change of light scattering while following a drogue deployed at 5 meters depth.

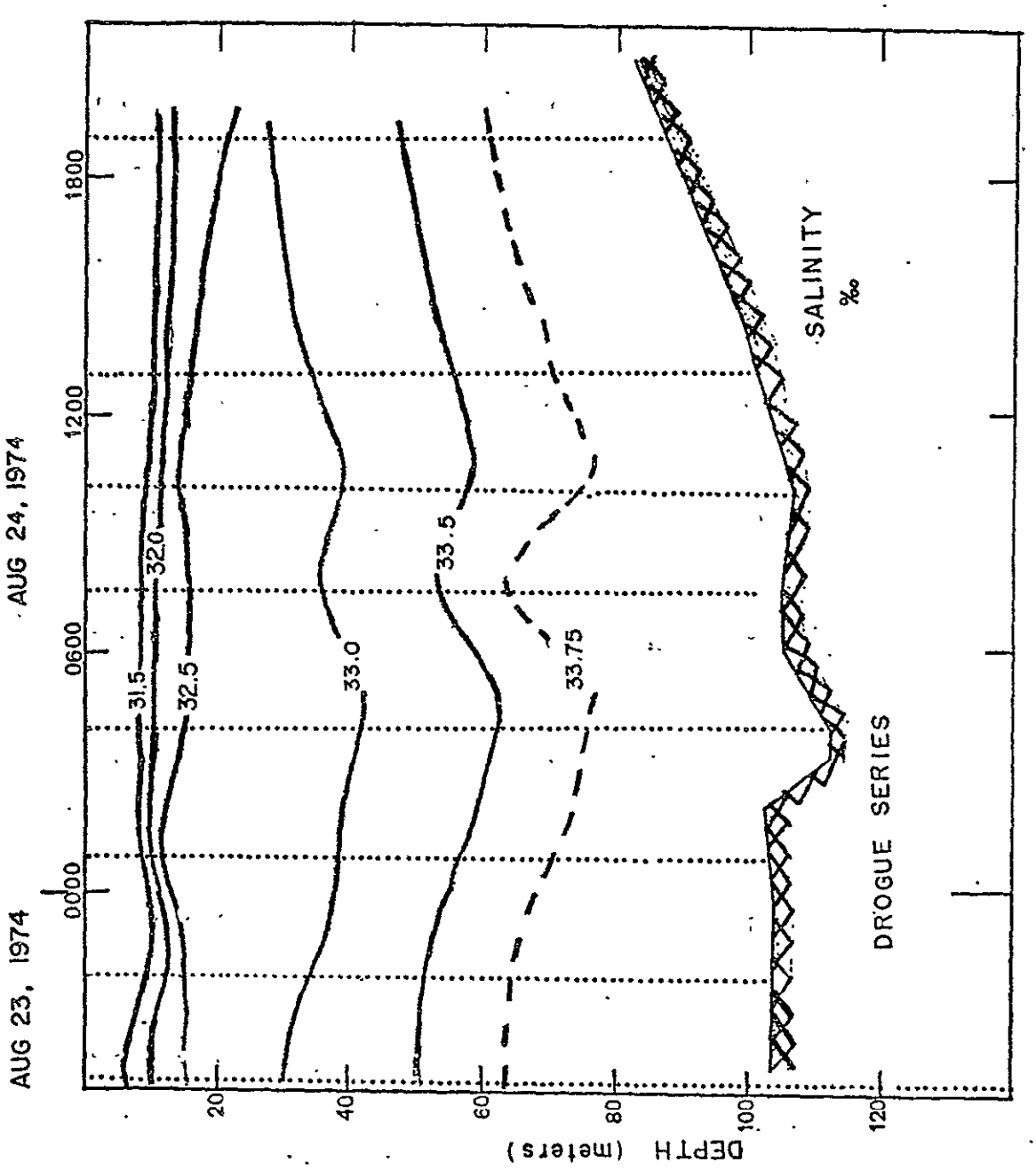

Figure 48. The time change of salinity while following a drogue deployed at 5 meters depth.

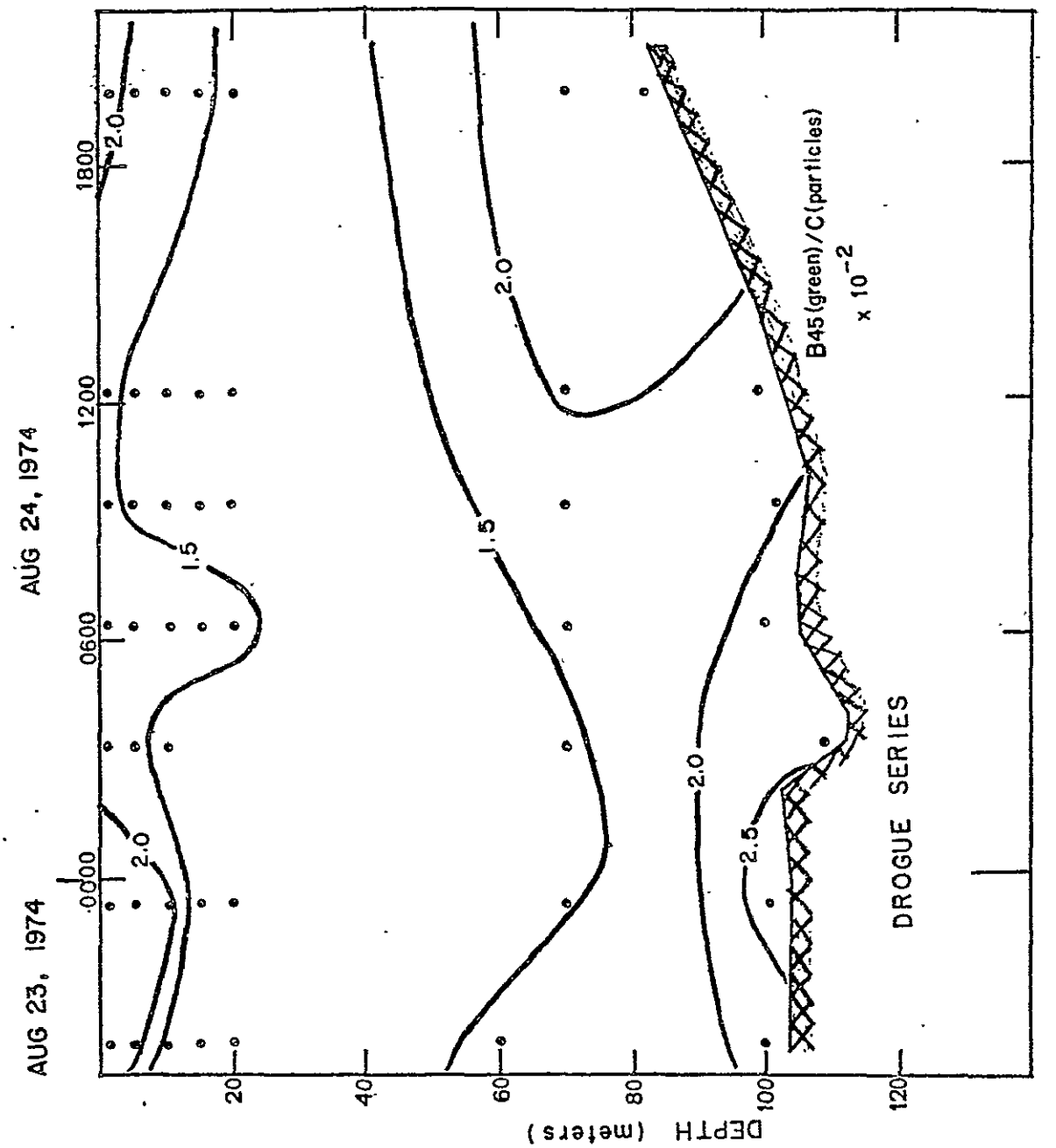

Figure 49. The time change of the ratio of light scattering while following a drogue deployed at 5 meters depth.

APPENDIX C

FORTRAN Program for One-Dimensional Model

```
      PROGRAM FIZ
      DIMENSION W(40),S(40),SN(40),SL(40),SNL(40),AN(40),ANN(40)
      DIMENSION AL(40),AZ(40)
      DATA(AL(I),I=1,40)=.81,.98,1.0,.94,.86,.78,.71,.62,.55,
     1.49,.44,.38,.34,.29,.25,.21,.19,.15,.12,.10,.08,.05,
     2.04,.01,0.,0.,0.,0.,0.,0.,0.,0.,0.,0.,0.,0.,0.,0.,0.,0.)
C
C     DEFINE CURRENT FIELD AND PARAMETERS
C
      VM=5.0E-6
      VML=1.0E-5
      WS=.0002
      WSL=.0005
      READ(10,1001)W
      READ(7,1002)S
      DO 1 I=1,40
1     SL(I)=S(I)
      READ(8,1002)AN
      READ(9,1001)AZ
      ALF=.3
C
C     CONVERT TO M/QHR UNITS
C
      AKL=400
      AK=50.
      VM=VM*900.
      VML=VML*900.
      WS=90.*WS/10.
      WSL=90.*WSL/10
      DO 8 N2=1,40
8     AZ(N2)=9.*AZ(N2)/(10.*10.)
C
C     NOTE W WAS NOT READ IN CGS UNITS ABOVE
      DO 9 N9=1,40
9     W(N9)=.090*W(N9)/10.
C
C     START LOOPING
C
      DO 10 IT=1,4
      DO 11 IS=1,200
C
C     SURFACE BOX
C
      SN(1)=S(1)-W(1)*(S(2)-S(1)).-WS*(S(1)).
      SNL(1)=SL(1)-W(1)*(SL(2)-SL(1)).-WSL*(SL(1)).
      SN(1)=SN(1)+AZ(10*(S(2)-S(1))
      SNL(1)=SNL(1)+AZ(1)*(SL(2)-SL(1))
      ANN(1)=AN(1)-W(1)*(AN(2)-AN(1))+AZ(1)*(AN(2)-AN(1))
```

```
C
C    INTERIOR BOXES
C
     DO 12 JT=2,39
     JM=JT-1
     JP=JT+1
     SN(JT)=S(JT).-W(JT)*(S(JP)-S(JT)
     SN(JT)=SN(JT)-WS*(S(JM)).
     SNL(JT)=SL(JT)-W(JT)*(SL(JP)-SL(JT))
     SNL(JT)=SNL(JT)-WSL*(SL(JT)-SL(JM))
     SN(JT)=SN(JT)+AZ(JT)*(S(JP)-S(JT)-AZ(JM)*(S(JT)*S(JM))
     SNL(JT)=SNL(JT)+AZ(JT)*(SL(JP)-SL(JT))-AZ(JM)*(SL(JT)
    1-SL(JM))
     ANN(JT)=AN(JT)-W(JT)*(AN(JP)-AN(JT))
     ANN(JT)=ANN(JT)+AZ(JT)*(AN(JP)-AN(JT))-AZ(JM)*(AN(JT)
    1-AN(JM))
  12 CONTINUE
C
C    PRODUCTION
C
     DO 13 JR= 1,24
     B=VM*AN(JR)*S(JR)*AL(JR)/(AK+AN(JR))
     BL=VML*AN(JR)*SL(JR)*AL(JR)/(AKL+AN(JR))
     SN(JR)=SN(JR)+B
     SNL(JR)=SNL(JR)+BL
     ANN(JR)=ANN(JR)-ALF*(B+BL)
  13 CONTINUE
C
C    REASSIGN VALUES
C
     DO 14 JF=1,39
     S(JF)=SN(JF)
     SL(JF)=SNL(JF)
  14 AN(JF)=ANN(JF)
     S(40)=SN(39)
     SL(40)=SNL(39)
     AN(40)=ANN(39)
  11 CONTINUE
     WRITE(1,1003)S,SL,AN
  10 CONTINUE
     CALL EXIT
1001 FORMAT(10F6.2)
1002 FORMAT(10F6.0)
1003 FORMAT(10F6.0)
     END
```

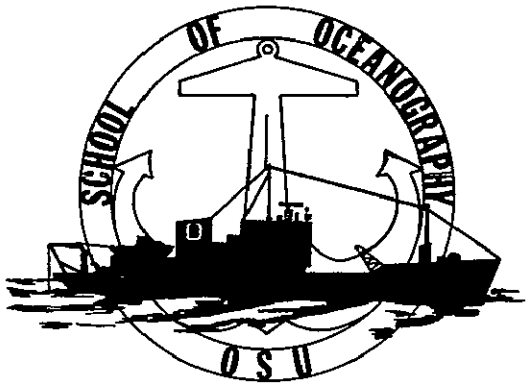
SCHOOL OF OCEANOGRAPHY
OSU